

2024

# Detecting spontaneous symmetry breaking and bound states in (1+1)-dimensional bosonic models with lightcone conformal truncation

---

<https://hdl.handle.net/2144/49938>

*Downloaded from DSpace Repository, DSpace Institution's institutional repository*

BOSTON UNIVERSITY  
GRADUATE SCHOOL OF ARTS AND SCIENCES

Dissertation

**DETECTING SPONTANEOUS SYMMETRY BREAKING AND  
BOUND STATES IN (1+1)-DIMENSIONAL BOSONIC MODELS  
WITH LIGHTCONE CONFORMAL TRUNCATION**

by

**KYRIAKOS GRAMMATIKOS**

B.S., University of Crete, 2016  
M.A., Boston University, 2022

Submitted in partial fulfillment of the  
requirements for the degree of  
Doctor of Philosophy

2024



Approved by

First Reader

---

Emanuel Katz, PhD  
Professor of Physics

Second Reader

---

Andrew Liam Fitzpatrick, PhD  
Associate Professor of Physics

## Acknowledgements

I would like to thank my advisor Emanuel Katz, for having the patience to support me throughout navigating this vast and rather complicated field of study. His wide knowledge base, physical intuition, and presentation feedback have been instrumental to the completion of this thesis and degree. I would like to thank my colleagues, Wei Li and Yuan Xin, for generously interacting with me during this learning process and offering interesting and insightful conversations. I would like to thank my committee members, Richard Brower, Anushya Chandran, Chris Grant, Zeynep Demiragli, Liam Fitzpatrick for their presence, comments and support.

Many thanks to the classmates, colleagues and friends Nikolay Shumovskyi, Jack Stropko, Janos Adam, Tamiro Villazon, Peco Myint, for making the first few and most formative years in this journey more bearable. Also, to the rest of the grad student community, older and younger, at BU physics for embracing me and supporting me emotionally during mentally difficult times.

The biggest shoutout goes to my family and friends for putting up with me through life-changing experience, and staying by my side through thick and thin. Special gratitude to my younger brother Ilias, for his nuggets of wisdom and mature attitude, and my parents Giorgos and Roula for igniting my interest in science, facilitating my transition to America and always being a listening ear. From my friends, I would especially like to thank Zhenghui Li, Erick Sechler and Antoine Ho, for keeping me the best company, and reminding me to have fun even during the hardest of times, my childhood friend Konstantina Morali, for support and commiseration during our simultaneous PhDs, and my favorite Cretan Vula Nikolidaki for her continued communication, support and fun vacation time we had together. This degree wouldn't have been possible without you, and is dedicated to you. Finally, I extend a heartfelt thanks to everyone who is not mentioned on this page that contributed to these bewilderingly wild 8 years in the United States.

**DETECTING SPONTANEOUS SYMMETRY BREAKING AND  
BOUND STATES IN (1+1)-DIMENSIONAL BOSONIC MODELS  
WITH LIGHTCONE CONFORMAL TRUNCATION**

**KYRIAKOS GRAMMATIKOS**

Boston University, Graduate School of Arts and Sciences, 2024

Major Professor: Emanuel Katz, Professor of Physics

ABSTRACT

Lightcone Conformal Truncation (LCT) is a relatively new Hamiltonian truncation method that proposes viewing QFTs as deformations of solvable conformal field theories (CFTs). LCT stands out from other truncation methods in fully preserving conformal invariance and probing the infinite volume limit directly. The output of the method is a discretized version of the spectrum of the underlying continuum theory, which can subsequently be used to calculate other QFT observables. We apply the method to two bosonic scalar field theories, with a quartic/sextic potential described by two dimensionless couplings. The theories exhibit textbook Landau-Ginzburg first order phase transitions at weak coupling, providing an ideal laboratory for the method to probe observables at criticality. The  $\phi^4$  theory requires the  $\mathbb{Z}_2$  symmetry to be broken by a  $\phi^3$  term to access the SSB phase, while the  $\phi^6$  theory requires no explicit breaking. We identify a method to detect a phase transition with our method and we present novel, quantitative, non-perturbative estimates for the shape of the phase transition lines and furthermore, we detect and quantify the emergence and weak coupling dependence of the bound states in the spectrum of the theories.

# Contents

<b>Title</b>	<b>i</b>
<b>Copyright</b>	<b>ii</b>
<b>Reader's Approval</b>	<b>iii</b>
<b>Acknowledgements</b>	<b>iv</b>
<b>Abstract</b>	<b>v</b>
<b>1 Introduction</b>	<b>1</b>
<b>2 LCT and its ingredients</b>	<b>12</b>
2.1 Free boson CFT and operator content . . . . .	16
2.2 Constructing CFT states . . . . .	22
2.3 Computing Hamiltonian matrix elements . . . . .	24
2.3.1 Wick contractions . . . . .	26
2.3.2 Radial quantization . . . . .	30
2.4 Spontaneous symmetry breaking in LCT . . . . .	37
<b>3 Spontaneous Symmetry Breaking in the <math>\phi^4</math> bosonic field theory in 1+1-D</b>	<b>43</b>
3.1 Implementing SSB in LCT . . . . .	46

3.2	Results . . . . .	51
3.3	Crossings . . . . .	60
3.4	Bound states . . . . .	70
<b>4</b>	<b>Phase transitions and bound states in <math>\phi^6</math> theory</b>	<b>79</b>
4.1	Effective LC description . . . . .	83
4.2	LCT simulations . . . . .	86
4.3	Crossings . . . . .	93
4.4	Bound states . . . . .	96
<b>A</b>	<b>Zero modes in LC</b>	<b>101</b>
A.1	A toy LC quantized field theory . . . . .	105
A.2	Zero modes in constrained first order classical systems . . . . .	108
A.3	The Dirac-Bergmann algorithm . . . . .	115
<b>B</b>	<b>Semiclassical results</b>	<b>118</b>
B.1	$\phi^6$ model semiclassics . . . . .	118
B.2	Critical surfaces of a general sextic potential . . . . .	120
<b>C</b>	<b>Avoided Crossings</b>	<b>124</b>
<b>D</b>	<b>Non-relativistic bound state in <math>\phi^4</math></b>	<b>130</b>

<b>List of Journal Abbreviations</b>	<b>136</b>
<b>References</b>	<b>137</b>
<b>Vita</b>	<b>146</b>

## List of Tables

1	Matrix sizes for a few $\Delta_{\max}$ values. . . . .	51
---	--	----

## List of Figures

1	SSB pattern in $\phi^4$ and $\phi^6$ . . . . .	39
2	VEV in the quartic theory with negative mass term . . . . .	44
3	Minima of classical $\phi^4$ potential with a $\phi^3$ deformation . . . . .	50
4	Perturbative gap correction from cubic interaction . . . . .	52
5	Approach to non-perturbative first order transition for $\lambda = 0$ . . . . .	53
6	Zero gap lines . . . . .	54
7	Zero gap lines at weak coupling . . . . .	56
8	Eigenvalue shower . . . . .	61
9	Individual avoided crossing width . . . . .	62
10	Crossing parameter scaling with $\Delta_{\max}$ . . . . .	64
11	Measurement of the half-width of the crossing . . . . .	65
12	Scaling of transition width measures with truncation level . . . . .	67
13	Existence of a near threshold bound state . . . . .	71
14	Bound state measurement on the phase boundary . . . . .	72
15	Extrapolated threshold bound state . . . . .	74
16	Bound state emergence curve . . . . .	75
17	Landau phase transition for $\phi^6$ potential . . . . .	79
18	Eigenvalue shower for sextic theory . . . . .	80

19	Existence of mass gap and near threshold bound state in sextic theory	87
20	Perturbative zero gap curve (sextic theory) . . . . .	88
21	Approach to first order transition line $\lambda_6 = 0$ . . . . .	89
22	Sextic theory unbroken phase boundary . . . . .	91
23	Transition width at weak coupling and crossing height in $\phi^6$ . . . . .	93
24	Transition width at strong coupling . . . . .	94
25	Two- and three-particle bound states . . . . .	97
26	Two- and three-particle bound states on the phase boundary . . . . .	99
27	Kinks of sextic theory . . . . .	119
28	Non-relativistic binding energy of threshold bound state . . . . .	134

# 1 Introduction

Quantum field theories in the continuum are not only hard to exactly solve, but also hard to approximate; the vast majority of the tools at your average field theorist's toolbox for calculating QFT observables up until the 1960s, were mostly based off of perturbation theory. Perturbation theory is a powerful tool that uses the states of a simpler, solvable theory as the basis for understanding the Hilbert space of an interacting theory. This tool spearheaded many quantitative, but also conceptual advances in the QFT realm; after the measurement of the Lamb shift in 1947, Bethe published a paper with a perturbative theoretical calculation that agreed with experiment. The success of that calculation not only brought QFT back to the game of modelling nature, but also shed some light into the biggest conceptual problem QFT posed at the time, the one of infinities. Bethe's ingenuity was to avoid taking into account modes of extremely high energy into account by imposing an explicit cutoff in terms of the mass of the electron. This kickstarted the process of understanding QFT as a theory that explicitly requires as input the energies of the phenomena it is supposed to describe, and that arrogantly assuming that the physics we understand holds to arbitrarily high energies is misleading.

Much like its predecessor, classical field theory, one can treat QFT as an effective, description for systems with a large number of degrees of freedom, that should break down as one zooms in to very small distances or equivalently, thanks to quantum mechanics and the uncertainty relation, very large energies. As an example of the breakdown of a classical field theory, hydrodynamics describes collective phenomena and assumes the density and velocity fields of a fluid are smoothly varying functions of space and time, however they appear smooth only if averaged over a large enough spatiotemporal volume; in fact the assumptions of hydrodynamics break down already at the  $\mu m$  scale, and this constitutes a UV cutoff for this theory, much like the rest frame energy of the electron was an appropriate cutoff for Bethe's calculation. The role of the cutoff scale as necessary input for the theory is further highlighted by the development of the renormalization group approach, which starts with the assumption

that the low energy physics (such as correlation functions, which can be measured through experiment) should not be varying with the choice of scale we made. This in turn is what has allowed several important developments, like the classification of QFTs upon their perturbative renormalizability, facilitating the understanding of the behavior of the theories at strong coupling, and detecting existence of possible critical points (usually described by strongly coupled CFTs), and enabling the Standard Model, which with only a few experimentally measured parameters, is able to describe without error all the relativistic particle physics we know for energies  $E \lesssim 13$  TeV.

Despite its monumental successes, perturbation theory has a few obvious shortcomings, and all of them are related to understanding the physics of the interacting model independently of any reference to a simpler, exactly solvable model. In particular, Haag showed ?? that there is no unitary transformation connecting the Hilbert spaces of a non-interacting and an interacting QFT while Anderson ?? showed that eigenvectors of interacting large  $N$  many body Hamiltonians generally have vanishingly small overlap with those of a non-interacting one, for arbitrarily weak coupling. In other words, interactions cause a massive rearrangement of the Hilbert space of a QFT and, as a result, one Hilbert space does not necessarily simulate the other well. This makes QFT quite unlike regular quantum mechanics of a few bodies and/or spins, where every basis of vectors can be used interchangeably when it comes to understanding the properties of a system.

This may seem to pose an impasse for quantum physics, yet it has not stopped physicists from trying to write down meaningful effective theories for systems with a large number of degrees of freedom, nor has it prevented the completion of this thesis. Instead, it has underscored the need for developing tools to access non-perturbative physics without having to resort to weak coupling approximations, but also writing effective theories with respect for the fact that the theories we write down are valid in a certain energy window, which has to be made explicit in the methods we employ. These tools generally put an emphasis on understanding what we call "low energy degrees of freedom", which are the states that should be robust under changes in the content of the physics at high energies, which we cannot claim to know anyway.

In this spirit, a variety of non-perturbative tools have been developed. In the following paragraphs, we will briefly describe 3 categories of tools that have aided non-perturbative understanding in QFT and were developed contemporaneously: lattice QFT, Hamiltonian Truncation and Conformal Field Theory (CFT), of which the latter two have been extensively used in constructing the LCT method.

One of the first non-perturbative tools that has laid the foundation for a truly non-perturbative definition of QFTs is lattice quantum field theory. Lattice methods, albeit tangentially interesting to the purposes of this thesis, are beyond the scope of this manuscript, however we deem that the methods deserve a quick mention, given the gravity of their contributions to our non-perturbative understanding of QFT. In the years before its conception, the perturbative standard model of physics had been created, summarizing the entirety of the knowledge that had been obtained on relativistic particle physics until then. However, axiomatically, QFT was standing on less than solid ground, and the knowledge of existence/well-posedness of interacting continuum field theories was limited to the perturbative regime, and slowly yet surely, the demand to understand QFT at strong coupling was rising. Lattice QFT, partly drawing inspiration from Feynman's path integral, tries to approach the limit of a continuum QFT by discretizing spacetime: the field can live only on discrete spacetime points, which usually belong to some kind of regular lattice, of lattice spacing  $a$ . While the lattice formulation explicitly breaks Poincaré invariance, and recovers it in only the continuum limit, it is a local approach to QFT that respects internal symmetries, which is very important for QFT. After a Wick rotation and imposing periodic boundary conditions, the continuum limit (assuming it exists) should be recovered as the lattice spacing is decreased:  $a \rightarrow 0$ . If a non-trivial continuum limit exists, it is known that the lattice model has to undergo a second order phase transition; in other words, the system develops long range correlations, and any relevant correlation lengths  $\xi$  have to be very large in units of the lattice spacing  $\xi \gg a$ . This statement makes perfect sense from an emergence standpoint; the individual components of a system need to remain correlated over macroscopic distances in order for interesting physics to emerge. Uncorrelated degrees of freedom give rise to Gaussian ensembles

in the thermodynamic limit; these correspond to quadratic field theories that are in essence interaction-free and hence uninteresting. Additionally, the lattice naturally highlights the intimate connection between  $D+1$  dimensional statistical physics models (like the Ising spin model) and QFTs in  $D$  spatial dimensions: for example the 2-D Ising model presents with a genuine second order phase transition when thermal fluctuations become strong and, as research has shown, there is a host of interacting 1+1-D QFTs that, when quantum fluctuations become strong exhibit the exact same phase transition patterns, demonstrating the universality of the underlying statistical model. One of the most important successes of the lattice was to lay down the fundamental tools for understanding asymptotically free theories like QCD. Theories of that kind are expected to have a well defined continuum limit due to their asymptotic freedom and approximate conformality at high energies. The vexing question about the dynamically generated bound state masses that are seen in QCD, despite the fact that at a classical level the particles involved are massless, was answered after some technical difficulties like the fermion doubling problem were solved. In more recent years, lattice QFT techniques like Quantum Monte Carlo (QMC) simulations have been applied to understand QFT in curved space and the gravitational path integral itself.

Another important tool for nonperturbative QFT, originally discovered in the context of string theory, is conformal field theories (CFTs). These field theories possess scale invariance (invariance under dilations of space) that is unbroken by quantum fluctuations- this alone makes them interesting, since this means that the quantum theory possesses no notion of energy or distance scale at all. This scale invariance is intimately connected with statistical systems (quantum or thermal or both) undergoing phase transitions of the second order or higher. These kinds of phase transitions have been found to be associated with development of long range correlations, divergence of a subset of correlation lengths, which leads to massless modes in the low energy spectrum. CFTs offer a very general framework to describe these transitions since they are characterized precisely by massless excitations and power law decaying correlations that lack the presence of a scale.

While there exist scale invariant theories that are non-relativistic in nature, many spin statistical systems that have been studied in the past present with spacetime symmetries described by an extension of the Poincaré group. More concretely, relativistic scale invariant theories actually possess even more symmetries than just Poincaré + dilatation, so that the symmetries form a group, the conformal group. Much like Poincaré invariance on its own, the conformal symmetry group in any dimension  $d > 2$  provides some information on the correlation functions of the theory, but not enough to completely determine them. On the other hand, in two spacetime dimensions, the conformal group includes all smooth conformal mappings on the complex plane, and is therefore infinite-dimensional; this is the source of the power of conformal symmetry and the reason why it has been studied so thoroughly in 2 spacetime dimensions.

Some of the triumphs of the analysis of conformal theory in two dimensions include:

1) A complete classification of theories with central charge  $c < 1$ , into a countably infinite family of models called minimal models. Many interesting systems that exhibit phase transitions can be described by these models in the vicinity of their critical points, and their critical exponents (which describe the scaling of correlation functions near the critical point) can be determined in terms of the dimensions of operators in these models. These models even include CFTs that are non-unitary and can describe transitions of non-Hermitian Hamiltonians or lossy quantum systems coupled to an environment.

2) The development of the conformal bootstrap. In the past, the critical exponents of a system had to be measured near criticality using an underlying lattice model or by performing MC simulations to collect information on the correlation functions. Instead, the conformal bootstrap works directly with the continuum version of the CFT. It utilizes the bootstrap equation, a very stringent requirement on the correlation functions of the CFT, to narrow down the possible sets of CFT data that satisfy the equation. The conformal bootstrap framework can pin down the candidate theory operator dimensions and OPE coefficients with stunning accuracy, only requiring with a relatively small amount of data on the candidate theory, like bounds on the

operator dimensions of the lowest lying operators.

3) The AdS/CFT correspondence, first proposed by Maldacena [1]. The proposition conjectures a duality between two types of theories, a QFT in an AdS space background and a CFT that lives on the boundary of that space. The two theories are conjectured to have a completely equivalent set of correlation functions, in the sense that once an appropriate dictionary between fields in the AdS bulk and the conformal boundary have been identified, the correlation functions containing those fields should match exactly, to all orders in perturbation theory and beyond. This correspondence is of the strong/weak flavor, in the sense that a weakly coupled field in the bulk induces a strongly coupled CFT on the boundary and vice versa. Like all dualities in physics, it is extremely useful since the implementation of a physical concept may be completely obvious in one description, while its interpretation in the other could be obscure, and therefore results in one theory may help bootstrap the other.

As we will see below, in our method CFTs are utilized as a starting point for understanding other interacting theories.

The cluster of Hamiltonian truncation methods, represent an attempt to approximate QFT Hilbert spaces by a finite matrix. Generally, the eigenfunctions to the Hamiltonian describing a QFT form a continuous spectrum, that can be labeled in terms of a, frequently infinite, set of parameters. Compared with spectra of typical quantum mechanical Hamiltonians, where the eigenstates can be labeled by just a few quantum numbers, QFT spectra are often vastly larger. One may argue that generic QFT spectra are not quite the right object to study and that the only objects that really make sense in a QFT are correlation functions. However, there are large classes of QFTs that are known to possess small sets of states that stand out: typically these are few-particle bound states that arise from introducing attractive interactions to an ensemble of particles. These states are the asymptotic particles of the system and they can be individually detected/identified in a scattering experiment. Such well-isolated states with reasonably long decay times are also usually low energy states in

generic QFTs. As it turns out, in case we are interested in the low energy spectrum of a QFT, it is possible to recover it with high accuracy from diagonalizing a finite matrix.

Several methods of constructing such approximations have been implemented in the literature, each one being more suitable for a specific class of theories. However, all of them share a common characteristic; they all resort to a *truncation* of the Hilbert space, that reduces its dimension by restricting the range of some parameter, either naturally by imposing appropriate boundary conditions, or by arbitrarily cutting off the range at a particular point. Generally, this procedure produces a sequence of finite matrices of increasing size, the eigenmodes of which should converge to the continuum limit as their size goes to infinity.

The method of truncating the Hilbert space was initially applied with great success to quantum mechanical systems like the anharmonic oscillator, usually to understand the behavior or energy levels in the intermediate regime [18][49], where both weak and strong coupling expansions fail. Applying the method to quantum field theory problems however remained elusive, until a breakthrough was made with the work of However a very important conceptual leap was made in the work of Brooks and Frautschi [11][12], where the first truncation flavored approach in QFT was developed. In the time prior, equal time quantization approaches had been employed like the Tamm-Dancoff approximation, but were posing difficulties. In particular, Tamm-Dancoff type approaches required technically refined renormalization procedures to approach physics in  $3 + 1$  dimensions, and the field was not mature enough yet to solve them completely. On the other hand, [12] circumvents the problem by limiting considerations to the Yukawa model in  $1 + 1$  dimensions, which reduces the number of divergences significantly. Their method was the beginning to what we today call Hamiltonian truncation. A few years later, the same model was considered in [71], with the model being quantized on the light-front (LF). LF quantization was pioneered by Weinberg in his seminal work [92] and it implied significant simplifications for theories quantized on such a surface. More specifically, the structure of the vacuum in this quantization is the same in both free and interacting theories, which

allows the construction of a Fock space using the free boson and fermion states, while in equal time quantization (ET) this is not possible immediately. This resulted in an unprecedented efficiency in the representation of field theories, and it was deemed to be warranting further investigation by the community. This laid the technical foundations for the family of discrete lightcone quantization (DLCQ) techniques, further extended in several works [88][47][38] to QED<sub>2</sub> and the  $\phi^4$  scalar field theory. Hamiltonian truncation has had some remarkable recent successes with the work of Rychkov and Eliás-Miro [37][36][76][77], where the method has been applied successfully to scalar field theories very general recipes have been devised to regulate energy truncated renormalizable theories with state dependent counterterms.

Incorporating lightcone quantization into numerical QFT methods was a significant step forward, as it provided knowledge on low energy excitations. However, early iterations of the method did not provide insight into the structure of theories around the so called fixed points. Fixed points (FPs) are, at a high level, regarded as fixed point solutions to the renormalization group flow of the theory under perturbation by one or more relevant local operators. They present with several interesting characteristics; they exhibit with long range order with power law decaying correlation functions and emergence of gapless modes in the spectrum. Studying the vicinity of an FP using the UV degrees of freedom is often a difficult endeavor; even in the earliest instances of numerically studying the classical Ising model using Monte Carlo simulations, the problem quickly becomes intractable around the critical point due to the fact that fluctuations become as big as the system itself and a local update algorithm takes exponentially long to approximate local field expectation values at a given temperature as we get closer and closer to the critical point. Fixed points, however, need not necessarily be described in terms of UV degrees of freedom: due to their scaling properties, they can oftentimes be recast as a conformal field theory. Qualitatively, knowledge of this CFT summarizes the most important RG scaling fields at the fixed point and their correlations, and allows to study the vicinity of the fixed point by using perturbations by relevant operators included in this CFT. Finding the scaling operator content of the theory is the most non-trivial part to this endeavor, but,

very fortunately, in 2 spacetime dimensions the scaling limits of many simple systems have been identified exactly, using the powerful Virasoro symmetry that these CFTs possess in work done by several pioneers of the field (Kac, Zamolodchikov, Yang etc.)

Numerical work in the field was very limited until the seminal work of Yurov and Zamolodchikov [90] [91] [56], where a new numerical method was developed for studying relevant deformations of CFTs. The essence of the method is that the starting Hilbert space of states of a CFT with known data is constructed by acting with primary operators and their descendants on the CFT vacuum up to a maximum scaling dimension  $\Delta_{\max}$ , so that the set of states obtained is finite. Subsequently, the perturbed Hamiltonian matrix elements are calculated in the UV CFT basis using the CFT data, and the resulting matrix is diagonalized for various values of the coupling. In the literature, this method is dubbed TCSA (truncated conformal space approach) or TFFSA (truncated free fermion space approach), depending on the UV theory perturbed. In TCSA the UV theory is usually a minimal model which has a finite number of primaries, while in TFFSA the starting point is the free massless fermion, which has an infinite family of primary operators. Otherwise, the two methods share similar fundamental principles of operation. The major success this truncation scheme achieved was the construction of the low energy spectrum of one parameter relevant operator perturbations of known CFTs to unprecedented accuracy. The method has found success in applications to integrable models resulting from such perturbations, where it is relatively simple to compare the low energy spectrum against predictions of integrability, but also in certain weakly coupled non-integrable models [65]. However, the method used ET quantized fields, which necessitated quantization on a circle of radius  $R$ , to control the divergence of the vacuum energy. This is a major drawback of the scheme, since both truncation and cutoff errors have to be controlled at the same time. At best, one has to hope that the truncation procedure has converged well enough before one considers the large volume limit, and this is exactly what happens when the model under consideration is integrable, and some of the symmetries of the UV theory are preserved. Lack of integrability however leads to slower convergence with increasing truncation size, which in turn leads to truncation artifacts at large

volumes. In a theory where little or no results are available for the spectrum, even if the TCSA results make sense at intermediate volumes, there is no concrete understanding of which value of the volume yields the best possible results at any given truncation; however it is clear that the best value increases as matrices are truncated at higher levels.

This work will be concerned with a specific framework called Lightcone Conformal Truncation, which was developed in a series of works [52][53][54]. This method draws elements from all the aforementioned nonperturbative CFT methods, but the major novelty that it brings to the table is the ability to simulate infinite volume interacting theories for all couplings, without depending on the Fock space formulation for a free boson/fermion. This change of basis, based on the underlying massless boson/fermion CFT, deals naturally with a lot of the issues of other lightcone quantization based methods while maintaining vacuum triviality, it offers excellent agreement with Feynman perturbation theory for weak coupling while maintaining reasonable phenomenology at strong coupling, which in turn allows the extraction of near critical observables in well-controlled theories. Finally, by taking full advantage of the conformal group structure in two dimensions, the framework features considerable computational speedups in computing the basis of states and its matrix elements with the Hamiltonian, leaving the diagonalization routine as the sole bottleneck of the computational problem.

In section 2, we will give a brief overview of the basic building blocks of LCT and we describe how each stage in the computation can be implemented, with a special focus on developing the tools necessary to simulate bosons in  $1+1$ -D with interactions that are polynomial in the fundamental field. More specifically, we describe the physics of lightcone quantized (LC) theories, while comparing to the intuition of the more conventional equal time (ET) quantization, then we describe how we can use conformal invariance to construct a new basis of states with appropriate quantum numbers for the free scalar, and we provide two different tools for computing overlaps between such states and Hamiltonian matrix elements. Finally, we give a short overview of spontaneous symmetry breaking in QFT, and how it can be probed in the context of

LCT. In section 3, we apply the method to an explicitly  $\mathbb{Z}_2$  broken  $\phi^4$  theory, probe its phase diagram and detect weakly coupled bound states. In section 4, we take on the most general  $\mathbb{Z}_2$  invariant sextic bosonic theory and we show that it exhibits similar breaking patterns. We match the weak coupling SSB predictions with our data, and we compute a quantitative estimate for the two-particle bound state that appears in the triple well potential, at criticality. We also verify theoretical predictions for the two- and three- particle bound states arising away from criticality, near the Gaussian fixed point. In section 5, we discuss our findings, propose future directions to be pursued, and conclude.

## 2 LCT and its ingredients

As discussed above, before LCT all attempts at putting QFT in 1+1-dimensions on a computer invariably require a double tuning between the volume and the truncation level. Even at finite volumes in ET quantization, the basis that needs to be considered is still infinite to obtain the full spectrum at that volume. It makes sense therefore that in the context of ET truncation methods, the limit of infinite truncation  $\Delta_{\max} \rightarrow \infty$  has to be taken before the limit of infinite volume  $L \rightarrow \infty$ , since simply taking the limit of infinite volume at finite truncation results in uncontrollable truncation artifacts. Ideally, the two limits would have to be taken together, keeping a parameter like  $\Delta_{\max}/F(ML)$  constant, for some empirically determined function of the volume  $F$ , and  $M$  a mass scale relevant to the theory. There is no universal answer to this question and to our knowledge, there is currently little theoretical understanding of the correct asymptotic combination of  $\Delta_{\max}, L$  to be taken, even for specific systems.

The biggest advantage of LCT is that it allows for the infinite volume limit to be taken first; LC quantization and starting from a known CFT are required to allow us to work directly with infinite volume wavefunctions. In more traditional Hamiltonian truncation approaches, it is technically difficult to work with infinite volume wavefunctions. For example, in approaches working with the Fock space of a free boson/fermion, like Tamm-Dancoff and DLCQ, working at infinite volume would prevent putting the theory on a computer, since there is an uncountable number of momentum modes below any energy cutoff  $E > 2m$ , with  $m$  the mass of the particle, while in TCSA quantizing the underlying CFT on a circle serves the purpose of regulating the vacuum energy divergent renormalization, so it can be represented in a finite matrix eigenvalue problem.

The method starts from an integrable CFT with known conformal dimensions and OPE coefficients (also known collectively as CFT data), quantized in lightcone coordinates. Lightcone quantization is particularly advantageous since it turns out that in order for the theory to have a well-defined energy and mass spectrum, the light-

cone momenta have to both be positive. More specifically, defining the lightcone coordinates and translation generators

$$\begin{aligned} x^\pm &= \frac{t \pm x}{\sqrt{2}} \\ P_\pm &= \frac{P_0 \pm P_1}{\sqrt{2}} \end{aligned} \tag{2.1}$$

we see that the invariant mass matrix of a lightcone quantized QFT in 1+1 dimensions can be written

$$M^2 = 2P_+P_- \tag{2.2}$$

For a QFT with well-defined spectrum, the Hamiltonian  $P_0$  should be bounded below and the mass matrix should be positive semidefinite (no tachyonic modes). We can always shift the energy by a constant to render it positive semidefinite as well, so we demand  $M^2, P_0 \geq 0$ . The generators  $P_+, P_-$  commute, so in a common basis of eigenvectors  $\{|n\rangle, P_\pm|n\rangle = \lambda_\pm|n\rangle\}$ , one can show that by the requirement above, all eigenvalues must satisfy simultaneously  $\lambda_+\lambda_- \geq 0$  and  $\lambda_+ + \lambda_- \geq 0$  and therefore, both LC momentum generators have to be positive semidefinite:

$$P_+, P_- \geq 0 \tag{2.3}$$

The above proof can be extended to arbitrary dimensions. The semidefiniteness of *both* generators has important consequences for LC quantized theories. The vacuum is defined as the state that satisfies simultaneously

$$P_+|0\rangle = P_-|0\rangle = 0 \tag{2.4}$$

We will consider "time" evolution here to be along slices of constant  $x^+$ , so that the LC Hamiltonian is given by  $H_{LC} \equiv P_+$ . With this convention,  $P_-$  is a kinematically defined generator with positive spectrum, while  $P_+$  contains all the dynamical information about the system. Unlike equal time quantization, where two single particle states can have opposite spatial momenta and can create a zero total momentum

state, in LC this is not possible, since particles can only have positive LC momentum. This is true irrespective of the form of the LC Hamiltonian and thus leads to the so called *non-renormalization of the vacuum*, which means that no interaction can possibly modify the state or eigenvalue of the vacuum, since higher momentum states cannot create a zero-momentum state that can mix with it, even when interactions are present.

One can then construct the interacting Fock space directly on the vacuum, by decomposing the (spin 0) field with an expression similar to regular quantization

$$\phi(x) = \int_0^\infty \frac{dp_-}{\sqrt{2p_-}} [a(x^+, p_-)e^{-ipx} + a^\dagger(x^+, p_-)e^{ipx}] \quad (2.5)$$

where the Fourier modes with negative momentum can be interpreted as antiparticles with positive momentum. The creation-annihilation operators satisfy the typical equal LC time commutation relation

$$[a(x^+, p_-), a^\dagger(x^+, q_-)] = 2\pi\delta(p_- - q_-) \quad (2.6)$$

The dependence of the Fock operators on time is non-trivial to accommodate interactions and specified by the dynamics of the problem and a full Fock space can be easily constructed. On one hand, building a Fock space on an interacting vacuum in ET, where the vacuum structure changes with the couplings, is intractable, since the structure of the vacuum is dynamically determined, and writing simple equations for their evolution is impossible. On the other hand, in the LC formalism it is possible to write integral equations that govern the wavefunctions assigned to each particle sector. More specifically, one can write any state in the interacting QFT as a sum

over Fock state wavefunctions<sup>1</sup>

$$|\Psi, P_-\rangle = \sum_{n=0}^{\infty} \int \prod_{i=1}^n \frac{dp_i}{(2\pi)\sqrt{2p_i}} (2\pi)\delta(p_1 + \dots + p_n - P_-) \psi_n(p_1, \dots, p_n) |p_1, \dots, p_n\rangle \quad (2.7)$$

where it is taken into consideration that the lightcone momentum  $P_-$  is a conserved quantity, so we work at a particular value of it. For Lagrangian theories that are perturbations of a free particle, whether fermion or boson, when one writes down polynomial interactions, these can only change the particle number (which is a conserved quantity in a free theory) by a few at most. Therefore it is possible to write an infinite set of coupled integral equations of finite length to solve the eigenproblem of the Hamiltonian. These coupled integral equations can be then truncated and solved [20][19][23][15], using an appropriate basis of functions for each of the  $n$ -particle wavefunctions. What's more, these wavefunctions require no finite volume or periodic boundary conditions to be realized. Such truncations of the Hilbert space, however, leave a lot to be desired when one attempts to reproduce more than just perturbative physics; it has been shown that nonperturbative phenomena like phase transitions can only be well represented when some information about very high particle sectors is included [19][21].

The LCT method proposes a different avenue of including the information coming from high particle sectors in the Hamiltonian, which relies on the fact that the free *massless* boson/fermion have conformal symmetry, circumventing several technical obstructions encountered in other methods. The simplicity of the scheme lies in the construction of an efficient basis for the free boson, that allows states of very high particle number to be included in the basis, while keeping the computational costs relatively low.

---

<sup>1</sup>This construction has been based on the assumption that the vacuum sector is trivial: there is a unique vacuum state that is the same as the non-interacting vacuum. While the construction of Fock states is rigorous for any type of interacting vacuum, it can be shown that the vacuum structure cannot always be trivial, or lightcone cannot reproduce non-perturbative effects such as symmetry breaking effects induced by interactions. Zero momentum modes can be found to be the culprit for this [89]. However, for free theories zero modes do not really pose an issue, as can be seen from canonical quantization (see zero mode discussion in a later chapter).

## 2.1 Free boson CFT and operator content

To take advantage of the conformal symmetry one needs to understand the irreps of the conformal group, which in  $d + 1$ -dimensions is isomorphic to  $O(d + 1, 2)/\mathbb{Z}_2$ . The analysis proceeds in a spirit similar to the analysis of irreps of other compact Lie groups. The group possesses a quadratic Casimir invariant, which can be used for classifying the irreps:

$$\mathcal{C} = D^2 + \frac{1}{2}(K^\mu P_\mu + P^\mu K_\mu) - L_{\mu\nu}L^{\mu\nu} \quad (2.8)$$

This operator can be diagonalized and its eigenvalues can be labeled by two quantum numbers given by

$$\mathcal{C} = \Delta(\Delta - d) + \ell(\ell + d - 2) \quad (2.9)$$

where  $\Delta$  is the conformal dimension of the primary operator, and  $\ell$  the spin. These quantum numbers are related to the holomorphic and antiholomorphic scaling dimensions of the operator in the corresponding Euclidean CFT. Once all the primary operators of the CFT have been determined, all other operators can be constructed as their descendants. All that remains is identifying a suitable basis for the Casimir operator eigenbasis. Due to the state-operator correspondence in CFTs it suffices to classify the operators, and then construct states by acting with those operators on the vacuum. For the free boson CFT in  $d = 1$  spatial dimension, there are several operator building blocks that merit closer examination. The naive scaling dimension of the bosonic scalar field is  $\Delta = 0$ , however, it is not possible to construct a primary operator in a unitary CFT with this scaling dimension, except the identity. The idea becomes intuitively clear when one considers the 2-point function of this operator. One can easily show that it is IR divergent at infinite volume:

$$D_{1/\epsilon}(x - y) \equiv \langle \phi(x)\phi(y) \rangle \sim -\frac{1}{2\pi} \ln \frac{|x - y|}{\epsilon} \quad (2.10)$$

where  $1/\epsilon$  is some IR mass scale required for the integration to converge. In a finite matrix computation, as one tunes the IR scale to zero, such operators are going to acquire infinite energy since the diagonal matrix elements will diverge and hence they are undesirable for building an appropriate basis. For the same reason, vertex operators, of the form,  $\mathcal{V}_a = e^{ia\phi}$  are also rejected, even though they can be shown to be truly primary in the continuum theory with conformal dimension  $\Delta_a = a^2/4\pi$ . The reason is that, similarly, their two point function is constructed from the two point function of the fundamental field:

$$\langle \mathcal{V}_a(x) \mathcal{V}_{-b}(y) \rangle = \delta_{ab} \exp(-a^2 D_{1/\epsilon}(x-y)) \sim \left( \frac{\epsilon}{|x-y|} \right)^{a^2/2\pi} \quad (2.11)$$

Even though the IR scale can be absorbed into a redefinition of the operator such that the two-point function is finite, the matrix elements of this operator with powers of  $\phi$  still depend on the IR scale, which means they will be lifted from the spectrum as well.

We need to use a building block that has a finite two point function and a well defined scaling dimension. The only candidate is the field  $\partial_- \phi$ , since the field  $\partial_+ \phi$  is constrained by the equations of motion and, as a result, it is non-dynamical in light-cone quantization. More specifically, LC is a singular quantization scheme, in the sense that when one quantizes the theory on worldlines of massless particles, right moving modes are explicitly determined by the motion of left moving modes; then right movers, since they don't have an equation of motion with a time derivative, they can be integrated out to give rise to an effective theory. In the free massless boson/fermion in 1+1-dimensions, this procedure of integrating out the right movers is especially simple; the Hamiltonian vanishes identically giving rise to a vanishing mass matrix, and furthermore the right and left movers decouple. As a result of the Dirac-Bergmann quantization algorithm, it can be shown that a consistent quantization can be achieved by setting either the right or the left moving components of the field to zero. This is equivalent to the quantization of an open bosonic string, where only half the modes survive quantization plus a zero mode corresponding to

the motion of the center of mass of the string. In this work we will be using only left movers so we set right moving modes to zero

$$\partial_+\phi = 0 \tag{2.12}$$

Since the fundamental field and vertex operators contain right moving components, they need to be discarded for quantization on the lightcone to be consistent.

We can create operators of arbitrary particle number by acting with multiple  $\partial_-\phi$  operators on the vacuum. Conformal dimension can be raised by taking minus derivatives on the basic building blocks, creating descendant operators. Multiplying these blocks on the same spacetime point and normal ordering them we can construct arbitrary dimension and particle number local operators. The most general operator of particle number  $n$  and conformal dimension  $\Delta \geq n$  can be constructed as linear combinations of the aforementioned operators, taking the form

$$\mathcal{O}_{n,\Delta}(x) = \sum_{\sum k_i = \Delta} C_{\mathbf{k}}^{\mathcal{O}} \partial_-^{k_1} \phi(x) \dots \partial_-^{k_n} \phi(x) \tag{2.13}$$

Clearly, this linear space has dimension exactly  $p_n(\Delta)$ , equal to the number ways one can partition the integer  $\Delta$  into exactly  $n$  parts. The problem is reduced to finding appropriate linear combinations that are orthogonal eigenstates of the Casimir invariant. One way to construct the basis is to write the action of the conformal Casimir on momentum space  $n$ -particle states (2.7). It takes the form

$$\mathcal{C} = -2 \sum_{j=1}^n \sum_{i=1}^{j-1} p_i p_j \left( \frac{\partial}{\partial p_i} - \frac{\partial}{\partial p_j} \right)^2 \tag{2.14}$$

We seek solutions to the eigenproblem  $\mathcal{C}\psi(p_1, \dots, p_n) = \lambda\psi(p_1, \dots, p_n)$ . Solving the problem for the lowest possible sectors, we notice that a general solution can be written for the amplitudes of the Casimir eigenstates of any particle number in terms

of Jacobi polynomials:

$$\psi_\ell(p_1, \dots, p_n) = p_1 \dots p_n |p_n|^{\ell_n} \prod_{i=1}^{n-1} |p|_{i+1}^{\ell_i} P_{\ell_i}^{(2|\ell_{i-1}+2i-1, 1)} \left( \frac{|p|_{i+1} - |p|_i}{|p|_{i+1}} \right) \quad (2.15)$$

where we defined the shorthand  $|p|_k \equiv \sum_{i=1}^k p_i$ . These states can be reduced to primary operators by taking  $\ell_n = 0$ . All the other quantum numbers are allowed to be any positive integer. The conformal dimension of the primaries constructed by those amplitudes is  $|\ell|_{n-1} + n$ , so it seems like there are as many primaries as monomials. However, it turns out that this eigenbasis is overcomplete; certain elements are linearly dependent on others, or exactly zero. This is due to the fact that this basis assumes that the quantum particles are distinguishable, therefore one needs to symmetrize in order to obtain the requisite CFT states.

For example, in the two particle sectors, the generating amplitude can be expressed in terms of a single Jacobi polynomial, labeled by one parameter:

$$\psi_\ell^{(2)}(p_1, p_2) = p_1 p_2 (p_1 + p_2)^\ell P_\ell^{(1,1)} \left( \frac{p_2 - p_1}{p_2 + p_1} \right) \quad (2.16)$$

Substituting  $p_i^k \rightarrow \partial_-^k \phi$  where  $\phi$  is a bosonic operator (commutes with other boson operators), naturally symmetrizes the polynomials in the momentum variables. Expanding the Jacobi polynomials explicitly and simplifying immediately shows that all polynomials with odd spin are trivial:  $\psi_{2m+1}^{(2)}(p_1, p_2) = 0$ . Every even spin solution yields a primary operator after symmetrization, for example

$$\begin{aligned} \psi_0^{(2)}(p_1, p_2) &\rightarrow (\partial\phi)^2 \\ \psi_2^{(2)}(p_1, p_2) &\rightarrow 6\partial^3\phi\partial\phi - 9(\partial^2\phi)^2 \\ \psi_4^{(2)}(p_1, p_2) &\rightarrow \partial^4\phi(\partial\phi)^2 - 10\partial^3\phi(\partial\phi)^3 + 10(\partial^2\phi)^2(\partial\phi)^2 \\ &\dots \end{aligned} \quad (2.17)$$

Here we dropped the minus from all derivative operators to reduce clutter. The same

process can be repeated for higher particle sectors to yield candidate primaries, and subsequently, when there are multiple operators with the same particle number and dimension, the Gram-Schmidt process must be used to orthonormalize the states with respect to the Fock inner product.

This process of constructing the basis operators is the most intuitive, but not the most expedient. In fact, thanks to a method by Penedones [73], we have a way of constructing these operators recursively, much more efficiently than what's achievable with the Fock basis. First, we define the double trace operation between two operators  $A, B$  with corresponding scaling dimensions  $\Delta_A, \Delta_B$ :

$$[AB]_\ell = \sum_{m=0}^{\ell} (-1)^m \binom{2\Delta_A + \ell - 1}{\ell - m} \binom{2\Delta_B + \ell - 1}{m} \partial^m A \partial^{\ell-m} B \quad (2.18)$$

For  $\ell \geq 0$ , this operation outputs an operator of scaling dimension  $\Delta_A + \Delta_B + \ell$ , by increasing its conformal spin by  $\ell$  units. It can be shown that this operator satisfies  $K_\mu [AB]_\ell = 0$  and is hence primary. For a free massless boson, it is simple to show that  $\partial\phi$  is a primary of dimension  $\Delta = 1$ , and from (2.15) it is the only single particle primary that can be constructed out of the fundamental field. This recipe can then be used recursively to find all primaries with scaling dimension less than a cutoff  $\Delta \leq \Delta_{\max}$ . Starting with the single particle primary, we can successively produce operators with higher dimensions by just sowing additional  $\partial\phi$ 's to all the operators that have been produced at each step and we are guaranteed to generate all possible primaries through this process.

If applied blindly, this sequence of operations will also generate an overcomplete basis; many operators will be linear combinations of others or zero. Fortunately there is a way to construct a complete basis, which we will outline here (readers seeking a more detailed treatment can refer to [1]). More specifically, one can construct all operators with particle number and conformal dimension  $(n, \Delta)$  from operators with one less particle with particle dimensions  $(n-1, \Delta' = \Delta - jn - 1)$ ,  $0 \leq j \leq \lfloor \Delta/n - 1 \rfloor$ . Denoting  $\mathcal{S}_{n,\Delta}$  the set of all non-trivial primaries of particle number and conformal

dimension  $(n, \Delta)$ , the elements of this set by  $\mathcal{O}_{n,\Delta}^k$  and its size  $N(n, \Delta)$ , the following recursive equation holds:

$$\mathcal{S}_{n,\Delta} = \bigcup_{j=0}^{\lfloor \Delta/n+1 \rfloor} \bigcup_{k=0}^{N(n-1,\Delta-jn-1)} [\mathcal{O}_{n-1,\Delta-jn-1}^k \partial\phi]_{jn} \quad (2.19)$$

and the recursion for the number of operators at any given level should satisfy

$$N(n, \Delta) = \sum_{j=0}^{\lfloor \Delta/n \rfloor} N(n-1, \Delta - jn - 1) \quad (2.20)$$

It was mentioned previously that the linear space spanned by monomial operators  $\partial^{k_1}\phi \dots \partial^{k_n}\phi$  at level  $(n, \Delta)$  has dimension  $p_n(\Delta)$ , equal to the ways of writing  $\Delta$  as a sum of  $n$  distinct integers. This function satisfies the same recursion (2.20) as  $N(n, \Delta)$ , but the boundary conditions are different. Since  $\partial\phi$  is the only single particle *primary* field, we assert that the count of primary fields must satisfy  $N(1, \Delta) = \delta_{\Delta,1}$ , in contrast to the boundary condition obeyed by the count of monomials  $p_1(\Delta) = 1$ . It is, however, easy to verify that there is an explicit solution in terms of integer partitions, given by

$$N(n, \Delta) = p_n(\Delta) - p_n(\Delta - 1) \quad (2.21)$$

This recursive structure is easily implementable on a computer and can be truncated at any order desired.

## 2.2 Constructing CFT states

Now, we are ready to construct the CFT states. Since the momentum  $P_-$  is conserved kinematically, we can diagonalize it immediately by working in momentum space, and simplify the calculations. More specifically, we will work with Fourier space operators acting on the LC vacuum:

$$|\mathcal{O}, p\rangle = \int dx_- e^{-ipx_-} \mathcal{O}(x_-)|0\rangle \quad (2.22)$$

We have only considered operators with spin  $\ell = \Delta$ , which for the Euclidean space free boson can be seen to be holomorphic operators. As such, after a Wick rotation, we see that these operators and their correlation functions only depend on the  $x_-$  coordinate. These are the only operators that are non-trivial for a free boson in LC quantization, since antiholomorphic operators/left movers form a separate Hilbert space, which is not appropriate for quantization on the  $x_+ = \text{const}$  surfaces. Henceforth, we will drop the subscripts, since the structure of the equations should be obvious from now on. Typically, in CFT applications the operators are orthonormalized against the momentum space 2-point function such that

$$\langle \mathcal{O}_i(x) \mathcal{O}_j(0) \rangle = \frac{\delta_{\Delta_i \Delta_j}}{x^{2\Delta_i}} \quad (2.23)$$

Our choice will be to make the Fourier transforms orthonormal, by imposing the orthogonality condition

$$\langle \mathcal{O}_i, p | \mathcal{O}_j, p' \rangle = 2\pi(2p)\delta(p - p')\delta_{ij} \quad (2.24)$$

However one can directly compute this overlap from the two-point function, using translational invariance

$$\langle \mathcal{O}_i, p | \mathcal{O}_j, p' \rangle = 2\pi(2p)\delta(p - p') \underbrace{\left[ \frac{1}{2p} \int_{-\infty}^{\infty} e^{ipx} \langle \mathcal{O}_i(x) \mathcal{O}_j(0) \rangle dx \right]}_{G_{ij}} \quad (2.25)$$

The quantity in brackets is called the Gram matrix of the basis chosen, and it is generally a non-diagonal hermitian matrix. To generate an orthonormal basis, one has to perform a Gram-Schmidt decomposition on this matrix. Due to the structure of this particular problem, operators with different particle numbers have no overlap, and due to primaryity, operators with conformal dimensions are also orthogonal by construction; hence the orthogonalization procedure can be done separately for all levels  $(n, \Delta)$ . The Gram matrix in free theory can be computed in various ways, Wick contractions being the most intuitive way. In fact, the two point functions between two operators of the same level are the only ones that are non-zero and they can be written in a simple form:

$$\langle O_{n,\Delta}^j(x) O_{n,\Delta}^k(0) \rangle = \frac{A_{jk}}{x^{2\Delta}} \quad (2.26)$$

The integral over momenta can therefore be done easily with an appropriate regularization; it is easy to see that

$$\int dx \frac{e^{ipx}}{(x - i\epsilon)^{2\Delta}} = 2\pi \frac{p^{2\Delta}}{\Gamma(2\Delta - 1)} \quad (2.27)$$

The number  $A_{jk}$  is a number depending on combinatorics and monomial coefficients only. It can be computed brute-force by simply writing the expressions for the operator basis obtained as, for example, in equation (2.17) and laboriously computing Wick contractions for all the operators involved. We will delve into efficient routines for computing free boson correlation functions in more detail shortly, but for the next chapter we will assume a fully orthonormal basis is available.

## 2.3 Computing Hamiltonian matrix elements

Now that a full basis of the free massless boson CFT has been constructed, we proceed to include self-interactions in the Hamiltonian and other conformal generators, so that the conformal algebra is preserved. This can be done consistently at least for local, Poincaré invariant Hamiltonian interactions of the form

$$P_{+, \text{int}} = \lambda \int \mathcal{O}_R(x_-) dx_- \quad (2.28)$$

where  $\mathcal{O}_R$  is a relevant operator. It is convenient if this operator is also primary, due to the fact that the correlations functions including it can be solved entirely in terms of known CFT data. In two dimensions, monomial operators of the form  $\phi^n$  are classically relevant and operators of the form  $\phi^n (\partial\phi)^2$  are marginal. We will not consider operators with derivatives in this work, and hence we will write Hamiltonians of the form

$$P_+ \equiv H_{LC} = \int dx_- \sum_{n>1} \frac{\lambda_n}{n!} \phi^n \quad (2.29)$$

However, as discussed before, the fundamental field itself is a composite operator in the free boson CFT, and hence it requires a more careful treatment in a CFT computation. This is just a technicality however, and it doesn't affect the discussion that follows.

We wish to understand the spectrum of the interacting theory, especially the low energy sector and the bound states, which in non-integrable models are usually in the low energy sector themselves. In order to extract the masses of these excitations, we can diagonalize the invariant mass operator, given by

$$M^2 = 2P_+P_- \quad (2.30)$$

in the CFT basis. Clearly, since the CFT basis we constructed is diagonal in  $P_-$ ,

matrix elements of the invariant mass will have the following general form

$$\langle \mathcal{O}, p_- | M^2 | \mathcal{O}', p'_- \rangle = 2\pi(2p_-)\delta(p_- - p'_-)\mathcal{M}_{\mathcal{O}\mathcal{O}'} \quad (2.31)$$

where the amplitude  $\mathcal{M}$  is related to the three-point function of the perturbing sandwiched by operators in our basis:

$$\mathcal{M}_{\mathcal{O}\mathcal{O}'} = \lambda \int dx dy e^{ip(x-y)} \langle \mathcal{O}(x)\mathcal{O}_R(0)\mathcal{O}'(y) \rangle \quad (2.32)$$

Again, if the perturbing operator is primary, the correlation function can be determined almost entirely by conformal symmetry

$$\langle \mathcal{O}_1(x)\mathcal{O}_2(y)\mathcal{O}_3(z) \rangle = \frac{C_{123}}{(x-y)^{\Delta_1+\Delta_2-\Delta_3}(y-z)^{\Delta_2+\Delta_3-\Delta_1}(z-x)^{\Delta_3+\Delta_1-\Delta_2}} \quad (2.33)$$

The coefficient  $C_{123}$  is called an OPE coefficient and determined dynamically. Once more, the 2-dimensional Fourier integral (properly regularized) can be done exactly via the formula

$$\int_{-\infty}^{\infty} \int_{-\infty}^{\infty} \frac{e^{ipx}}{x^A z^B (x-z)^C} dx dz = \frac{4\pi^2 \Gamma(A+B-1) p^{A+B+C-2}}{\Gamma(A)\Gamma(B)\Gamma(A+B+C-1)} \quad (2.34)$$

For a CFT with a known list of operator dimensions and OPE coefficients, the matrix elements are extremely simple to compute. In practice, such a list is available only in the case of very simple CFTs like the minimal models. Even for the free boson and the free fermion, that are under complete analytical control, OPE coefficients of primaries can only be constructed recursively; no analytic formula has been found thus far.

There are multiple ways of computing the aforementioned two- and three-point functions in a free theory, since one has complete analytical control over various tools, like the spectrum, the path integral, the propagators, etc. However, for the purpose of computing an increasing in size hierarchy of such expectation values efficiently, we

need algorithmic techniques that lend themselves to automated and fast implementation on a computer.

Historically, there have been three main approaches to computing overlaps and matrix elements. The first is a Fock space technique, which relies on the representation (2.7) for the primary operators. The technique reduces to computing simple integrals over symmetric polynomials of the momenta (there are as many as the particle number of the state). We will not get into details of this technique, since it is relatively inefficient for computations.

### 2.3.1 Wick contractions

The most versatile technique of matrix element computation is Wick contractions. The free boson is a CFT with a quadratic Lagrangian, and therefore Wick's theorem holds. In a few words, Wick's theorem essentially states that cumulants of any order  $n$  ( $n$ -point correlation functions) of a multivariate normal random variable (quadratic field Lagrangian) can be computed directly from the second moments (two-point correlation functions). Typically, one rescales the field so that the linear terms in the Lagrangian disappear, and this also makes all odd-point functions vanish. All other  $2n$ -point functions can be contracted by choosing all possible pairings of normal-ordered operators, and computing their 2-point functions. In the example below, we calculate a 4-point function of four normal ordered fields in terms of the field propagators:

$$\begin{aligned} \langle \phi_1(x)\phi_2(y)\phi_3(z)\phi_4(w) \rangle &= \langle \phi_1(x)\phi_2(y) \rangle \langle \phi_3(z)\phi_4(w) \rangle + \langle \phi_1(x)\phi_3(z) \rangle \langle \phi_2(y)\phi_4(w) \rangle + \\ &+ \langle \phi_1(x)\phi_4(w) \rangle \langle \phi_2(y)\phi_3(z) \rangle \end{aligned} \tag{2.35}$$

Higher point functions can be computed similarly. We apply this fundamental result to our problem at hand. The basic building blocks that we have to compute are two-point functions of arbitrary monomials of the same particle number, and three

point functions of those monomials with the perturbing operator as well. Typically, the perturbing operator can change the particle number, so which particle numbers contribute to the matrix elements will be important for the discussion below. One can use Wick contractions, for example to compute the Gram matrix. This can be done by computing the two-point function for  $n$ -particle monomial building blocks. To reduce clutter in the result we will often define multiindices  $\mathbf{k} = \{k_1, \dots, k_n\}$  and a shorthand for monomial operators  $\partial^{\mathbf{k}}\phi = \partial^{k_1}\phi \dots \partial^{k_n}\phi$ . The two-point function looks like the following:

$$\langle \partial^{k_1}\phi(x) \dots \partial^{k_n}\phi(x) \partial^{k'_1}\phi(y) \dots \partial^{k'_n}\phi(y) \rangle = \frac{A_{\mathbf{k}\mathbf{k}'}}{(4\pi)^n (x-y)^{\Delta+\Delta'}} \quad (2.36)$$

Here, the numerator is the Wick contraction coefficient, which keeps track of possible pairings of operators but also factors coming from two-point functions of arbitrarily high dimension descendants of the fundamental field. It is given by the formal expression

$$A_{\mathbf{k}\mathbf{k}'} = \sum_{\sigma(\mathbf{k},\mathbf{k}')} \prod_{i,j} \Gamma(k_i + k'_j) \quad (2.37)$$

The sum runs over all the  $(2n)!/2^n n!$  distinct pairings of the two sets. Any  $n$ -particle primary at level  $(n, \Delta)$  can be written in terms of monomials as

$$\mathcal{O}_{n,\Delta}(x) = \sum_{\mathbf{k}} C_{\mathbf{k}}^{\mathcal{O}} \partial^{\mathbf{k}}\phi(x) \quad (2.38)$$

With this expression, for primaries at the same level in our basis, one can explicitly compute the non-zero Gram matrix entries to be

$$G_{\mathcal{O}_i \mathcal{O}_j} = \frac{p^{2\Delta-1}}{4^n \pi^{n-1} \Gamma(2\Delta-1)} \sum_{\mathbf{k}\mathbf{k}'} C_{\mathbf{k}}^{\mathcal{O}_i} C_{\mathbf{k}'}^{\mathcal{O}_j} A_{\mathbf{k}\mathbf{k}'} \quad (2.39)$$

Wick contractions can also be applied to the calculation of matrix elements (2.32). In this work we will be interested in self-interactions of the form (2.29), with  $n \leq 6$ . These operators are not primary, which means that their correlation functions do not

take on the simple form (2.33). Despite this minor inconvenience, Wick's theorem holds true for all operators composed of powers and derivatives of the fundamental field. Even though, the two-point function of the fundamental field contains an IR divergence, its two-point functions with its descendants has the right decay properties at long distances and is IR finite:

$$\langle \phi(x) \partial^\ell \phi(y) \rangle = -\frac{1}{4\pi} \frac{(\ell-1)!}{(x-y)^\ell} \quad (2.40)$$

We will present Wick contraction based computations of the matrix elements of monomials in our basis with the operators  $\mathcal{O}_R = \phi^2, \phi^3, \phi^4, \phi^6$ . Let us start with the simplest one, the mass term. In LC quantization, the mass term conserves particle number, due to the positivity of lightcone momenta; the integral over  $x_-$  forces the LC momenta of the two-particle creation or annihilation operators to sum to zero, which means that the only way for this operator to produce particles is if they are zero momentum modes (whose contributions we ignore in this method). Hence, there is only one type of matrix element that we need to compute, in the form

$$\langle \partial^{\mathbf{k}} \phi, P | \int dy \frac{m^2}{2} \phi^2(y) | \partial^{\mathbf{k}'} \phi, P' \rangle = \frac{m^2}{2} \int dx dy dz e^{i(Px-P'z)} \langle \partial^{\mathbf{k}} \phi(x) \phi^2(y) \partial^{\mathbf{k}'} \phi(z) \rangle \quad (2.41)$$

where  $\mathbf{k}, \mathbf{k}'$  are multiindices as defined above, of length  $n$ , with total dimension  $|\mathbf{k}| = \Delta, |\mathbf{k}'| = \Delta'$ . All other matrix elements vanish for this interaction. To compute the non-zero ones, we take one fundamental field from the left and one from the right, contract them with  $\phi^2(y)$ , and then contract the remaining  $(n-1)$ -particle monomials with each other. This is equivalent to writing

$$\langle \partial^{\mathbf{k}} \phi(x) \phi^2(y) \partial^{\mathbf{k}'} \phi(z) \rangle = \sum_{i,j} \langle \partial^{k_i} \phi(x) \phi^2(y) \partial^{k'_j} \phi(z) \rangle \langle \partial^{\mathbf{k} \setminus k_i} \phi(x) \partial^{\mathbf{k}' \setminus k'_j} \phi(z) \rangle \quad (2.42)$$

The second term in the summand is computed in (2.36), while the first term is simply

$$\langle \partial^{k_i} \phi(x) \phi^2(y) \partial^{k'_j} \phi(z) \rangle = \frac{2}{(4\pi)^2} \frac{\Gamma(k_i) \Gamma(k'_j)}{(x-y)^{k_i} (y-z)^{k'_j}} \quad (2.43)$$

The final result, after doing the configuration space integrals and factoring out the usual momentum-conserving delta function, the monomial mass matrix connecting  $n \rightarrow n$  operators reads

$$\mathcal{M}_{\mathbf{k}\mathbf{k}'}^{\phi^2(n \rightarrow n)} = m^2 \frac{P^{\Delta+\Delta'-2}}{4^n \pi^{n-1} \Gamma(\Delta + \Delta' - 1)} \sum_{ij} \Gamma(k_i + k'_j - 1) A_{\mathbf{k} \setminus k_i, \mathbf{k}' \setminus k'_j} \quad (2.44)$$

The  $\phi^3$  matrix elements present no additional difficulty: the only non-zero matrix elements are those that connect  $n \rightarrow n + 1$  particles. The result of the computation yields:

$$\mathcal{M}_{\mathbf{k}\mathbf{k}'}^{\phi^3(n \rightarrow n+1)} = \lambda_3 \frac{P^{\Delta+\Delta'-2}}{4^{n+1} \pi^n \Gamma(\Delta + \Delta' - 1)} \sum_{i,j>\ell} \frac{\Gamma(k_i + k'_j + k'_\ell - 1) \Gamma(k'_j) \Gamma(k'_\ell)}{\Gamma(k'_j + k'_\ell)} A_{\mathbf{k} \setminus k_i, \mathbf{k}' \setminus k'_j k'_\ell} \quad (2.45)$$

Higher order powers of the field yield increasingly many types of matrix elements that have to be taken into account. More concretely, a  $\phi^N$  interaction will give rise to  $\lfloor N/2 \rfloor$  different types of matrix elements, connecting particle sectors  $n \rightarrow n + N - 2m$  with  $1 \leq m \leq \lfloor N/2 \rfloor$ . These computations are simple to perform, albeit tedious, so we just state the results here for  $\phi^4, \phi^6$ :

$$\begin{aligned} \mathcal{M}_{\mathbf{k}\mathbf{k}'}^{\phi^4(n \rightarrow n)} &= \frac{\lambda_4}{4\pi} \mathcal{N}_{\mathbf{k}\mathbf{k}'} \sum_{i>j,\ell>m} \frac{\Gamma(k_i + k_j + k'_\ell + k'_m - 1) \Gamma(k_i) \Gamma(k_j) \Gamma(k'_m) \Gamma(k'_\ell)}{\Gamma(k'_m + k'_\ell) \Gamma(k_i + k_j)} A_{\mathbf{k} \setminus k_i k_j, \mathbf{k}' \setminus k'_\ell k'_m} \\ \mathcal{M}_{\mathbf{k}\mathbf{k}'}^{\phi^4(n \rightarrow n+2)} &= \frac{\lambda_4}{(4\pi)^2} \mathcal{N}_{\mathbf{k}\mathbf{k}'} \sum_{i,j>\ell>m} \frac{\Gamma(k_i + k'_j + k'_\ell + k'_m - 1) \Gamma(k'_j) \Gamma(k'_m) \Gamma(k'_\ell)}{\Gamma(k'_m + k'_\ell + k'_j)} A_{\mathbf{k} \setminus k_i k_j, \mathbf{k}' \setminus k'_j k'_\ell k'_m} \end{aligned} \quad (2.46)$$

$$\begin{aligned} \mathcal{M}_{\mathbf{k}\mathbf{k}'}^{\phi^6(n \rightarrow n)} &= \frac{\lambda_6}{(4\pi)^2} \mathcal{N}_{\mathbf{k}\mathbf{k}'} \sum_{\substack{i>j>\ell \\ m>n>r}} \Pi_0(k_{ij\ell}, k'_{mnr}) A_{\mathbf{k} \setminus k_{ij\ell}, \mathbf{k}' \setminus k'_{mnr}} \\ \mathcal{M}_{\mathbf{k}\mathbf{k}'}^{\phi^6(n \rightarrow n+2)} &= \frac{\lambda_6}{(4\pi)^3} \mathcal{N}_{\mathbf{k}\mathbf{k}'} \sum_{\substack{i>j \\ \ell>m>n>r}} \Pi_2(k_{ij}, k'_{\ell mnr}) A_{\mathbf{k} \setminus k_{ij}, \mathbf{k}' \setminus k'_{\ell mnr}} \\ \mathcal{M}_{\mathbf{k}\mathbf{k}'}^{\phi^6(n \rightarrow n+4)} &= \frac{\lambda_6}{(4\pi)^4} \mathcal{N}_{\mathbf{k}\mathbf{k}'} \sum_{\substack{i \\ j>\ell>m>n>r}} \Pi_4(k_i, k'_{j\ell mnr}) A_{\mathbf{k} \setminus k_i, \mathbf{k}' \setminus k'_{j\ell mnr}} \end{aligned} \quad (2.47)$$

where we have used the shorthand definitions:

$$\begin{aligned}
\Pi_0(k_{ij\ell}, k'_{mnr}) &= \frac{\Gamma(k_i + k_j + k_\ell + k'_r + k'_m + k'_n - 1)\Gamma(k_i)\Gamma(k_j)\Gamma(k_\ell)\Gamma(k'_m)\Gamma(k'_n)\Gamma(k'_r)}{\Gamma(k'_m + k'_n + k'_r)\Gamma(k_i + k_j + k_\ell)} \\
\Pi_2(k_{ij}, k'_{\ell mnr}) &= \frac{\Gamma(k_i + k_j + k'_\ell + k'_r + k'_m + k'_n - 1)\Gamma(k_i)\Gamma(k_j)\Gamma(k'_\ell)\Gamma(k'_m)\Gamma(k'_n)\Gamma(k'_r)}{\Gamma(k'_\ell + k'_m + k'_n + k'_r)\Gamma(k_i + k_j)} \\
\Pi_4(k_i, k'_{j\ell mnr}) &= \frac{\Gamma(k_i + k'_j + k'_\ell + k'_r + k'_m + k'_n - 1)\Gamma(k'_j)\Gamma(k'_\ell)\Gamma(k'_m)\Gamma(k'_n)\Gamma(k'_r)}{\Gamma(k'_j + k'_\ell + k'_m + k'_n + k'_r)}
\end{aligned} \tag{2.48}$$

$$\mathcal{N}_{\mathbf{k}\mathbf{k}'} = \frac{p^{\Delta+\Delta'-2}}{4(4\pi)^{n-1}\Gamma(\Delta + \Delta' - 1)} \tag{2.49}$$

With these results we can compute matrix elements for any Hamiltonian used in this work.

### 2.3.2 Radial quantization

The method of Wick contractions is very general and simple to implement computationally, but it does not make any use of the fact that the bosonic free theory is a CFT. For example, one of the consequences of this fact, it is observed that in the basis of monomial operators, it is not clear why operators of the same particle number and different scaling dimension should be orthogonal to each other. From this point of view, a massive cancellation of terms must occur to accommodate this- however from the point of view of the conformal basis, this fact is trivial. In this section we will briefly discuss using radial quantization to use as much information about the CFT as possible, while gaining efficiency and performing no redundant calculations. As a matter of fact, the use of radial quantization has allowed us to efficiently generate significantly larger Hamiltonians up to  $\Delta_{\max} \simeq 45$ , whereas with Wick contraction based algorithms, the computation times became difficult to handle past  $\Delta_{\max} \simeq 34$ .

In Euclidean space in 2 dimensions, we can use conformal symmetry to map the flat metric to any other metric related to it by a conformal mapping, given by a change

of coordinates  $z' = f(z)$ , where  $f$  is an arbitrary function. This technique is very powerful in the classical setting, since it allows solutions to the Laplace equation (the euclidean equivalent of the wave equation) to be produced by just knowing its solution for a simple choice of boundary, such as a circle, and mapping it to other boundary shapes using specific conformal transformations. It is also very powerful in the quantum setting: in two dimensions, any choice of conformal mapping is a Weyl transformation. Conformally invariant theories are especially well behaved against such transformations; it is a simple matter to construct correlation functions on the space produced by a conformal mapping. Radial quantization is a specific choice of coordinate transformation that shows that a CFT quantized on  $\mathbb{R} \times S^1$  is<sup>2</sup> equivalent to a theory quantized on  $\mathbb{R}^2$ . To wit, the Euclidean cylinder metric is locally flat, and performing the change of coordinates  $t = \ln r$  the metric becomes

$$ds^2 = dt^2 + dx^2 = r^{-2}(dr^2 + r^2 dx^2) \quad (2.50)$$

The metric in the new coordinates is conformally equivalent to a planar geometry expressed in spherical coordinates. This can also be written in complex coordinates  $z = re^{ix}$  as

$$ds^2 = \frac{dzd\bar{z}}{z\bar{z}} \quad (2.51)$$

This reparametrization is very powerful, since it can turn many problems in 2-D CFT into ones of complex analysis of one variable, where very powerful tools are available. A technical subtlety here is that  $z, \bar{z}$  have to be considered as independent variables, unrelated by complex conjugation for certain applications, but the upshot is that the structure of the Virasoro algebra in two dimensions allows for a clean factorization of the  $z, \bar{z}$  dependences. We will mostly be concerned with holomorphic fields  $\varphi(z)$ .

One question that arises, is how can one express correlation functions given two spaces that are conformally equivalent. By definition, operators with conformal dimension

---

<sup>2</sup>Here space has been compactified to form a cylinder with circumference  $2\pi$ ;  $x \sim x + 2\pi$ .

and spin  $\Delta, s$  on some space  $S_1$  behave as follows under a conformal transformation:

$$\mathcal{O}^{(S_1)}(z(w), \bar{z}(\bar{w})) = \left(\frac{dz}{dw}\right)^h \left(\frac{d\bar{z}}{d\bar{w}}\right)^{\bar{h}} \mathcal{O}^{(S_1)}(z, \bar{z}) \quad (2.52)$$

where  $2h = \Delta + s$ ,  $2\bar{h} = \Delta - s$ . Correlation functions behave similarly, as dictated by the Weyl transform

$$\langle \mathcal{O}^{(S_1)}(z(w), \bar{z}(\bar{w})) \dots \rangle = \left(\frac{dz}{dw}\right)^h \left(\frac{d\bar{z}}{d\bar{w}}\right)^{\bar{h}} \langle \mathcal{O}^{(S_1)}(z, \bar{z}) \dots \rangle \quad (2.53)$$

The correlation functions as defined above do not possess the simple form (2.26) for arbitrary conformal transformations. To maintain their scale invariant form, we define native operators on the target space  $S_2$  defined by the mapping  $S_1 \rightarrow S_2 : z = f(w)$

$$\mathcal{O}^{(S_2)}(z, \bar{z}) = \left(\frac{dw}{dz}\right)^h \left(\frac{d\bar{w}}{d\bar{z}}\right)^{\bar{h}} \mathcal{O}^{(S_1)}(z(w), \bar{z}(\bar{w})) \quad (2.54)$$

The factor in front is the inverse of the Weyl factor. For example, for the free boson theory in radial quantization, a fundamental field  $\phi(z, \bar{z})$  can be constructed that satisfies the equations of motion  $\partial_z \partial_{\bar{z}} \phi = 0$ :

$$\phi(z, \bar{z}) = \phi_0 - \frac{i\pi_0}{4\pi} \ln(z\bar{z}) + \frac{i}{\sqrt{4\pi}} \sum_{n>0} \frac{1}{\sqrt{n}} (a_n^\dagger z^{-n} + a_n z^n + \bar{a}_n^\dagger \bar{z}^{-n} + \bar{a}_n \bar{z}^n) \quad (2.55)$$

The unbarred/barred creation operators of non-zero momentum create a left/right moving particle of momentum  $n$  and obey the usual bosonic commutation relations. The operators  $\phi_0, \pi_0$  correspond to a zero momentum mode, which corresponds to the motion of the center of mass of the configuration. The two point function of this field does not obey the form (2.26), showing that the field cannot be primary:

$$\langle \phi(z, \bar{z}) \phi(w, \bar{w}) \rangle = \frac{1}{4\pi} (\ln(z-w) + \ln(\bar{z}-\bar{w})) \quad (2.56)$$

However, it is easy to show by virtue of (2.56) that the holomorphic/left-moving field

$\partial_z\phi(z, \bar{z}) \equiv \partial\phi(z)$  two point function has the correct scaling for a field of dimension and spin  $\Delta = 1, s = 0$ :

$$\langle \partial\phi(z)\partial\phi(w) \rangle = -\frac{1}{4\pi(z-w)^2} \quad (2.57)$$

This field is the Wick rotated equivalent of the left-moving Minkowski field  $\partial_-\phi$  that we are going to use as a building block for our calculations. The zero mode of the free boson doesn't contribute to correlation functions of fields that are good representations of the conformal algebra, and although in an interacting LC quantized theory it can give rise to dynamically constrained zero-modes of the field, it is consistent within the framework of LCT to ignore it for any subsequent computations. The form of building block  $\partial\phi(z)$  in radial quantization that we will use is:

$$\begin{aligned} \partial\phi(z) &= \frac{i}{\sqrt{4\pi}} \sum_{n=1}^{\infty} \sqrt{n} (a_n z^{-n-1} + a_n^\dagger z^{n-1}) \\ [a_k, a_{k'}^\dagger] &= \delta_{kk'} \end{aligned} \quad (2.58)$$

However, the biggest simplifications to the calculations of overlaps and matrix elements do not come from just reparametrizing the coordinates. Radial quantization is a special quantization scheme for conformal theory conceptually and quantitatively, since it highlights the most important features of the theory, while permitting the construction of a natural positive definite measure on the states of any CFT.

We start by noting that a time translation on the cylinder  $t \rightarrow t + a$  is mapped on to a dilation on the radially foliated plane  $r \rightarrow e^a r$ . Therefore, it is intuitive to demand that to reproduce CFT on the cylinder, one needs to consider evolution along concentric spheres on the plane, since equal time slices on the cylinder are mapped onto these concentric spheres. Radial quantization maps the infinite past to  $r = 0$  and the infinite future to  $r = \infty$ , while the infinitesimal generator that is equivalent to moving along time slices is the dilatation operator  $D = r\partial_r$ . Operators inserted at the origin with well defined scaling properties obey the following commutation

relation

$$[D, \mathcal{O}_\Delta(0)] = i\Delta \mathcal{O}_\Delta(0) \quad (2.59)$$

As a result, in a theory with a well-defined vacuum that satisfies  $D|0\rangle = 0$ , the states  $|\Delta\rangle = \mathcal{O}_\Delta(0)|0\rangle$  diagonalize the dilatation operator:

$$D|\Delta\rangle = i\Delta|\Delta\rangle \quad (2.60)$$

The operators can also have a well defined spin quantum number, since  $[D, M_{\mu\nu}] = 0$ . Importantly, the momentum and special conformal transformation generators  $P_\mu, K_\mu$  act as raising and lowering operators for the conformal dimension due to the commutation relations

$$[D, P_\mu] = iP_\mu, \quad [D, K_\mu] = -iK_\mu \quad (2.61)$$

Similar to the analysis of the harmonic oscillator, we postulate that there exist operators called primary satisfying

$$[K_\mu, \mathcal{O}_\Delta(0)] = 0 \quad (2.62)$$

Other operators in the theory can be generated by acting on these operators using  $P_\mu$  forming an infinite tower, called the family of descendant operators. Finally, very importantly, in this quantization scheme it is possible to define the notion of an inner product between two primary states in the theory:

$$\langle \Delta | \Delta' \rangle = \lim_{r \rightarrow \infty} x^{2\Delta} \langle 0 | \mathcal{O}_\Delta(x) \mathcal{O}_{\Delta'}(0) | 0 \rangle \quad (2.63)$$

It can be shown that this overlap is non-negative. As a result, primary operators can be orthonormalized with respect to this inner product, or in other words, a basis of operators  $\mathcal{O}_\Delta^i$  exists such that

$$\langle \mathcal{O}_\Delta^i(x) \mathcal{O}_{\Delta'}^j(0) \rangle = \frac{\delta_{ij} \delta_{\Delta\Delta'}}{x^{2\Delta}} \quad (2.64)$$

The big technical simplification that radial quantization brings to LCT is the fact that creation and annihilation operators are orthogonal to each other. For this part of the discussion we follow closely [1], Chapter 7. The reader should refer to it for a more complete treatment. Denoting  $\mathbf{k} = (k_1, \dots, k_n)$  one prove that

$$\begin{aligned} \langle 0|a_{\mathbf{k}}a_{\mathbf{k}'}^\dagger|0\rangle &= \|\mathbf{k}\|^2\delta_{\mathbf{k}\mathbf{k}'} \\ \|\mathbf{k}\|^2 &= \prod_{i=1}^{\infty} N_i! \end{aligned} \tag{2.65}$$

where  $N_i$  counts how many times a boson with  $i$  derivatives appears in the vector  $\mathbf{k}$ . As an example, if  $\mathbf{k} = (1, 1, 2, 4, 4)$ , the bincount vector is  $N = (2, 1, 0, 2, 0, \dots)$ . Unsurprisingly, one can easily prove that monomials acting on the origin can be described as a product of creation operators

$$\partial^{\mathbf{k}}\phi(0)|0\rangle = \mathcal{N}_{\mathbf{k}}a_{\mathbf{k}}^\dagger|0\rangle \tag{2.66}$$

If the monomials were primary operators, this would be the end of the story, since we could prove that the bra  $\langle 0|\partial^{\mathbf{k}}\phi(\infty)$  is proportional to the hermitian conjugate of the RHS of (2.66). However, a more careful calculation shows that  $\langle 0|\partial^{\mathbf{k}}\phi(\infty) \neq \langle 0|\mathcal{N}_{\mathbf{k}}a_{\mathbf{k}}$ . It turns out that this is not so important, since we can show that for primaries the bra is truly the hermitian conjugate of the ket:

$$\begin{aligned} \mathcal{O}_{\Delta}(0)|0\rangle &= \sum_{\mathbf{k}} C_{\mathbf{k}}^{\mathcal{O}}\mathcal{N}_{\mathbf{k}}a_{\mathbf{k}}^\dagger|0\rangle \\ \langle 0|\mathcal{O}_{\Delta}(\infty) &= \sum_{\mathbf{k}} C_{\mathbf{k}}^{\mathcal{O}}\mathcal{N}_{\mathbf{k}}\langle 0|a_{\mathbf{k}} \end{aligned} \tag{2.67}$$

As long as we calculate matrix elements only between primaries, we can pretend monomial bras behave like bras of primaries, and this simplifies the bookkeeping significantly. With radial quantization, the problem of orthonormalizing primaries against the Fourier transformed two-point function (1.38) has therefore been trivialized; orthogonality between primaries of different dimension is now explicitly man-

ifest, and any non-zero inner products have been reduced to a simple dot product calculation on a computer.

The utility of radial quantization doesn't stop there: we can also compute matrix elements of the interaction Hamiltonian with our primary basis. However, the operators  $\phi^n$  are not primary, and we cannot directly use the machinery above to calculate the three point functions (1.45). Expressing  $\phi$  as an integral over primaries is simple, however:

$$\phi^n(x) = \int^{y_1} dy'_1 \partial\phi(y'_1) \dots \int^{y_n} dy'_n \partial\phi(y'_n) \Big|_{y_1=\dots=y_n=x} \quad (2.68)$$

The lower boundaries of the integrals are fixed a posteriori, by demanding that the correlator after integration obeys the cluster decomposition principle and hence vanishes as  $y_i \rightarrow \infty$ . The computation of the matrix elements  $\langle O_i(x) \partial\phi(y_1) \dots \partial\phi(y_n) O_j(z) \rangle$  is not as daunting as it seems, owing to the simplicity of the radial quantization expansions. We relegate the details to ch. 7 of [1], and we only cite the final result

$$\begin{aligned} \mathcal{M}_{\mathcal{O}\mathcal{O}'}^{(\frac{\phi^n}{n!})} &= 2 \frac{(-1)^{\Delta-\Delta'} N_{FT}}{(4\pi)^{n/2} N_{\mathcal{O}} N_{\mathcal{O}'}} \sum_{\mathbf{k}\mathbf{k}'} C_{\mathbf{k}}^{\mathcal{O}} C_{\mathbf{k}'}^{\mathcal{O}'} \mathcal{N}_{\mathbf{k}} \mathcal{N}_{\mathbf{k}'} \sum_{\substack{\mathbf{k} \setminus k_i = \mathbf{k} \setminus k'_j \\ |k_i| + |k'_j| = n}} \|\mathbf{k} \setminus k_i\|^2 \frac{\mathcal{I}(\{k_i\}, \{k'_j\})}{\prod_i k_i^{\frac{1}{2}} \prod_j k'_j^{\frac{1}{2}}} \\ \mathcal{I}(\{k_i\}, \{k'_j\}) &= \sum_{\substack{A_+ \subset k_i \\ A_- \subset k'_j}} (-1)^{d(A_+) + d(A_-)} \min \left( \sum_{k_i \in A_+} k_i, \sum_{k'_j \in A_-} k'_j \right) \end{aligned} \quad (2.69)$$

The above formula is simple to implement and offers considerable speedup in calculations compared to Wick contractions. We have used radial quantization liberally in this work to perform our biggest simulations efficiently, however, some parts of the work have been done using Wick contractions only.

## 2.4 Spontaneous symmetry breaking in LCT

Spontaneous symmetry breaking is a very important phenomenon in QFT that occurs in systems that are invariant under a symmetry transformation. We say that spontaneous symmetry breaking occurs if, as one tunes a parameter of the system, the eigenstates of the system may cease being explicitly invariant under the symmetry, despite the Hamiltonian being explicitly invariant under it. These changes in the behavior of the system are sudden in the thermodynamic limit and hence discontinuous, and they are commonly the reason that a system experiences a phase transition; in this phase transition paradigm, a phase transition is in essence a radical change of the macroscopic behavior of the system, which also requires a massive reshuffling of its microscopic degrees of freedom. This macroscopic change in behavior can be studied by calculating large scale observables in the theory, such as correlation functions.

Any observable that can trace a phase transition is called an *order parameter*. Typical order parameters that we can use in a QFT may differ depending on the order of the phase transition that we are interested in. For example, good order parameters for a first order transition are one point functions of operators in the vacuum  $\langle \Omega | \mathcal{O}(0) | \Omega \rangle$ , since they will exhibit discontinuous behavior along a first order phase boundary. In second order phase transitions, expectation values are continuous, but their first derivatives may be discontinuous along the phase transition. This type of phase transition is very interesting in the QFT/statistical physics setting, since it usually signifies scaling behavior for the critical system. The system becomes scale invariant at the critical point, and develops long range (proportional to the system size) correlations between the degrees of freedom; this implies also that two-point functions develop power law tails, instead of the typical exponential decay encountered in the relativistic QFT setting, and as a result, the existence of massless excitations in the theory. Whenever the scaling ansatz holds, the appearance of a CFT is a common occurrence.

SSB can also typically be associated with a rapid rearrangement of the spectrum of the quantum theory while one varies a parameter of the system; the symmetry under

which the system is invariant is reduced to one of its subgroups and the remaining generators of the group that became "broken" can be used to distinguish between ground states of the same energy.

A very well understood example of an SSB transition is the thermal 2-D Ising model with no external magnetic field. The Hamiltonian of the Ising model is quadratic in the spins and hence is invariant under flipping all spins simultaneously:  $\sigma_i \rightarrow -\sigma_i$ . This is a  $\mathbb{Z}_2$  symmetry of the microscopic Hamiltonian. At high temperatures  $T \gg |J|$ , the expected value of the total magnetization of the system is zero, since the system has enough thermal noise to make noise flips highly probable and the resulting typical configurations look essentially random. On the other hand, at  $T \ll |J|$  ground state physics dominates. There are two ground states, the all-up and all-down states, and the  $\mathbb{Z}_2$  symmetry generator changes one into the other, and this signals the breaking of the symmetry. Between those two phases, in the continuum limit, there is a critical point at temperature  $T_c \propto J$ , where the system transitions from one phase into the other. In any real system, obviously this situation is metastable and which state will dominate the ensemble after a long time evolution depends heavily on the initial conditions/other interactions that may explicitly break the symmetry. In the example above, the degeneracy can be broken by a magnetic field, which below the critical temperature will split the ground states energetically, making the alignment with its direction energetically favorable.

A cartoonish, phenomenological way of viewing these transitions is to write a classical potential that can have one or two vacua depending on its parameters. This potential can be used to model an order parameter, in this case the magnetization, since, rather surprisingly, minima of polynomials can reproduce any order of phase transition required, as long as the polynomial is of high enough degree. For the Ising model, the lowest degree  $\mathbb{Z}_2$  polynomial that satisfies the phenomenology is

$$V(\phi) = \lambda\phi^4 + \mu\phi^2, \quad \mu = f(T - T_c) \quad (2.70)$$

Analysis of the minima shows that the polynomial develops two degenerate minima for

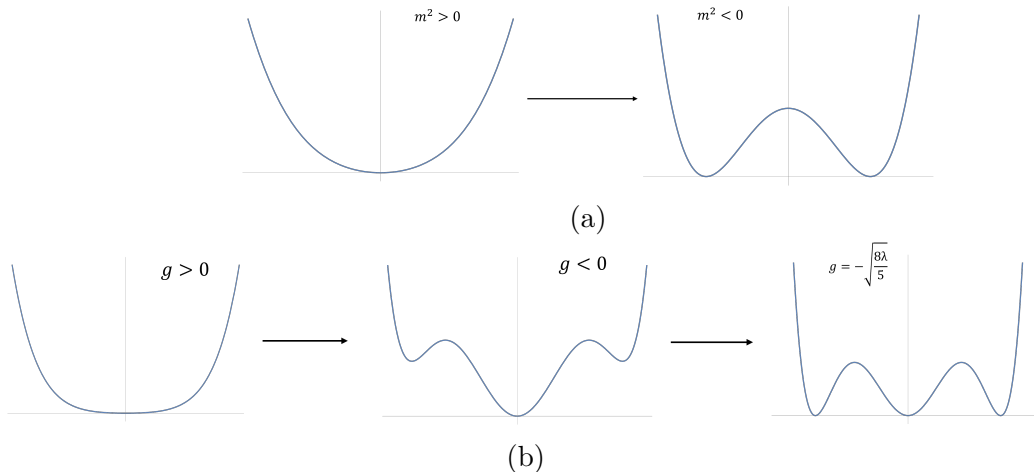


Figure 1: A cartoon of the spontaneous symmetry breaking transitions exhibited by the classical Hamiltonians (2.71)-shown in (a)-,(2.72)-shown in (b). The quartic potential (a) develops two degenerate minima and the sextic potential develops three. The number and properties of minima like width are important for determining weak coupling SSB physics such as kinks and bound states.

$\mu < 0$ , while it only has one when  $\mu \geq 0$ . There is a first order at  $\mu_c = 0$ , and as long as  $f(0) = 0$ , the transition happens at the right critical temperature. This framework is called Landau mean field theory, and it captures well most qualitative aspects of phase transitions, however, especially in low dimensional spaces, it cannot be used for quantitative predictions. In this work we are directly interested in analyzing bosonic Lagrangians in 2-D with a polynomial potential, and in these models Landau mean field theory can make quantitative predictions for weak coupling. In a fully quantum theory, one way to analyze SSB at arbitrarily large coupling would be to compute the quantum effective potential (QEP). Knowledge of the QEP turns the quantum problem into a classical one, and hence the configurations that correspond to absolute minima of the QEP should reflect the vacuum structure of the theory. This object is quite difficult to compute, but at tree level (semiclassical approximation) the QEP has the same form as the classical potential, so we expect that the vacua of the theory are described by the classical ones to a good degree of approximation for weak coupling. In this regime, the quantum behavior of these models is d by their semiclassical behavior.

This class of models can exhibit symmetry breaking patterns not only at weak, but

also strong coupling as well; as a matter of fact, strongly coupled bo there is a close connection to a class of CFTs called minimal models [94]. Bosonic polynomial models belong to the same critical universality class as minimal models, meaning that the CFTs encountered at the second order critical points correspond to a minimal model. Additionally, in the case of Ising field theory- which is the  $\mathcal{M}(4, 3)$  minimal model- small deviations from criticality written in terms of the relevant operators of the CFT can describe small deviations from criticality in the bosonic model.

In ET quantization, studying criticality is relatively straightforward conceptually, but analytically difficult to approach, due to the fact that the vacuum structure is radically different than the free theory at strong coupling, so one usually resorts to computational approximations. For example, the phase diagram of  $\phi^4$  theory has been studied in detail numerically and analytically in [76][77][81][79].

Naively, in LC quantization, this problem becomes much easier, owing to the triviality of the vacuum; one can build excitations on top of the non-interacting vacuum at *any coupling*. This statement, that LC trivializes strongly coupled QFT, has been strongly contested in the past. In works like [89] it has been shown that assuming the vacuum is completely trivial (in other words, it is the only state in the zero  $P_-$  sector) in LC quantization leads to various inconsistencies when quantizing the theory, and, to make matters worse, the theory cannot reproduce phenomena related to spontaneous symmetry breaking. Indeed, to all orders in perturbation theory, expectation values of operators in the vacuum cannot be modified, since all tadpole diagrams are set to zero by vacuum triviality. The crux of the issue is that assuming the vacuum is the unique state that satisfies  $P_-|0\rangle = 0$  ignores certain states constructed from zero momentum modes of the fundamental field. These modes are dynamically constrained, in a similar way to how Gauss's law is a constraint in gauge theory; LC demands that the excited modes with non-zero momentum determine zero momentum operators through a coupled operator equation that contains no derivatives of the time dependence. They are responsible for providing operators with non-zero expectation values in the vacuum, and including them in calculations is required for

LC to reproduce ET physics.<sup>3</sup>

Due to zero modes being dynamically constrained, it can be argued that all the information about symmetry breaking is contained in the excitations above the vacuum, albeit in a complicated way. An early argument in favor of this point of view was provided by [75], where a variational calculation using coherent states was performed for the  $\phi^4$  theory with a negative mass term, and vanishing with the volume splitting between variational ground states was observed at weak coupling. Also, independently, Burkardt [14] showed that, at least in perturbation theory, the effects of zero modes can be included in a lightcone calculation by adding back all the vanishing tadpole diagrams to the theory with the trivial vacuum, and as an added bonus these interactions are never of higher order than the original polynomial potential. This means that LC quantization of the naive theory must be able to reproduce the correct phase diagram of the theory, with the caveat that the position of the transition line may be shifted in comparison to the corresponding equal time calculation. In this light, LC becomes an effective model for understanding QFTs, and some external input is needed for LC to be a complete scheme, but the advantage of sped up calculations and conceptual simplicity remains attractive. In this work we will show, by working on specific bosonic models, that it is indeed the case, that LCT can indeed reproduce important phenomenology, such as the phase diagram and the bound states of the theory. In both models that we consider, perturbative and nonperturbative symmetry breaking takes place, in slightly different settings. More specifically, the models we are interested in are described by the following interaction Hamiltonians

$$H_1 = \int dx_- \left( \frac{\lambda}{4!} \phi^4 + \frac{m^2}{2!} \phi^2 \right) \quad (2.71)$$

$$H_2 = \int dx_- \left( \frac{\lambda}{6!} \phi^6 - \frac{g}{4!} \phi^4 + \frac{m^2}{2!} \phi^2 \right) \quad (2.72)$$

The semiclassical potential for both models exhibits a  $\mathbb{Z}_2$  breaking transition, going

---

<sup>3</sup>For a more detailed discussion of zero modes, the reader is encouraged to refer to Appendix A.

from a potential with a single vacuum as shown in Fig. 1, to one with multiple vacua, symmetrically placed around the origin. For the first Hamiltonian, the phase  $m^2 > 0$  has been studied recently numerically and analytically using LC or ET truncation in several works [2][76][77][81][79], and the existence of a strongly coupled SSB transition is well established. The broken phase has not been studied using LCT thus far. For technical reasons, LCT is unable to accurately simulate  $H_1$ . To make a study of broken phase possible, we instead simulate the Hamiltonian

$$H'_1 = \int dx_- \left( \frac{\lambda}{4!} \phi^4 + \frac{g}{3!} \phi^3 + \frac{m^2}{2!} \phi^2 \right) \quad (2.73)$$

which explicitly breaks the mirror symmetry, but the symmetry is restored as we approach the curve  $g^2 = 3\lambda m^2$ , at least at weak coupling. The sextic model described by  $H_2$  has the added benefit of being invariant under the symmetry, while LCT simulation gives reasonable results, unlike for  $H_1$ . With this setup, we proceed to analyze both models in the following sections.

### 3 Spontaneous Symmetry Breaking in the $\phi^4$ bosonic field theory in 1+1-D

As noted in the previous chapter, zero modes in LC quantization are instrumental for producing a spontaneous symmetry breaking (SSB) pattern of an underlying symmetry group at the level of the vacuum sector. Traditionally, SSB is detected by picking a suitable order parameter of the form:

$$F_{\mathcal{O}}(\lambda_1, \dots, \lambda_n) = \langle \Omega | \mathcal{O}(0) | \Omega \rangle \quad (3.1)$$

where  $\lambda_1, \dots, \lambda_n$  are the interaction couplings of the theory. Well chosen order parameters exhibit singular behavior for some value of the couplings. The order parameter itself may not diverge, but some of its derivatives might. If the  $n$ -th derivative of the order parameter exhibits a discontinuity, the transition is also called an  $(n + 1)$ -th order phase transition. We would like to explore this using the LCT method. Since LCT doesn't take into account zero modes, the textbook diagnostic tool for SSB is uncalculable within our scheme. However, typically the spectrum also undergoes some sort of discontinuous behavior when crossing the phase transition point/line; one way to justify this is to think of the spectrum eigenvalues and eigenvector components in some basis as a highly nonlinear function of nonlocal operator VEV's and hence conclude that they are very likely to experience a transition themselves.

We will begin our investigation with the Hamiltonian

$$\mathcal{H}_1 = \frac{\lambda}{4!} \phi^4 + \frac{m^2}{2!} \phi^2 \quad (3.2)$$

Thanks to an important result due to Chang [25], that relates the strongly coupled unbroken/broken phase  $|m^2| \gg \lambda$  to a weakly coupled broken phase  $|m^2| \ll \lambda$ , where the dynamics is under analytical control, the phase diagram of  $H_1$  under the vacuum expectation value (VEV) of the field  $\langle 0 | \phi | 0 \rangle$  is completely known.

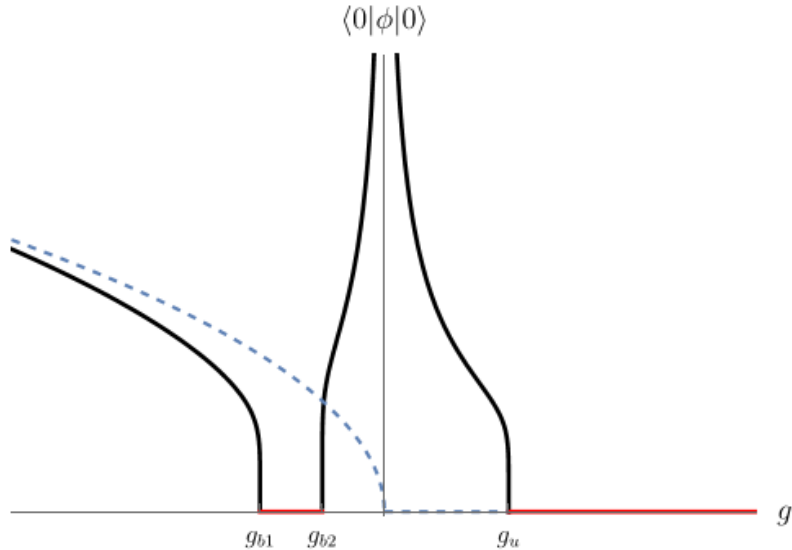


Figure 2: Qualitative plot of the VEV  $\langle 0|\phi|0\rangle$  vs the ratio  $g = m^2/\lambda$ , informed by Chang duality. The red lines represent the unbroken phase of the model, and the black ones the broken phase. The semiclassical prediction is shown in dashes.

In Figure 2, a qualitative drawing of the behavior of the VEV as one varies the dimensionless ratio  $g = m^2/\lambda$  parameter is shown. The semiclassical prediction is shown in dashed lines; an analysis of the minima of the classical potential defined by  $H_1$  shows that at weak coupling there is one minimum at  $\phi = 0$  when  $m^2 > 0$  and two minima  $\phi = \pm\sqrt{-6m^2/\lambda}$  when  $m^2 < 0$ . More explicitly, when  $\lambda \ll m^2$ :

$$\langle 0|\phi|0\rangle = \begin{cases} 0 & m^2 > 0 \\ \pm\sqrt{-\frac{6m^2}{\lambda}} & m^2 < 0 \end{cases} \quad (3.3)$$

In the absence of explicit breaking, in the broken phase the system is going to be in a superposition of its two degenerate ground states. If a small explicit breaking is introduced and then removed, the system will be brought to live in the vacuum which was energetically favored by the breaking. These considerations hold in the weak coupling limit  $|g| \gg 1$ , but they do not represent the phase diagram of the quantum theory well if taken at face value.

However, due to Chang duality, knowledge of the phase diagram at weak coupling is

sufficient to determine the entire phase diagram. The duality allows us to prove that the system exhibits a second order critical point at strong coupling  $g_u$  as we approach from weak coupling in the unbroken phase on the right, and two critical points  $g_{b1}, g_{b2}$  (that are exactly the same in nature as  $g_u$ ) as we approach from the weakly coupled broken phase on the left. We use the duality and the second order criticality to argue that the regions  $(-\infty, g_{b1}), (g_{b2}, 0), (0, g_u)$  to conclude that the simplest way the VEV can depend on the coupling while obeying the known asymptotic relations in those regions is shown in Fig. 2, and in the remaining regions the VEV is exactly zero, since it is known that the theory is exactly  $\mathbb{Z}_2$  invariant for  $g > g_u$ . Of course, the accuracy of the figure is limited due to the fact that we don't have exact knowledge of the behavior of the VEV in the unbroken phase, but we know that at least in the neighborhood of  $g = -\infty, 0, g_{b1}, g_{b2}, g_u$  the picture is correct.

The phase diagram of  $H_1$  is fairly rich, with 4 distinct points where the theory exhibits a phase transition, and we note further that, as seen from the diagram, the transition at  $g = g_{b1}, g_{b2}, g_u$  is second order, while the phase transition at  $g = 0$  is first order. The region  $(g_u, \infty)$  has been well studied in LCT, and we want to study the perturbatively accessible broken phase end,  $(-\infty, g_{b1})$ .

However, LC quantization with a trivial vacuum cannot calculate VEVs, so it is not entirely clear how one could obtain signatures of a first order phase transition that do not rely explicitly on zero mode contributions. The main issue with first order transitions is that they do not exhibit scaling. The theories arising at first order points are perfectly ordinary, massive QFTs, and the only way to diagnose them is to explicitly measure a discontinuity in the spectra/correlation functions. In applying LCT to the model, we will focus on the spectral signatures of the phase transition, and especially the low energy states of the model, as we will discuss in the following sections.

### 3.1 Implementing SSB in LCT

It has been shown in previous work (see [40], [2], [53], [52] and [41]) that LCT can detect second order phase transitions relatively easily. This is possible due to the fact that second order phase transition points are oftentimes described by a CFT. These critical points are usually strongly coupled, but the CFT framework provides a simple emergent description of the degrees of freedom present at that specific point, taking advantage of the scaling behavior near it. The 1+1-D  $\phi^4$  theory (3.2) with a positive mass term possesses a strongly interacting fixed point which lies in the same universality class as the 2-D Ising model critical point, which has an emergent CFT description given by the  $\mathcal{M}(4, 3)$  minimal model, a rational CFT whose data is completely known. The flow of this theory to the Ising model is implemented in LCT in [2]. Furthermore, it is a well known fact that CFTs describe massless excitations, and this implies that the lightcone mass matrix must eventually have some zero eigenvalues, and this phenomenology is indeed present in LCT implementations in the vicinity of a 2nd order phase transition. However, it is not a priori clear how our method can model 1st order transitions, since the spectrum of finite matrices cannot present with explicit discontinuities, and additionally, the critical theory has no long range correlations.

The most naive approach to obtaining an LCT implementation of such a first order phase transition would be to take the canonical lightcone Hamiltonian

$$P_+ = \int dx_- \left( \frac{\lambda}{4!} \phi^4 + \frac{m^2}{2!} \phi^2 \right) \quad (3.4)$$

and compute its matrix elements with the free massless boson basis, and subsequently find the eigenvalues and eigenvectors. The coupling space is effectively one-dimensional, due to the fact that one can always rescale the fundamental field and set any of the coupling constants to unity; the only relevant quantity here is the ratio  $m^2/\lambda$ . However this approach fails to reproduce non-perturbative features for  $m^2 < 0$ . More worryingly, LCT seems to pose a spectrum interpretability problem

for these theories: the lowest eigenvalue is negative and therefore, since we assumed that the vacuum energy is zero in the underlying CFT, this indicates that the trivial vacuum ansatz does not work properly when one attempts to diagonalize the Hamiltonian around the unstable vacuum  $\phi = 0$ . Qualitatively, it is simple to see that the vacuum structure is much different than the assumed one; in fact due to SSB, at infinite volume we expect that if LCT was representing the system well, the excited modes would have to built upon a doubly degenerate ground state, with one state even and the other odd under the  $\mathbb{Z}_2$  symmetry. It is not surprising that the naive approach fails, since we hardwired a different vacuum structure into the theory by assuming that the spectrum must be close to a free boson around the unstable point.

In order to overcome this obstacle, the idea is to find the correct effective description of the theory so that at least the perturbative spectra are positive, and hence interpretable. An enlightening way to find the correct perturbative LC Hamiltonian is to construct it from the equal time theory [14]. Generally, for a bosonic theory with polynomial potential, the interacting Hamiltonians of ET and LC quantized theories given by

$$\begin{aligned}
 V_{ET}(\phi) &= \sum_{n=0}^N \lambda_{n,ET} \frac{\phi^n}{n!} \\
 V_{LC}(\phi) &= \sum_{n=0}^N \lambda_{n,LC} \frac{\phi^n}{n!}
 \end{aligned}
 \tag{3.5}$$

produce the same physical predictions to all orders in perturbation theory, if and only if:

$$V_{LC}(\phi) = \sum_{n=0}^N \langle 0 | V_{ET}^{(n)}(\phi) | 0 \rangle \frac{\phi^n}{n!}
 \tag{3.6}$$

Here, the VEV's are computed order by order in perturbation theory around the ET non-interacting vacuum. Note that the equivalence relation forces the two potentials to be of the same order and have the same highest power coefficient. Only the lower order terms of the Hamiltonian are affected, and they contain VEV's of powers of the field operator. In LCT with a trivial vacuum, the mapping is effectively uncom-

putable, but it can guide our intuition for writing down the correct form of effective Hamiltonians required for LCT to give well-behaved spectra.

Specializing to a bosonic theory with polynomial potential of degree 4 given by  $V(\phi) = \lambda\phi^4/4! + g\phi^3/3! + m^2\phi^2/2! + h\phi$ , the recipe to generate the LC effective Hamiltonian is given by

$$\begin{aligned}
\lambda_{LC} &= \lambda_{ET} \\
g_{LC} &= g_{ET} + \lambda_{ET} \frac{\langle 0|\phi|0\rangle}{1!} \\
m_{LC}^2 &= m_{ET}^2 + g_{ET} \frac{\langle 0|\phi|0\rangle}{1!} + \lambda_{ET} \frac{\langle 0|\phi^2|0\rangle}{2!} \\
h_{LC} &= h_{ET} + m_{ET}^2 \frac{\langle 0|\phi|0\rangle}{1!} + g_{ET} \frac{\langle 0|\phi^2|0\rangle}{2!} + \lambda_{ET} \frac{\langle 0|\phi^3|0\rangle}{3!}
\end{aligned} \tag{3.7}$$

Here, both Hamiltonians are assumed to be normal-ordered, so that their vacuum energies are set to zero. In LCT, a linear interaction term is invisible, due to the fact that it is only comprised of zero modes, and hence all of its matrix elements in our basis are zero in the trivial vacuum approximation. This could potentially be an issue, but at least at weak coupling  $h_{LC}$  vanishes identically. To show this, select the appropriate couplings for the broken  $\phi^4$  theory  $(\lambda, g, m^2, h)_{ET} = (\lambda, 0, -m^2, 0)$  and plugging in the semiclassical regime VEVs given by

$$\langle 0|\phi^n|0\rangle = (\pm)^n \left( \frac{-6m^2}{\lambda} \right)^{\frac{n}{2}} \tag{3.8}$$

we find that the LC effective Hamiltonian contains a cubic term:

$$(\lambda, g, m^2, h)_{LC} = (\lambda, \pm\sqrt{-6m^2\lambda}, -2m^2, 0) \tag{3.9}$$

This means that LC quantization is rearranging the Hamiltonian naturally, so as to be located in one of the two true vacua of the theory. This is a strong indication that the LCT implementation will be successful if one considers the original theory with

a cubic term:

$$P_+ = \int dx_- \left( \frac{m^2}{2!} \phi^2 + \frac{g}{3!} \phi^3 + \frac{\lambda}{4!} \phi^4 \right) \quad (3.10)$$

In this particular theory there are no additional issues to resolve concerning the linear term, since one can always shift the field by a constant to center the theory around its classical true vacuum to make the linear term disappear, and hence, the theory can always be written in the form (3.10). Additionally, as shown above, at weak coupling, no additional shifting of the Hamiltonian is required to put it in the requisite form.

The extra cubic term explicitly breaks the  $\mathbb{Z}_2$  symmetry and under the  $\phi \rightarrow -\phi$  operation, we find that positive and negative cubic coupling perturbations have the same effect. In other words, the matrices  $P_+(m^2, g, \lambda), P_+(m^2, -g, \lambda)$  are isospectral and without loss of generality we can keep  $g, \lambda > 0$ . In order to maintain the interpretability of the spectrum intact, we also need to keep the mass positive and we expect that this restriction will allow us to only explore certain phases of the theory. We also notice that all these quantities are small when the quartic coupling is small. This affords us the certainty that in at least a small region around the Gaussian fixed point (GFP) the effective Hamiltonian (3.10) provides us with a faithful description of the ET broken phase theory. It is shown in our simulations that the region of validity is indeed finite- we could only gain access to the broken phase of the theory, and we cannot see past the critical point into the unbroken phase. However, this feature was not surprising, since it has been a feature of the LCT unbroken phase as well [2]. Very generally, if we assume that we have  $g_{ET} = 0$  in (3.7) and the equal time theory is in the broken phase  $m_{ET}^2 < 0$ , one can convince themselves that as long as the VEVs involved in the expressions for the couplings of the effective Hamiltonian are differentiable functions, there exists a mapping

$$\frac{g_{LC}}{m_{LC}^2} = \mathcal{F} \left( \frac{\lambda_{LC}}{m_{LC}^2} \right) \quad (3.11)$$

which sends the interval  $(-\infty, g_{b1})$  to a curve in the LC quantized theory (see Fig. 2). The form of this mapping is completely general, and is not affected, even when

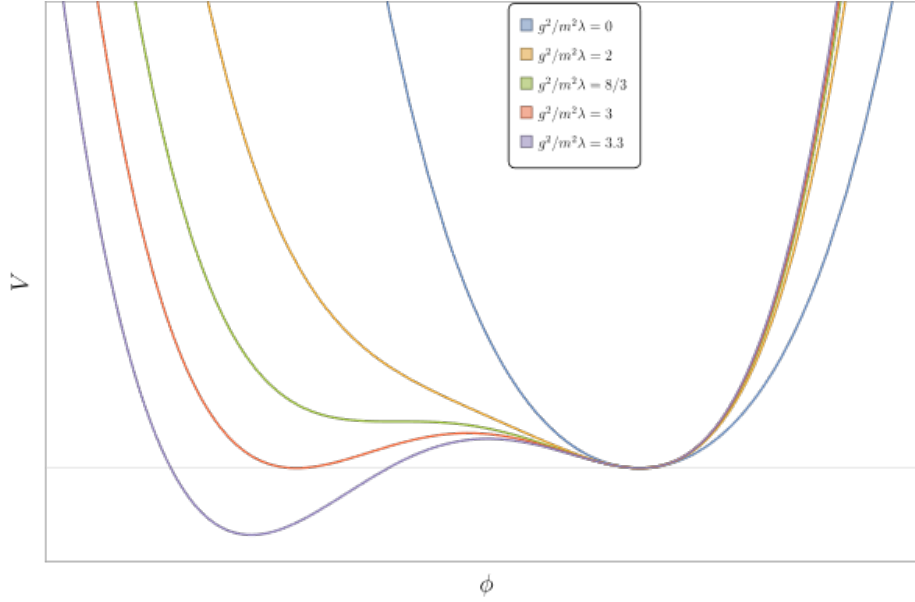


Figure 3: The shape of the classical potential (3.10) for increasing cubic coupling strength  $g$ . The minimum is unique until  $g^2 = 8\lambda m^2/3$ , where a local minimum and maximum appear. The vacuum is still at  $\phi = 0$ , however, until the cubic coupling reaches the value  $g^2 = 3\lambda m^2$ , past which the true vacuum is located at the other minimum. LC quantization should fail past that first order transition point, since the vacuum has been assumed to be at  $\phi = 0$ .

a field shift to the true vacuum is required to reproduce the effects of a linear term in the theory. We thus expect to reproduce the entirety of the physics of the SSB  $\phi^4$  model by studying the LC Hamiltonian near this curve. In this work, we will quantify this mapping nonperturbatively and study the spectrum of the theory near this phase transition curve. Furthermore, the shape of the mapping is known at weak coupling, from analyzing the minima of the potential (3.10). The result of the analysis can be seen in Fig. 3, where it is clear that the SSB theory at weak coupling must occur on the line  $g^2 = 3m^2\lambda$ , which in the language of the aforementioned mapping reads:

$$\mathcal{F}(x) \approx \sqrt{3x}, \quad x \ll 1 \quad (3.12)$$

Incidentally, the correct form of the LC Hamiltonian at weak coupling could have also been guessed in a more traditional way, by performing the field shift  $\Phi = \phi - v$  with  $\lambda v^2 = -6m^2$ .

### 3.2 Results

We have implemented the theory (3.10) in LCT, in a similar spirit to [2]. Since the  $\mathbb{Z}_2$  symmetry is broken explicitly in this Hamiltonian by the cubic term, odd and even particle sectors mix under said interaction term and therefore we have to diagonalize the full Hamiltonian to obtain the spectrum, so for large matrices we suffer a slowdown of about a factor of 4 compared to Hamiltonians with  $g = 0$ . Also, we are dealing with a two-parameter coupling space  $(\lambda/m^2, g/m^2)$  makes the exploration of the coupling space rather computationally intensive, and computations have been performed in a computing cluster for any  $\Delta_{\max} > 25$ . The size of the matrices in question is given by  $p(\Delta_{\max})$ , where  $p(n)$  stands for the number of partitions of positive integer number  $n$  into (any number of) positive integers.

$\Delta_{\max}$	$p(\Delta_{\max})$	$\Delta_{\max}$	$p(\Delta_{\max})$
15	176	35	14883
20	627	40	37338
25	1958	45	89134
30	5604	50	204226

Table 1: Matrix sizes for a few  $\Delta_{\max}$  values.

For reference, the sizes of matrices for some representative values of  $\Delta_{\max}$  are shown in the table above. One immediately sees that the size of the matrices grows fast with the truncation level. Asymptotically, the dependence on the  $\Delta_{\max}$  is subexponential, since  $p(\Delta) \sim \Delta^{-1}e^{\sqrt{C\Delta}}$ , with  $C = 2\pi^2/3$ . Calculating the matrix elements of the Hamiltonian in the free boson basis could also become computationally difficult for high truncation levels, but their generation is relatively fast until about  $\Delta_{\max} = 50$  using the radial quantization routine; also it has to be done only once for each value of the truncation level. This makes diagonalizing the matrices the main bottleneck of this computation. Our code uses the innate Mathematica functions to diagonalize the matrix, which is good enough for our purposes and allows us to push the diagonalizations safely to about  $\Delta_{\max} = 40$ . The first question we attempt to answer is approximating the gap of the theory for various values of the couplings, and whether

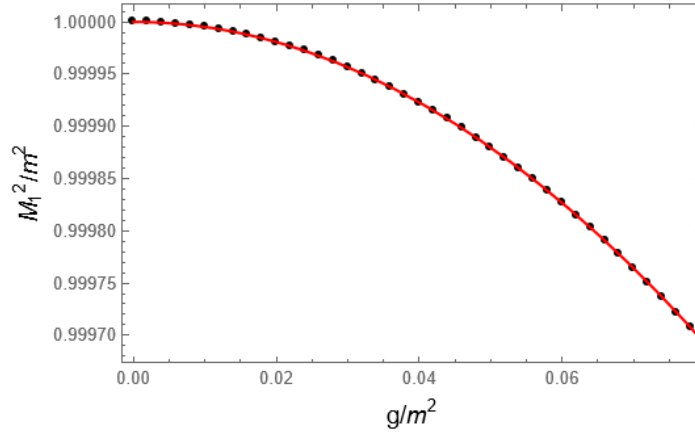


Figure 4: LCT data for the gap at weak coupling,  $\lambda = 0, g \ll m^2$ . There is excellent agreement between the raw data for  $\Delta_{\max} = 25$  and the leading order perturbative correction to the mass, given by  $M_1^2 = m^2(1 - \frac{g^2}{12\sqrt{3}})$  (shown in red).

this quantity contains any information about SSB in this theory. To this end we diagonalized  $M^2 = 2P^+P^-$  and computed the gap in units of the bare mass  $m^2$  for various values of the couplings. We know that perturbatively, the gap value is well-defined and therefore assuming that the vacuum is trivial is a good approximation.

We can verify this statement by testing the predictions of LCT against perturbation theory. In particular, we could test the perturbation theory prediction for the correction to the single particle pole against the single particle mass, which appears as the lowest mass eigenvalue at weak coupling. We denote the lowest mass eigenvalue by  $M_1^2(g, \lambda)$ . The comparison between the two quantities is shown in Fig. 4, where we find by fitting an even quartic polynomial to the  $\Delta_{\max} = 25$  data for the lowest eigenvalue that

$$\frac{M_1^2}{m^2} = 1 - \alpha_2 \left(\frac{g}{m^2}\right)^2 - \alpha_4 \left(\frac{g}{m^2}\right)^4 + \mathcal{O}(g^6 m^{-12}) \quad (3.13)$$

$$\alpha_2 = 0.0481125, \quad \alpha_4 = (3.4 \pm 0.2)10^{-3}$$

The quadratic coefficient agrees with negligible error with the exact value  $\alpha_2 = (12\sqrt{3})^{-1}$ .

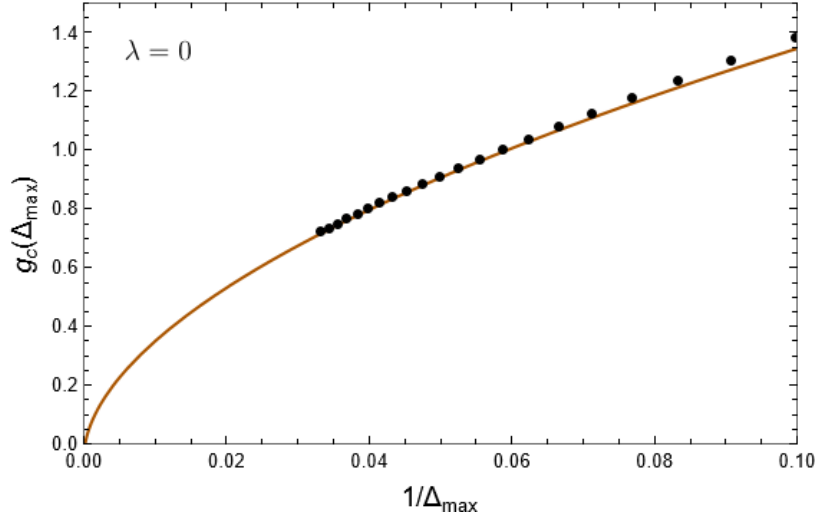


Figure 5: LCT data for the breakdown of the vacuum ansatz in the case of vanishing quartic coupling. The breakdown point slowly approaches its continuum value, and a reasonable model for the approach is given by  $g_c = g_c(\infty) + \gamma\Delta^a$ . Our maximum truncation level in this plot is  $\bar{\Delta}_{\max} = 30$ . The optimal, refined to eliminate bias, estimate for the exponent given the data is  $a = -0.55 \pm 0.03$ . The error on the exponent is obtained from the difference of the biased and bias subtracted measurements.

A subtlety that needs to be addressed is why LCT does not directly see that the theory that we are simulating to extract the perturbative coefficients is unbounded from below for any  $g \neq 0$ , since we set the quartic coupling to zero. It should be clear that this phenomenon is non-perturbative and not hardwired into our assumptions about the vacuum, so we should expect that an LCT simulation will reproduce the correct breakdown point in the continuum limit. Indeed, at some large enough cubic coupling depending on the truncation level  $g_c(\Delta_{\max})$  the LCT spectrum will signal a breakdown of the vacuum ansatz, exhibiting negative eigenvalues. The breakdown point is a monotonic function of the truncation level with decreasing rate. We expect that in the limit of large truncations we will recover the non-perturbative result:  $g_c(\infty) = 0$ . We define the breakdown point as the solution to the equation

$$g_c : M_1^2(g_c(\Delta_{\max}), 0) = 0 \quad (3.14)$$

In Fig. 5 we find this point for various truncation levels and we attempt to estimate the infinite truncation limit  $g_c(\infty)$  by fitting a power law to the curve. We can find a

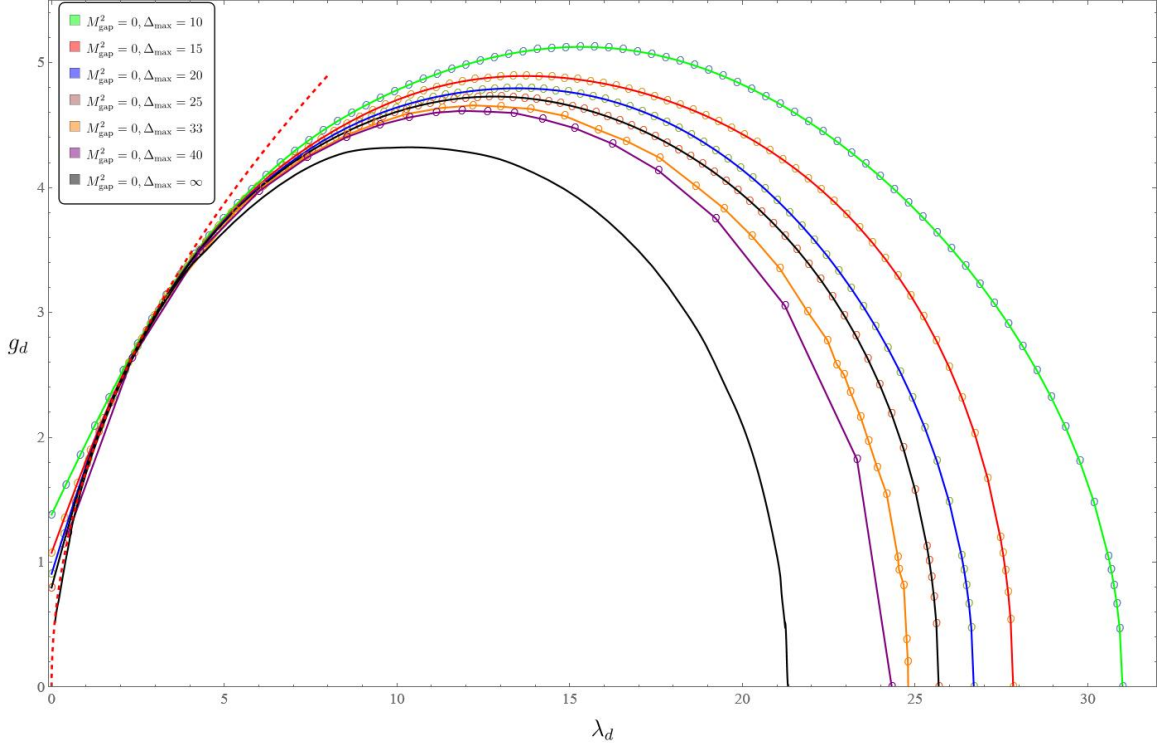


Figure 6: Plot of the lines of zero gap for various values of  $\Delta_{\text{max}}$  plotted in the space of dimensionless couplings of the theory,  $(\lambda_d, g_d) = (\lambda/m^2, g/m^2)$ . The red dashed line indicates the semiclassical prediction for the phase transition  $g_d^2 = 3\lambda_d$ . The black line shows an extrapolation of the curves to  $\Delta_{\text{max}} = \infty$ .

candidate exponent by performing OLS estimation  $\log g_c = \alpha \log \Delta_{\text{max}} + \beta$ . It turns out that adding more data changes this exponent significantly however. To correct for this bias, we perform separate OLS estimates for data up to truncation level  $\Delta \leq \bar{\Delta}_{\text{max}}$ , where  $\bar{\Delta}_{\text{max}}$  is the maximum truncation level included in our simulations, and then we extrapolate  $\alpha(\Delta)$  to infinity. In this case the exponents are well behaved as a function of  $\Delta$ , and a crude estimate of the refined estimate of the exponent is obtained by fitting another power law to  $\alpha(\Delta)$ .

Clearly, the transition from the theory with  $\lambda = g = 0$  to the one with  $\lambda = 0, g \neq 0$  is a first order transition, since the vacuum has now disappeared and configurations with large values of the field are favored, so we expect the VEV to diverge. However, there is no clear indication of a discontinuity in the spectrum of the finite matrices produced by LCT. What happens instead is that the spectrum goes from being well-

defined and positive to a having several large negative eigenvalues. The transition from one regime to another is fairly sudden and it gets sharper as one increases the truncation level (see next subsection for a discussion). It turns out, that in this model the only concrete way LCT can approximate a transition is by loss of positivity of the mass spectrum. The reason for this is that LCT with perturbative effective Hamiltonian corrections (3.7) has no access to the unbroken phase of the model, due to the fact that the VEVs exhibit discontinuities. In essence the mapping between LC and ET quantization is a several-to-one mapping; the same theory in ET quantization requires different effective LC descriptions to be fully simulated. For this model, we believe that simulating (3.10) is all that is required to understand the broken phase of the most general quartic theory (see Appendix B for an argument that works at weak coupling).

Although the order of the phase transition cannot be distinguished phenomenologically via an LCT computation, the simulation presents us with concrete evidence that a phase transition is happening. In the context of an LCT model that cannot represent both sides of the phase transition, we see the following phenomenology when the couplings are increased past the transition line at the current  $\Delta_{\max}$ :

- The spectrum undergoes a rearrangement: the lowest eigenvalues start strongly mixing with the higher ones. This phenomenon is generally expected at strong coupling, but becomes especially prominent near phase transitions.
- There are multiple crossings between low eigenvalues with higher ones descending in energy (see Fig. 9).
- The threshold to massgap expected ratio  $M_2^2/M_1^2 \approx 4$  is violated. The low energy eigenstates have support on all particle sectors, and the line separating the discretum from the continuum is blurred.
- One or more eigenvalues cross the  $M^2 = 0$  line, which is the assumed eigenvalue of the vacuum. This indicates that our assumption of vacuum triviality has been violated.

In the vicinity of the first order transition line of the model, all 4 of these phenomenological characteristics are found in the spectrum and even though each one of them is a distinct event happening at different values of the coupling, these values are very close to each other. We can therefore safely consider these proxys as equivalent in the region of interest, but we will primarily focus on the last criterion to make quantitative predictions. Conceptually, the last criterion is particularly convenient, given that in the known second order phase transition point at  $(\lambda_c, g_c) \approx m^2(24, 0)$ , it is an exact statement: the emergent description at that point is a CFT, which is a theory with gapless modes. In the first order transition region it is a non-exact proxy of the phase transition, but due to the evidence suggesting that all of these 4-criteria converge to the same limit, it interpolates smoothly between the two regions of the phase diagram.

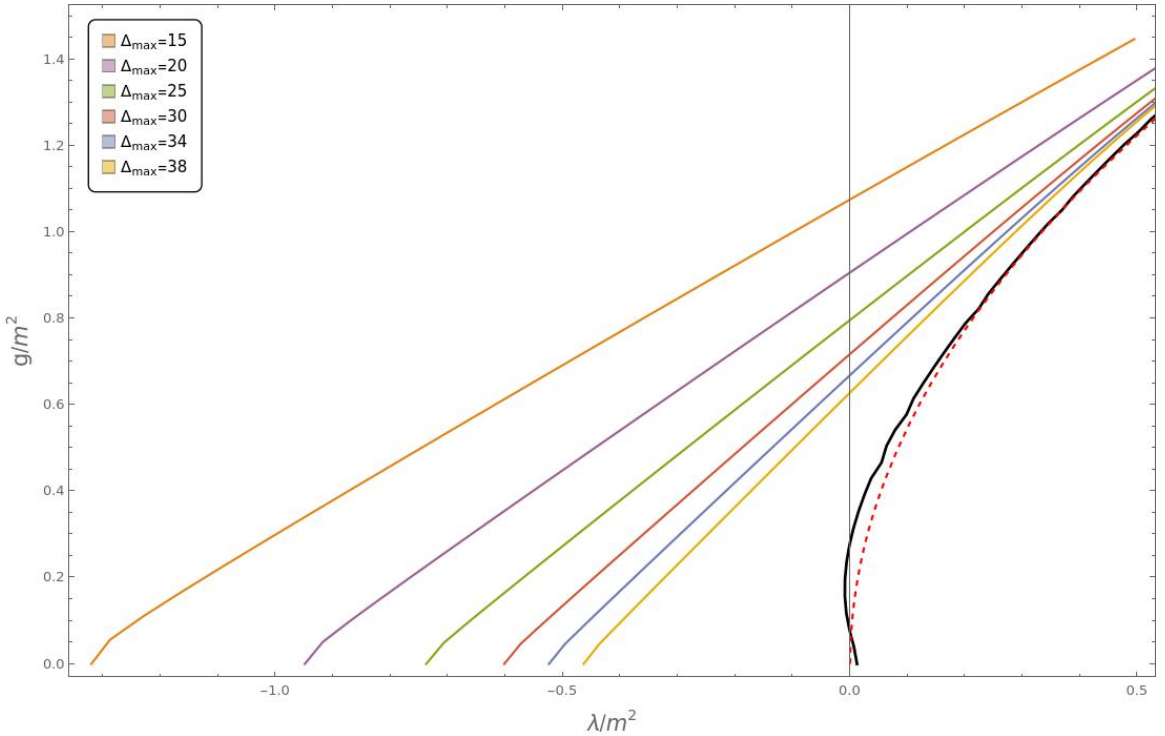


Figure 7: Zoom in to the bottom left corner of Fig. 6, which emphasizes what happens in the semiclassical region. The line of zero gap is extrapolated to infinity (black curve) and we see that the fit to the expected curve  $g = \sqrt{3\lambda m^2}$  is good to within 10% accuracy (measured against the distance of our most expensive simulations from the expected answer). The convergence is slowest in the vicinity of the origin, but after correcting for the infinite  $\Delta_{\max}$  estimator bias, the results are much more accurate.

The criterion can be probed numerically for the entire coupling space  $(g, \lambda)$ , similarly to the way it was probed in Fig. 5. From low  $\Delta_{\max}$  simulations, we expect the transition line to look like a simple closed curve. The curve doesn't pass through the origin for any finite truncation level (it should in the continuum limit however), and hence we will be able to trace the entire transition curve defined by  $M_1^2(\frac{g}{m^2}, \frac{\lambda}{m^2}; \Delta) = 0$ , by simulating the theory along rays emanating through a point. The result of an extensive exploration of the interaction coupling space parametrized by  $\lambda_d = \lambda/m^2, g_d = g/m^2$  is shown in Fig. 6. To generate the plot, we employed a bisection based algorithm that finds roots of the one variable equation

$$s_{\Delta}(\theta) : M_1^2(g_0 + s(\theta) \sin \theta, \lambda_0 + s(\theta) \cos \theta; \Delta) = 0 \quad (3.15)$$

The root essentially represents the distance of the point along the ray defined by an angle  $\theta$ , measured from  $(g_0, \lambda_0)$ . The angle  $\theta$  was varied in  $(0, \pi)$ , since the symmetry  $g \rightarrow -g$  fixes the rest. The starting point can be chosen arbitrarily. We chose it slightly away from the origin  $g_0 = 0, \lambda_0 = 5$ ; this choice improves the angular resolution of the transition curve at  $\pi/2 < \theta < \pi$ .

However, we notice immediately that the convergence to the continuum phase transition curve is somewhat slow; and even at the highest truncation possible we do not reproduce the shape of the curve expected even at weak coupling. This comes as no surprise; the convergence of LCT when simulating QFTs is usually some power law in  $\Delta_{\max}^{-1}$ , and especially in non-integrable theories, the truncation levels required for convergence are way beyond current computational capabilities. This necessitates the development of a scheme to estimate the values of accessible observables at the infinite truncation limit.

Most of the groundwork has been laid in the construction of Fig. 4. We can calculate an estimate for where the line of zeroes is going to converge, if for each direction we plot the distance  $s_{\Delta}$  of the zero from the center point for several values of  $\Delta_{\max}$  and

we fit the data set  $\{(\Delta_i, s_i(\theta_k))\}$  to a function of the form

$$s(\theta_k) = s_\infty(\theta_k) + \frac{A_k}{\Delta_{\max}^{\alpha_k}} \quad (3.16)$$

and obtain an OLS estimate for every direction  $\theta_k$ . The exponent  $\alpha_k$  is generally different for different directions. To calculate it independently and also have a measure of how good the above ansatz is, we first check that the discrete derivative of the data presented above, given by the points  $(\bar{\Delta}_i, \nabla_\Delta s_i) = \left\{ \frac{\Delta_i + \Delta_{i+1}}{2}, \frac{s_{i+1} - s_i}{\Delta_{i+1} - \Delta_i} \right\}$ , is fitted well by the function

$$\nabla_\Delta s(\theta_k) = \frac{\gamma(\theta_k)}{\bar{\Delta}^{\alpha+1}} \quad (3.17)$$

Importantly for numerical fitting purposes, the discrete  $\Delta$ -derivative vanishes in the limit of large truncation level, since we expect that the zero gap line is a proxy to the phase transition curve. Because of this, we can take a logarithm in (3.17) and directly perform OLS estimation:

$$\log \nabla_\Delta D(\theta_k) = (\alpha(\theta_k) + 1) \log \bar{\Delta} + \beta(\theta_k) \quad (3.18)$$

The logarithm is calculated from the slope of the line of best fit. We note here that the extrapolations have been performed in high enough truncation such that the above fit to a line is a good approximation ( $R^2 \gtrsim 0.98$ ).

The expected positions of the zeroes  $(\lambda_0 + s_\infty(\theta_k) \cos \theta_k, g_0 + s_\infty(\theta_k) \sin \theta_k)$  are shown in black in Fig. 6 and 7, connected to each other by interpolation for visualization purposes. We note that the agreement between the extrapolated data and the phase transition line is excellent in the regime where the semiclassical analysis of the system holds. As seen in Fig. 5, the extrapolation improves the quality of the curve by a lot, and the final estimate is very close to the known answer in the continuum. With a few more data points at higher  $\Delta_{\max}$ , double extrapolations like the one performed for Fig. 4 should become possible and a very good estimate of the infinite truncation limit at both strong and weak coupling should become possible. Currently, our expected error is on the order of 5-10% relative to the distance of the phase transition estimates for

the maximum possible value of truncation level from the origin (here the maximum level we obtain data at is  $\Delta_{\max} = 40$ ).

### 3.3 Crossings

As discussed above, it is readily observed that in LCT simulations phase transitions are represented by multiple concurrent phenomena. In fact, the collapse of the gap to zero as one increases the distance from the origin in coupling space given any line that passes through it, of slope  $g/\lambda$ , one encounters in close proximity to the point of vanishing gap, several avoided crossings happening in the low energy sector (see Figure 8). The low energy eigenstates of the continuum theory are well reproduced by LCT in the region of couplings where a LC quantized description is valid. We reason that any features of the spectrum that imply rapid rearrangements of it within small coupling windows or tend to discontinuities, such as avoided crossings among the low energy states that become sharper and sharper as one approaches the limit of infinite truncation, should be taken as evidence of a phase transition.

However, these events do not take place at a single point. At finite  $\Delta_{\max}$  events like a crossing of an eigenvalue with the vacuum (which is set to zero energy) happen at different couplings for a given value of the slope. However, importantly, as one increases  $\Delta_{\max}$ , the aforementioned phenomena happen increasingly more proximally to one another, which hints that they are converging to a single point. We would like to have a quantitative measure of the width of the phase transition, that allows us to quantify the speed of convergence near the phase transition. Avoided crossings are instrumental in achieving this goal at weak and intermediate couplings; they appear right before and after the gap closes at any given truncation level and there is a proliferation of them, creating the illusion of a shower of eigenvalues falling through. The closing of the phase transition window implies that the individual crossing widths have to go to zero, since it is impossible to have two eigenvalues ( $E_1, E_2$ ) of a finite matrix nearly collide while presenting a true discontinuity in the quantity  $E_2 - E_1$ , in tandem with the fact that a non-zero crossing minimum height defined by

$$h_0 = \min_{\lambda} |E_2(\lambda) - E_1(\lambda)| \quad (3.19)$$

implies an effective crossing width (henceforth denoted by  $w_0$  which is proportional to the height), guarantees that crossings found around the vacuum ansatz breakdown must converge towards the phase transition point. Pairwise avoided crossings can be assigned a well defined notion of height and width (see Appendix C for more details) and we will use them to construct a family of well-behaved measures of the width of the phase transition in the following discussion.

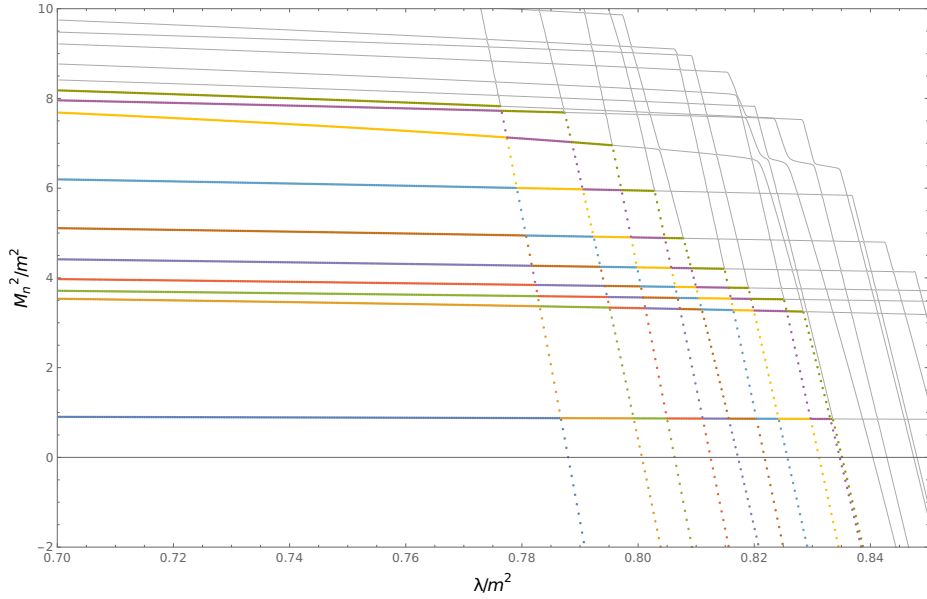


Figure 8: A plot of the lowest 20 eigenvalues along the line of slope  $g/\lambda = 2.0$ , near the phase transition. The LCT matrix has been diagonalized on a total of 1500 points in the plot range shown. The first 10 are shown in color, and the last 10 in gray continuous lines, to provide a cleaner visual representation. Note the closely avoided crossings between neighboring eigenvalues around the neighborhood of the point  $\lambda/m^2 = 0.789$  creating an "illusion" of high energy eigenvalues crashing down on lower energy ones.

## LCT measurements

We choose a particular direction in the  $(g, \lambda)$  coupling space ( $g/\lambda = 2.0$ ) and we diagonalize densely at truncation level  $\Delta_{\max} = 25$ . The result is shown in Fig. 8(a), and one immediately notes in the neighborhood of the coupling value where the first eigenvalue vanishes  $\lambda/m^2 = 0.789$  multiple avoided crossings take place. At the scale presented, the crossings look discontinuous, but upon a zoom-in, it is clear that the

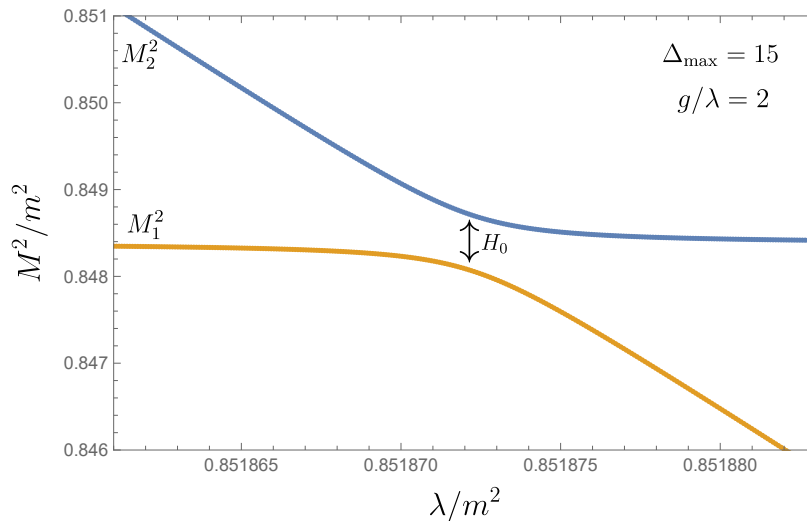


Figure 9: Plot of the width of the unique crossing between the two lowest energy levels vs. the truncation level. The approach to vanishing crossing width is exponential, roughly modeled by  $CW \sim e^{-\lambda\Delta^\gamma}$ , which is optimized given the data for  $\gamma \simeq 1.5$ .

features present no discontinuity as shown in the same Fig. 9. For the purposes of monitoring crossings, we only keep track of the eigenvalues obtained by diagonalization sorted in ascending order, and we say an avoided crossing between the  $n$ -th and  $n + 1$ -th eigenvalue has occurred when the difference between them approaches a (local or global) minimum. The crossings between this pair of eigenvalues is defined as the set of couplings that solve the equation

$$\mathcal{S}_n = \left\{ \lambda_0 : \left. \frac{d}{d\lambda} [M_{n+1}^2(s\lambda, \lambda) - M_n^2(s\lambda, \lambda)] \right|_{\lambda_0} = 0 \right\} \quad (3.20)$$

and we call these the  $(n|n + 1)$  crossings for short. Obtaining an explicit form for the eigenvalues in terms of the couplings and solving the above equation is generally intractable and we have to resort to numerical evaluations to approximate them. In the example shown in Fig. (8) we rely on obtaining dense enough measurements to detect that two eigenvalues are approaching each other, but the density of points that we have used is below the threshold required to completely resolve each individual crossing (for reference, in the example our resolution is  $\delta\lambda/m^2 \approx 2.7 \times 10^{-4}$  which much less than the typical crossing width  $w_0 \sim 10^{-7}$ ). This is not a hindrance at

detecting a crossing, however, since the average separation between crossings is much larger than our resolution. This guarantees that we will see every possible crossing in the low energy sector even with resolution a few orders of magnitude smaller than the average crossing width. Using appropriate fits, accurate estimates for all parameters that describe the crossings can be obtained from our analysis, including the height (see Appendix C). Finally, we notice that, at least for the lowest eigenvalues (small  $n$ ) the crossings sets grow linearly in size; in particular, the  $(n|n+1)$  crossing set is of size exactly  $n$ . This stems from the observation that higher order eigenvalues descend into the low energy sector without crossing each other, and it reinforces the "eigenvalue shower" picture.

To understand the behavior of the crossings, we first look at the scaling of the height parameter  $h_0$  with increasing truncation level. In particular, we choose to look at the (12) avoided crossing (between the first and second eigenvalue) due to the fact that these eigenvalues have a well-defined physical meaning for small and intermediate couplings and hence any avoided crossing between them indicates that the relationship between bound states and their respective towers of continuum states has been muddied by the strong interactions present. Additionally, the (1|2) crossing is unique and its position sequence with  $\Delta_{\max}$  is decreasing, making it a premium candidate for a truncation scaling analysis.

Obtaining measurements for  $h_0$  is relatively simple, due to the uniqueness of the minimum of the function  $D_{21} = M_2^2 - M_1^2$ , shown in Fig.11a: one can employ any convergent algorithm for finding the position of the global minimum with sufficient accuracy, and then the parameter  $h_0$  can be directly measured by diagonalizing at the reported value of the minimum. In our analysis, we use the golden section search algorithm to pin down the position of the minimum to perform direct measurements of the (12) crossing height for  $s = 2.0$  at various truncation levels, as seen in Fig. 10a. Of note is that the crossing gap vanishes exponentially with  $\Delta_{\max}$ . Interestingly, as we will explain below, this observation allows us to conclude that, purely from a probabilistic point of view, the amount of avoided crossings that require a three- or higher level treatment to be understood, is of measure zero as the truncation level

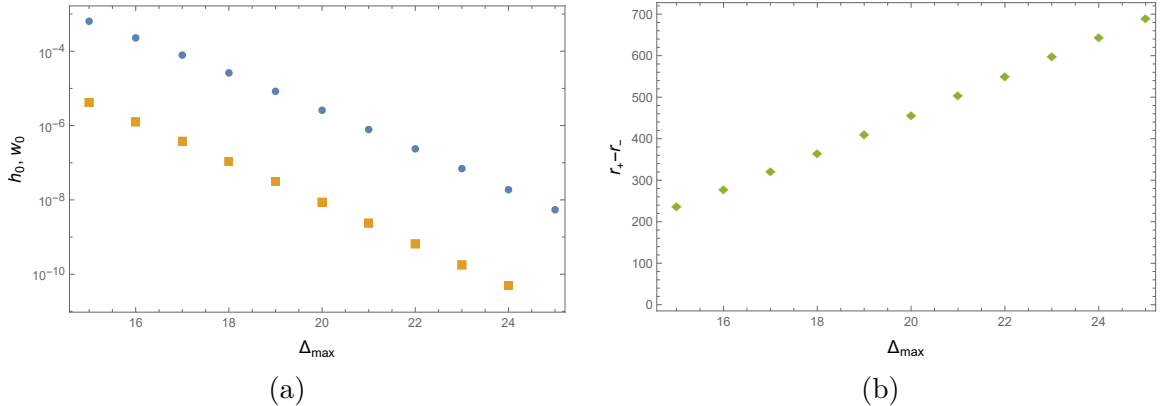


Figure 10: (a) Measurements of the height (blue) and the width (orange) of the crossing vs the truncation level. Both quantities decay exponentially. (b) The difference between the incoming and outgoing slopes of the avoided crossing. This quantity increases approximately linearly with the truncation level.

goes to infinity. To refine our understanding of the exponential decay, we fit the crude model

$$h_0 = A \exp(-B\Delta^\alpha) \quad (3.21)$$

For a given value of the exponent  $\alpha$ , the model fitted can be linearized, and the optimal solution is readily found via OLS. Then we can proceed to choose the exponent that minimizes the sum of squared residuals and we find that the best fit is given by an exponent  $\alpha = 1.5$ . The measurement of this exponent is however, sensitive to the  $\Delta_{\max}$  range that we choose for the fit, and we conclude that in order to get a more accurate estimate of the asymptotic behavior, data at higher truncations need to be included. We defer a more detailed study of this behavior to future work.

Information on the other parameters of the two-level crossing fit approximation, can be obtained in various ways, as explained in Appendix C. As stated there, the width of the crossing is not an independent two-level crossing parameter; it can be determined in terms of the crossing gap  $h_0$  and the asymptotic slopes of the two eigenvalues involved with increasing coupling. For a more concrete definition of the crossing width, we define it as the full width at half maximum of the function  $D''_{21}(\lambda)$ , where the primes denote derivatives with respect to the coupling along the line chosen. It is simple to show that the function has a single maximum for a two-level crossing

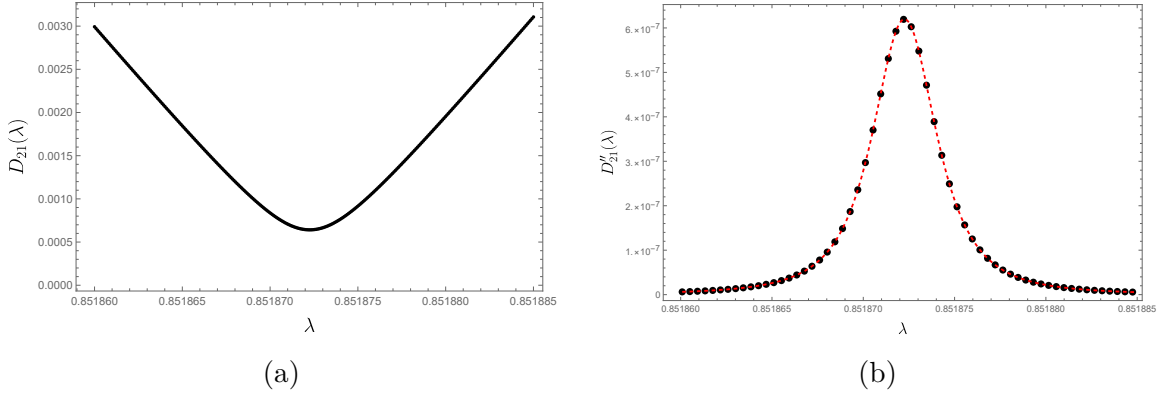


Figure 11: (a) Plot of difference between neighboring eigenvalues vs. the coupling. (b) Plot of the second derivative of said difference, the half-width of this function is well-defined.

at the same position as the center of the crossing defined in equation (3.20). The typical shape of the energy difference function and its second derivative is shown in Fig. 11, as measured for the (12) crossing for  $s = 2.0$ , at truncation level  $\Delta_{\max} = 15$ . A measurement of the width of the crossing requires very good resolution around the crossing center, on the order of 10% the value of the width itself, and can be subsequently achieved by fitting the data points to the functional form

$$(D_{21})^2 = A + B(\lambda - \lambda_c)^2 \quad (3.22)$$

where  $\lambda_c$  is the crossing center, that is already assumed to be known. A plot of  $D_{21}$  and its second derivative is shown in Fig. 11. For values of  $15 \leq \Delta_{\max} \leq 25$  we sample the two lowest mass matrix eigenvalues at couplings sufficiently close to the crossing center (somewhat surprisingly, the measurements can be spaced much wider than the crossing width itself and we still obtain a robust estimate of  $A, B$ ). From its definition as the FWHM of the second derivative of the energy difference, the crossing width is determined by the formula

$$w_0 = 2(2^{2/3} - 1)^{1/2} \sqrt{\frac{A}{B}} \quad (3.23)$$

A measurement of the crossing height and width is shown in Fig. 10a. Of note is

that they approximately decay at the same rate to leading order in  $\Delta_{\max}$ . On the other hand Fig.10b shows the difference of eigenvalue slopes far away from the crossing center and experimentally we find that it increases linearly with increasing truncation level. This happens because, as expected, the slope of the eigenvalue that is crashing down from the higher sectors increases with  $\Delta_{\max}$ , in accord to our expectation that the crash should become sharper as we approach the continuum limit. but since it is proportional to the ratio  $h_0/w_0$  as shown in equation (C.11), it follows that to next to leading order, the width decays faster than the height.

### Transition width

So far in our analysis, an outstanding problem has been to describe an appropriate measurement for understanding the accuracy with which LCT approximates the phase transition. As we have mentioned before, since we are merely approximating the continuum theory with a finite size truncation of its Hilbert space, the region where an instability is observed has some non-zero width. More specifically, in order for higher order eigenvalues to descend and destabilize the robust states of the system, such as the two-particle threshold, the bound states and eventually go negative, which means the structure of the LC ansatz vacuum has been compromised, the coupling has to be increased by a certain, relatively small amount. One can see this effect in Fig. 8. One could certainly argue here that violating positive definiteness of the Hamiltonian is a hallmark of a breakdown of the LC quantization assumptions and should serve as the de facto critical value for that truncation level. However, it is not correct to say that all couplings before the lowest eigenvalue hits zero have LCT spectra that make sense physically, since from semiclassical considerations we know that the theories on either side of the phase transition are gapped with at most two bound states, and this picture is violated at slightly lower coupling than the one where the vacuum ansatz becomes unstable. Another issue is that even though we should have an emergent  $\mathbb{Z}_2$  symmetry at the phase transition, LCT spectra do not show direct signs of states becoming exponentially degenerate with the scaling parameter

due to the fact that by explicitly breaking the symmetry we have effectively made a choice of vacuum- in infinite volume the tunneling between vacua is exponentially suppressed and as a result, lightcone cannot see the states built on top of the other vacuum. Multiple, fast converging, clustered avoided crossings remain, however, an indicator that the truncated basis is trying to reproduce these nonperturbative effects despite the lack of an appropriate vacuum structure. This is further reinforced by the observation that LCT simulations break down exactly on the expected curve for weak coupling.

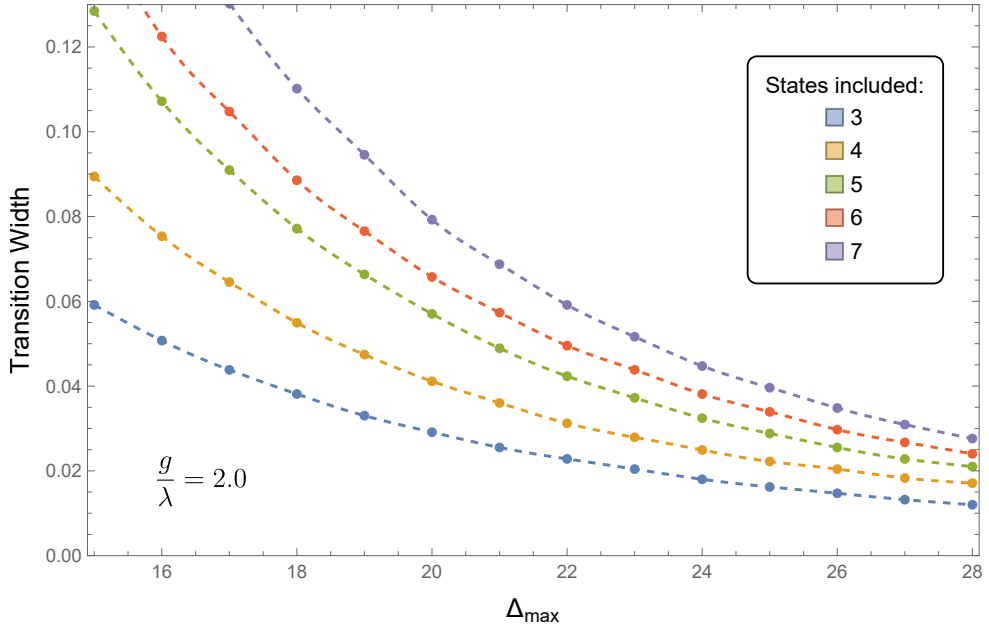


Figure 12: Plot of various possible definitions of the transition width with the truncation level. To generate this plot, along the line with slope  $g/\lambda = 2.0$  for each truncation level we progressively included crossings of more low lying eigenvalues, measuring the quartic coupling difference between the first and last crossing. As expected, the transition width slowly decreases as we approach the continuum limit. The dashed lines indicate interpolations between the data points, and are intended as an eye guide.

Operating provisionally, we take for the sake of argument an agnostic point of view as far as to where exactly LCT prefers the phase transition to be for a given truncation level, and we attempt to define a suitable measure for the width of the phase transition within the ansatz. There are two width proxies one can immediately devise; the first one is to measure the inverse slope of any of the rapidly descending eigenvalues at any point within the vicinity of the vacuum breakdown. This slope has the correct

units and can be roughly interpreted as the distance between the coupling strengths needed to cause a breakdown of the first excited state and the vacuum. Figure 10b is a good approximation for the slope at that point.

A more interesting family of width measurements can be obtained by considering all the crossings between the first few eigenvalues and reporting the range of that set. In notation, the family of widths can be defined as

$$W_m = \sup \bigcup_{k=1}^m \mathcal{S}_k - \inf \bigcup_{k=1}^m \mathcal{S}_k \quad (3.24)$$

This proxy should also go to zero as the transition window becomes smaller with increasing truncation. Indeed, our intuition is corroborated by numerical evidence, as shown in Figure 12. The fits of these quantities can be fit very well by the functional forms  $A/\Delta^\beta$ , with  $2.7 < \beta < 3.2$  depending on how many states have been included in the analysis. We see that as long as the size of the set of eigenvalues considered is much smaller than the order of the Hamiltonian at that truncation level, the width measurement above is a well-behaved estimator for the precision to which LCT approximates the phase transition.

We note here that avoided crossings are a good measure of transition width only in the weak and intermediate coupling regime. At strong coupling the eigenvalue shower picture breaks down, and the gap becomes zero before any significant crossings happen at the low energy sector. The behavior of crossings around the critical point is not as predictable as at weak coupling, so a different proposal is required to quantify the width. Such a measure is the distance between the zeros of two eigenvalues based on the definition (3.15):

$$W'_k = |s_\Delta^{(k)}(\theta) - s_\Delta^{(1)}(\theta)| \quad (3.25)$$

$$s = s_\Delta^{(k)}(\theta) : M_k^2(g_0 + s \sin \theta, \lambda_0 + s \cos \theta; \Delta) = 0 \quad (3.26)$$

We expect that this measure will work for both weak and strong coupling and we will pursue precise quantification of the width using this metric in an upcoming publication.

### 3.4 Bound states

One question that arises when examining a particular QFT is how to obtain information on the particle content of the theory. This piece of information is quite important, since it determines the states in the theory that are asymptotically free when separated far from one another, and hence can be used as scattering probes. Knowledge of the particle content can also place very strong constraints on other properties of the theory, like correlation functions and form factors. The spectrum of a generic massive QFT usually contains a low-energy discretum (usually comprised of a few states with masses  $m_1, m_2, \dots$ ) and the multiparticle continua that arise by acting with multiple creation operators for any of the particle types on the vacuum. The discrete states with energy below the lowest multiparticle threshold  $2m_1$  are stable and are the particle content of the theory. Discrete states with higher energy than that are generally metastable, since they can decay into the continuum with an arbitrarily small energy injection, if they have overlap with neighboring continuum states. It should be noted however, that this does not preclude the existence of stable bound states that are well within the multiparticle thresholds, but are protected by symmetry or integrability (as, for example, in the case of the  $\sigma$ -deformation of the Ising CFT, where 5 of the 8 scattering bound states are stable despite being above the lowest two-particle threshold).

Generally, finding bound states in a field theory is a non-perturbative problem. This is due to the fact that, more often than not, the theories we consider are perturbations of a free theory. Free theories have simple spectra, that may not be able to analytically deform into the spectra of even weakly coupled deformations thereof. Despite this, there is a class of bound states for which asymptotic expansions can be found: a weakly attractive potential can help two particles loosely bind together, which reduces the mass of the resulting state by an amount equal to the negative interaction energy of the pair. Some analytical work has been done in this direction in [43],[44],[82],[83], involving polynomial bosonic theories with a positive quadratic and a negative quartic term in the potential, while all other terms have been kept positive. It should be

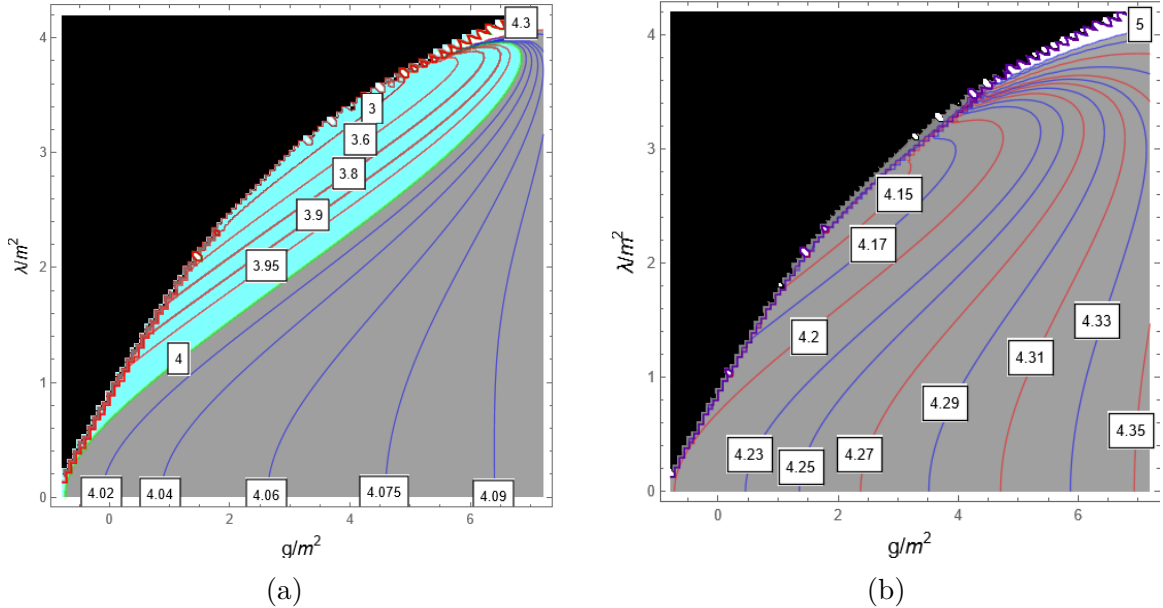


Figure 13: (a) A contour plot of the ratio of the two lowest eigenvalues in the spectrum,  $r_2 = M_2^2/M_1^2$  vs. the cubic and quartic couplings. The light blue coloring indicates the region where  $r_2 < 4$ , where a bound state forms below the two-particle threshold. In black is the region where the lowest eigenvalue has become negative. (b) Here we show the ratio  $r_3 = M_3^2/M_1^2$  for the same coupling values. We note that in the allowed region  $r_3 > 4$  which means that it always stays above the two particle threshold, hence confirming that a 3rd bound state below threshold never forms. The data here has been collected at truncation level  $\Delta_{\max} = 20$ .

clear that a negative  $\phi^4$  term is required to create a slightly attractive interaction, to guarantee the existence of the threshold bound state. We will study a  $\phi^6$  theory of exactly this form in the next chapter.

The theory we would like to study does not fall into the former category, since the potential contains a negative quadratic term and in order to study this perturbatively we need to perform a field shift, which generates a cubic term and hence explicitly breaks the  $\mathbb{Z}_2$  symmetry. Therefore we have to rely on a different technique to get an estimate for the trajectory of the near-threshold bound state. In fact, a semiclassical estimate has been obtained [64] for the spontaneously broken  $\phi^4$  theory by using integrability techniques. It can be argued that the stable bound state spectrum under threshold contains two states, using familiar techniques from elastic integrable scattering. The first one corresponds to a dressing of the one-particle state, while the

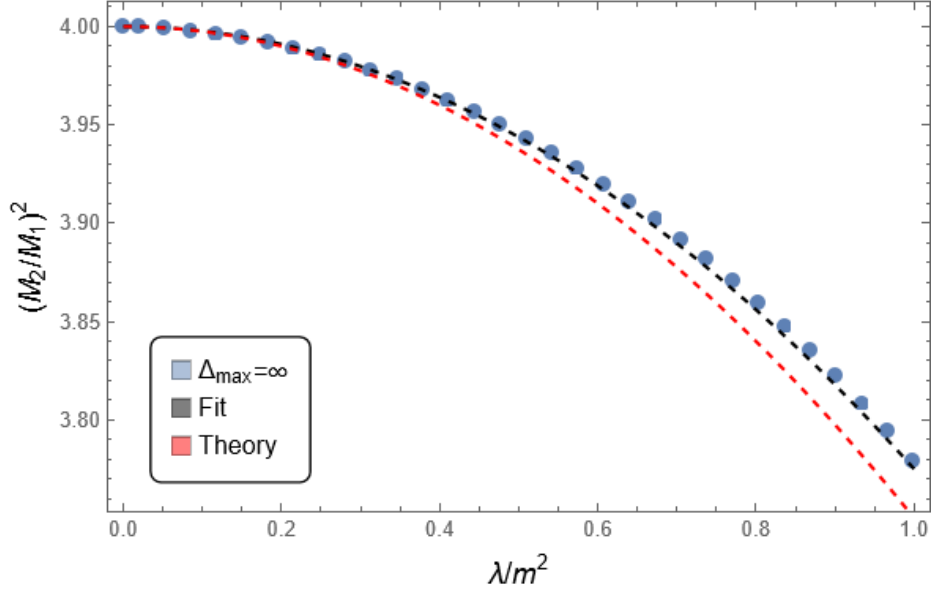


Figure 14: The ratio  $R = M_2^2/M_1^2$  of eigenvalues of the first two bound states of the truncated theory with  $g^2 = 3\lambda$ , shown at the truncation level  $\Delta_{\max} = 40$  and at infinite truncation level via an extrapolation. The prediction of (3.29) is shown by the red dashed line. The points shown are fit very well by a parabola with equation  $R = 4.0 - 0.225\lambda/m^2$  (black dashed line), which agrees with the semiclassical prediction at the 10% level.

second one can be adequately described as a loose bound state of two fundamental particles. It is predicted for the theory with potential  $\mathcal{V}(\phi) = \lambda\phi^4/4! - m^2\phi^2/2!$  that the trajectory of the first two bound states of the theory is given by

$$M_1 = 2M_{\text{kink}} \sin(n\pi\xi/2) \quad , \quad M_2 = 2M_{\text{kink}} \sin(n\pi\xi) \quad (3.27)$$

where  $M_{\text{kink}}$  is the kink mass and the quantity  $\xi$  given by the equation

$$\xi = \frac{\bar{\lambda}}{1 - c\bar{\lambda}} \quad , \quad \bar{\lambda} = \frac{\lambda}{2\pi m^2} \quad , \quad c = \frac{3}{2} - \frac{\pi}{4\sqrt{3}} \quad (3.28)$$

Expanding to leading order, the ratio of masses-squared is given by

$$\frac{M_2^2}{M_1^2} = 4 \left( 1 - \frac{\lambda^2}{16m^4} \right) + \mathcal{O}(\lambda^3 m^{-6}) \quad (3.29)$$

Verifying this asymptotic expansion is within the reach of LCT. From semiclassical considerations, analyzing the theory with Hamiltonian given by (3.10) can grant us access to some dynamical quantities associated with the negative mass  $\phi^4$  theory, if we look close to the semiclassical transition line  $g^2 = 3\lambda m^2$ .

To establish whether LCT has the potential to reproduce the phenomenology of a near threshold bound state, we conducted diagonalizations on a dense grid at low  $\Delta_{\max}$ , to map out the spectrum with good resolution. The results are shown in Fig. 13. The second eigenvalue has values consistently smaller than the two-particle production threshold for most of coupling space, except in the petal shaped region shown in the plot. For consistency, we also show the values of the third eigenvalue and we see that it remains consistently above threshold, confirming that only two bound states form. Thus, we expect that within the petal, the two bound states will converge to the correct infinite volume eigenvalue. Furthermore, the eigenvectors in the low energy sectors should converge as well, and in particular, their overlap with the  $T_{--} = (\partial\phi)^2$  component of the stress tensor should converge to a finite value, in direct contrast with continuum states, whose stress tensor overlap should vanish. At the edge of the petal the bound state is the precisely the one of the  $\phi^4$  theory with a negative mass term and a measurement of it is possible, and will be described in the next paragraphs. As is evident in the figure, the bound state only exists for a finite interval on the transition curve; this result is consistent with works [5][79], where it is argued that both bound states disappear for a strong enough value of the quartic coupling. In fact, in LCT the one-particle bound state also disappears at strong enough coupling, but this effect can only be seen approximately by extrapolation. Finally, showing the existence of a bound state at weak coupling in a quartic theory with a cubic term is, to our knowledge, a novel result.

We will attempt to quantify the bound state properties by exploring high truncations and extrapolating to infinite  $\Delta_{\max}$ . To this end we diagonalized matrices of  $\Delta_{\max}$  in the 20 – 40 range for a discrete set of points located exactly on that line, and all the points have small quartic coupling  $\lambda/m^2 < 1$ . Using the techniques described in previous subsections, we extrapolated the first and second eigenvalues to infinite

$\Delta_{\max}$ , using a simple fitting function  $M^2 = M_\infty^2 + A/\Delta_{\max}^c$ , where  $c$  is determined by the log of the discrete derivative of the data. The ratio values obtained for those points are shown in Figure 14. We see that there is a reasonable agreement between the prediction (3.29) and the simulations. The LCT data points are fitted very well by a parabola  $R = R_0 - R_2(\lambda/m^2)^2$ , and the target coefficient  $R_2 = 0.225 \pm 0.01$  agrees with the semiclassical prediction at the  $3\sigma$  level. Here, we estimated the error on the coefficient by varying the range of quartic couplings included in the fit.

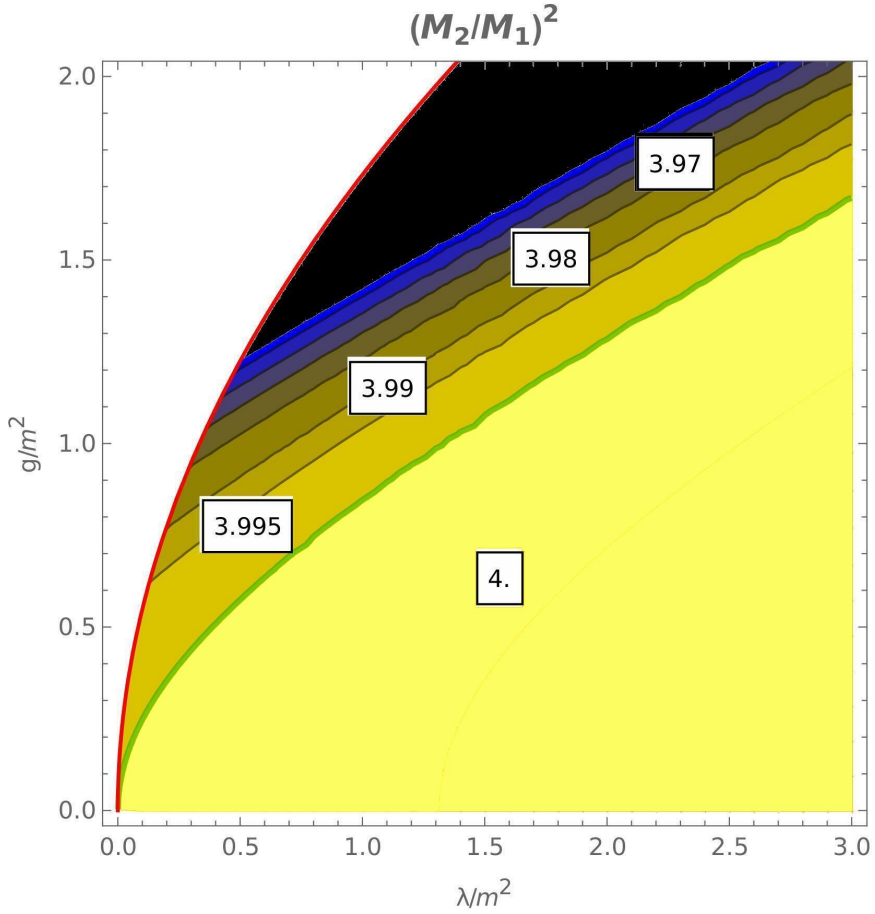


Figure 15: Contour plot of the ratio of the two lowest eigenvalues in the spectrum of the mass matrix  $M^2$ . For each point in this plot the ratio has been evaluated for  $\Delta_{\max}$  in the range 18 – 33 and extrapolated to infinity. For a large region (shown in bright yellow below the green line) the ratio extrapolates to exactly 4 to within errors of order  $\sim 10^{-4}$ , indicating the absence of a bound state. Above the green line, a bound state slowly descends through the 2-particle threshold. At the red line, and for small couplings, the ratio approaches the limiting values presented in Figure 14.

Having verified that LCT is producing reasonable results for the negative mass term  $\phi^4$

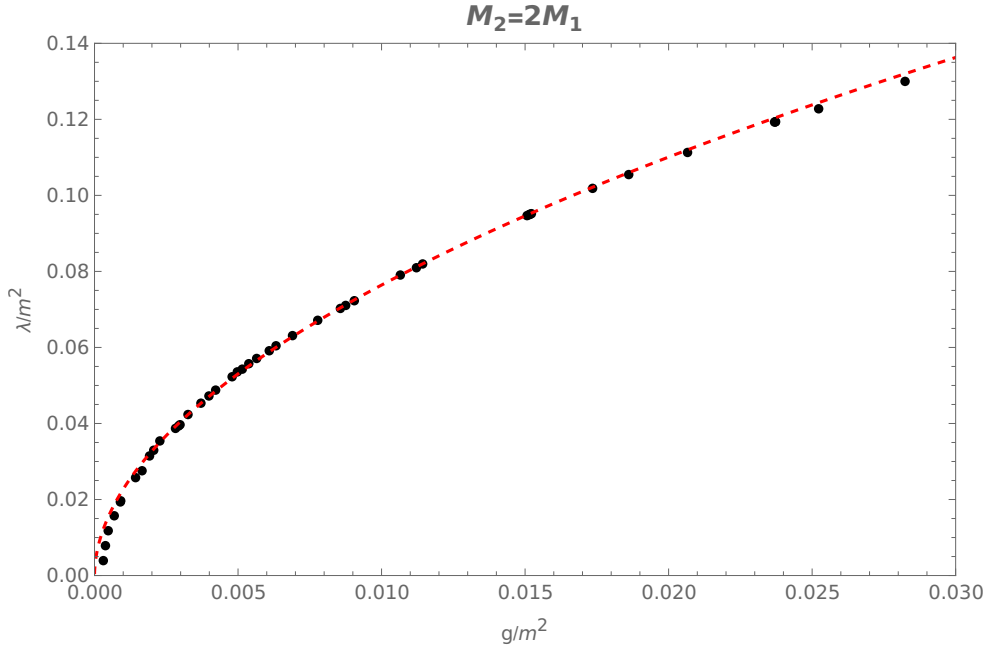


Figure 16: Isolated points at small coupling taken from the line  $M_2^2 = 4M_1^2$  indicated in Figure 15 by a solid green line. The line is fit best by a power law near the origin,  $g = A\lambda^\beta$ . The fit shows a clear preference for a square root type power law:  $\beta = 0.52 \pm 0.02$ . The coefficient  $A$  is of order unity, estimated at  $A = 0.87_{-0.02}^{+0.15}$  and is rather sensitive to the details of the fitting procedure.

gives us confidence that the bound state exists for values of the cubic coupling that are subcritical. We can now extend our search to include couplings away from the critical line, and we can take measurements at various  $\Delta_{\max}$  to quantify the convergence of the bound state in the limit of infinite truncation. We choose to sample the region  $\Omega = \{(g, \lambda) | g \leq \sqrt{3\lambda}, 0 \leq \lambda \leq 3\}$ , where the couplings are small enough to guarantee the existence of both bound states, and we do so in a dense rectangular grid of points, that allows us to draw precise contours of the bound state mass. A contour plot of the ratio of the first two eigenvalues  $M_2^2/M_1^2$  is shown in Fig. 15. In this plot, the values shown have been extrapolated to  $\Delta_{\max} = \infty$ . What allows this extrapolation to be accurate is the fact that, for weak coupling, the calculated values of the low lying spectrum converge very fast, leaving very little wiggle room for significant errors to develop; in most parts of the map, the bound state masses are accurate to 3 digits after the decimal point. Very importantly, the distinction between a threshold bound state and lack thereof is very clear: the bright yellow region shown below the green line in Fig. 15 is always consistent with the threshold of the single particle, carrying

very small errors of order  $\sim 10^{-4}$  for this range of couplings.

It is not surprising that LCT succeeds in reproducing the descent of a near-threshold bound state close to the line shown in green, since this transition is expected to be smooth. More precisely, in the non-relativistic limit, the quartic interaction dominates at leading order and is repulsive, but the cubic interaction produces subleading attractive contributions to  $2 \rightarrow 2$  scattering that for strong enough coupling allow the formation of a "two-particle" bound state. In non-relativistic QM, the emergence of a near threshold bound state in one dimension implies the energy dependence is approximately quadratic for weak coupling:  $E - E_{th} = \mathcal{O}(\lambda^2)$  (see [8]), and hence weakly coupled near-threshold bound states in QFT should emerge smoothly from the multiparticle continuum and their mass must be a smooth function of the couplings.

We can also quantify the shape of the green line, where the bound state first emerges. To probe this prediction for the shape of the curve where the bound state emerges, we isolate the points produced in Fig. 15 where the ratio of eigenvalues is exactly equal to 2. Those points are fit using a log-log OLS model

$$\log g(\lambda) = q \log \lambda + q' \tag{3.30}$$

to extract the leading power law. The result is shown in Fig. 16, and we see that the power law produces a good fit, and the optimal exponent is consistent with our expectations to within 5%. The best parameters are found to be

$$q = 0.52 \pm 0.02, \quad q' = 0.87 \pm 0.10 \tag{3.31}$$

As before, we tuned the number of points included to extract an error for the fitting procedure, which shows that the exponent is not too sensitive to the fit, while the constant of proportionality  $q'$  is moderately sensitive. Despite the sensitivity to the fitting details, the proportionality constant is smaller than the phase transition curve coefficient  $g/\sqrt{\lambda} = \sqrt{3}$ , thus leaving plenty of space for a bound state to arise at perturbative values of the coupling, connected to the Gaussian point at the origin.

This result doesn't seem like a coincidence, since, as seen in Fig. 15, the line where the bound state emerges is not the only one that looks like it has a square root shape at weak coupling. Lines of constant ratio  $M_2/M_1 = 2 - \epsilon$  also appear almost parallel to the emergence line, strongly suggesting that their shape can be described by equations of the form

$$\frac{M_2}{2M_1} = 2 - \epsilon \Rightarrow g^2 = a(\epsilon)\lambda + b(\epsilon) \quad (3.32)$$

We can argue that the most general, well-behaved function that can be defined in the sliver of coupling space defined by  $\gamma_1 \leq \frac{g^2}{\lambda m^2} \leq \gamma_2$ , that vanishes identically when  $g^2 = \gamma_1 \lambda m^2$  should have the form

$$\frac{M_2}{M_1} - 2 = \sum_{n=0}^{\infty} (\lambda/m^2)^n \left( \frac{g^2}{\lambda m^2} - \gamma_1 \right)^{q_n} f_n \left( \frac{g^2}{\lambda m^2} \right) \quad (3.33)$$

where  $f_n$  are functions that are nowhere vanishing. It is known that when  $g^2 \rightarrow \gamma_2 \lambda m^2$ ,  $\gamma_2 = 3$  the bound state binding energy is  $\mathcal{O}(\lambda^2)$ , which immediately implies that

$$f_0(\gamma_2) = f_1(\gamma_2) = 0 \quad (3.34)$$

Without making any further assumptions, this is about as much information as we can milk from this series expansion. However, if we demand additionally that this function is analytic at the origin, then the form of the functions  $f_n$  is severely restricted; they become polynomials of degree  $\deg f_n = n - q_n$ . Due to this restriction, it follows that  $f_0 = f_1 = 0$ . The expansion of the function to lowest order is given by following leading terms,

$$\frac{M_2}{M_1} - 2 = \left( \frac{\lambda}{m^2} \right)^2 \left[ a_1 \left( \frac{g^2}{\lambda m^2} - \gamma \right) + a_2 \left( \frac{g^2}{\lambda m^2} - \gamma \right)^2 \right] + \dots \quad (3.35)$$

The difference between the two terms is the shape of contours that they produce—only the latter term produces contours of the form (3.32). Hence, we conjecture that

to leading order the binding energy is given by

$$\frac{M_2}{M_1} = 2 - \left( a_0 \frac{\lambda}{m^2} - a_1 \frac{g^2}{m^4} \right)^2 + \dots \quad (3.36)$$

This conjecture can be justified by performing a non-relativistic approximation to the  $2 \rightarrow 2$  scattering, which allows us to compute the bound state energy by solving a one dimensional QM problem, of a particle in a potential. We attempt to fit the above relation to our data using the following linear model:

$$\left( 4 - \frac{M_2^2}{M_1^2} \right)^{1/2} = C + V_0 \frac{\lambda}{m^2} + V_1 \frac{g^2}{m^4} \quad (3.37)$$

And we find  $C = 0.008$ ,  $V_0 = 0.12 \pm 0.01$ ,  $V_1 = -0.20 \pm 0.02$ , with corresponding  $R^2 = 0.985$ . This is in reasonable agreement with (3.29), since it implies that on the SSB phase,

$$\frac{M_2^2}{M_{\text{gap}}^2} = 4 - r_2 \frac{\lambda^2}{m^4}, \quad r_2 \approx 0.23 \quad (3.38)$$

Also it implies that equation of the emergence line is  $g^2 = 0.6\lambda$ , which is qualitatively consistent with (3.31). The main reason for the quantitative discrepancy is the sensitivity of the LCT extrapolation procedure to small errors to the determination of the value of  $M_2$ . These errors are  $\mathcal{O}(10^{-4})$ , which may seem insignificant, but they are important for the accurate determination of the emergence line. This is especially true at weak coupling, since there such errors become important in comparison to the overall local variation of  $M_2$ . More dense data than the ones we obtained are expected to improve the linear fit, which includes taking data at points not too close to the origin so that the overall fit is less sensitive to extrapolation errors.

For more details, on how to derive (3.36) from a first principles approximate non-relativistic calculation, refer to Appendix D.

## 4 Phase transitions and bound states in $\phi^6$ theory

The  $\phi^4$  model is well studied in the quantum and the classical realm, due to its importance as a toy model in understanding Landau-Ginzburg theory. However, such a model cannot possibly be the last word on studying phase transitions. It has been known for some time that there are materials (like  $^3\text{He}/^4\text{He}$ ) that exhibit a variety of phase transitions eg. whole lines of first order transitions that end in critical endpoints or even tricritical points. This can be studied by enlarging the symmetry group of the model or increasing the degree of the polynomial interactions. The simplest model

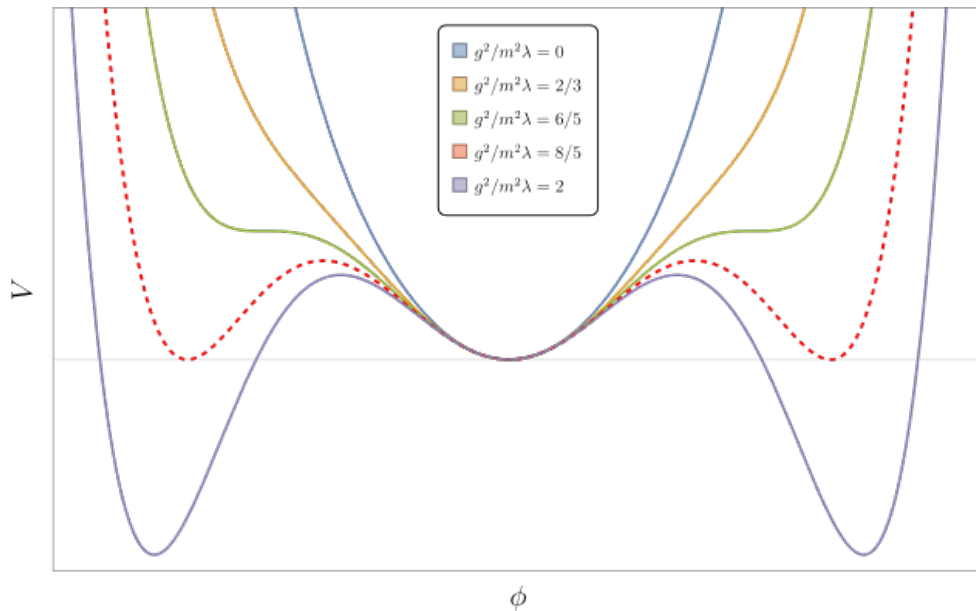


Figure 17: The form of the classical potential (4.1) for  $g < 0$ , with the other parameters kept constant. Note that two minima related to each other by symmetry descend at  $g^2 = 6\lambda m^2/5$  and the symmetry is broken at  $g^2 = 8\lambda m^2/5$ . Past that point we expect the LCT vacuum ansatz to fail at weak coupling.

that one can study in LCT that is bounded from below and has interesting first order transitions, that are perturbatively accessible from the Gaussian point is:

$$V(\phi) = \frac{\lambda}{6!}\phi^6 + \frac{g}{4!}\phi^4 + \frac{m^2}{2!}\phi^2 \quad (4.1)$$

This model is  $\mathbb{Z}_2$  invariant, but unlike the broken  $\phi^4$  theory, it already has interesting weak coupling phenomenology, without a negative mass term. This is a big advantage for LCT, since, as we will show, it means that the LCT Hamiltonian density can be taken to be identical in form as (4.1), without any further corrections. Said in other words, the above potential with  $\lambda, m^2 > 0$  has its true vacuum centered at  $\phi = 0$  at weak coupling, which allows direct application of our computational method.

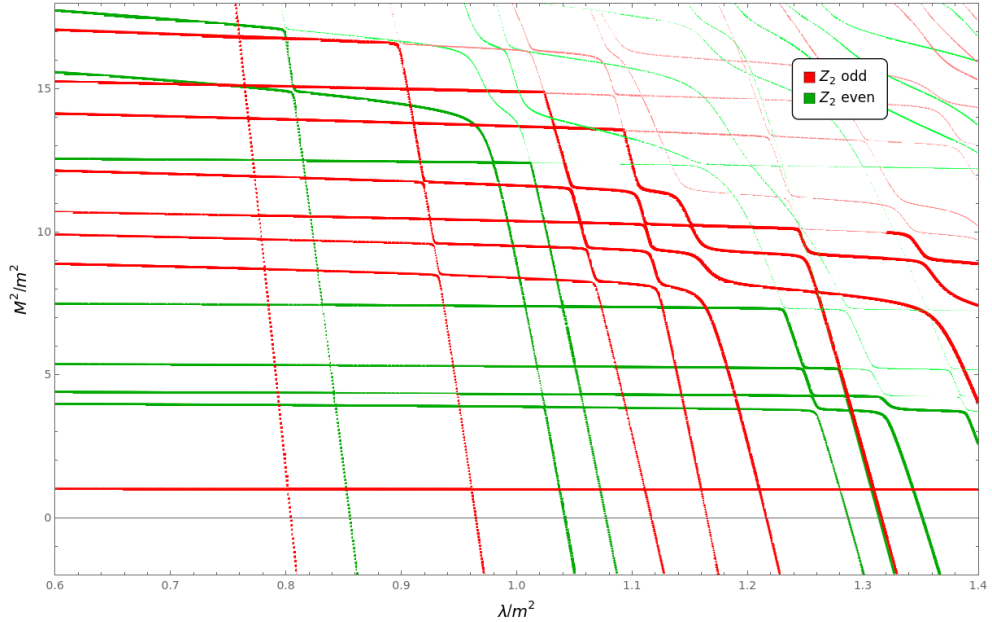


Figure 18: Isolated points at small coupling taken from the line  $M_2^2 = 4M_1^2$  indicated in Figure 15 by a solid green line. The line is fit best by a power law near the origin,  $g = A\lambda^\beta$ . The fit shows a clear preference for a square root type power law:  $\beta = 0.526_{-0.01}^{+0.03}$ . The coefficient  $A$  is of order unity, estimated at  $A = 0.864_{-0.02}^{+0.15}$  and is rather sensitive to the details of the fitting procedure. It is much smaller than the phase transition coefficient  $g/\sqrt{\lambda} = \sqrt{3}$ , thus leaving plenty of space for a bound state to arise at perturbative values of the coupling, connected to the GFP to the origin.

More specifically, the potential for  $g > 0$  has a single minimum at  $\phi = 0$ . For  $g < 0$ , we repeat the analysis cited above and we find that the potential always has a minimum at  $\phi = 0$  and the relevant phenomenology of the minima at various values of the ratio  $r = \frac{g^2}{\lambda}$  can be summarized as:

- $0 < r < 2/3$ : There is a unique minimum at  $\phi = 0$ .
- $2/3 \leq r < 6/5$ : There is still a unique minimum at  $\phi = 0$  and 4 inflection points

$$I_{\pm}^2 = -\frac{12g}{\lambda} \left(1 \pm \sqrt{1 - \frac{2}{3r}}\right)$$

- $6/5 \leq r < 8/5$ : There are still 4 inflection points now with 2 maxima  $\pm\phi_-$  and 2 minima  $\pm\phi_+$  satisfying  $\phi_{\pm}^2 = -10\frac{g}{\lambda} \left(1 \pm \sqrt{1 - \frac{6}{5r}}\right)$ . The absolute minimum is still at the origin.
- $r \geq 8/5$ : At  $r_c = 1.6$  the three minima  $(0, \phi_+, -\phi_+)$  coincide and at the quantum level  $\mathbb{Z}_2$  is broken. A first order transition occurs semiclassically, because the classical minima of the action change discontinuously.

A picture of the above phases of the classical potential can be seen in Fig. 17. It should be clear from the analysis in Chapter 3 that for small values of the coupling, we expect LCT to succeed in reproducing the first order transition line at  $g^2 = 1.6\lambda m^2$ . In order to study the properties of the lightcone Hamiltonian and connect them to the its equal time counterpart we write the naive LC expression

$$P_+ = \int dx_- \left( \frac{\lambda}{6!} \phi^6 + \frac{g}{4!} \phi^4 + \frac{m^2}{2!} \phi^2 \right) \quad (4.2)$$

We couldn't have applied this reasoning to the case of  $\phi^4$  theory, since the first-order transition takes place at  $m^2 = 0$ , which our method has no access to, due to a lack of an appropriate CFT that can potentially describe the emergent degrees of freedom on both sides. In this model, at least for low values of the couplings  $g, \lambda$  some properties of the phase transition taking place can be measured and compared to ET quantization by directly studying the naive Hamiltonian. However, the same critical line may also be approached in the LCT framework from a theory that has its  $\mathbb{Z}_2$  symmetry explicitly broken, resulting in a Hamiltonian of the form

$$H_{\text{broken}} = \sum_{k=2}^6 \frac{\lambda_k}{k!} \phi^k \quad (4.3)$$

It is not hard to see that the theory contains this transition, by writing out the form

of the critical classical theory  $V_c = \lambda\phi^2(\phi^2 - v^2)^2$  and shifting variables to  $\phi' = \phi - v$ , ignoring a constant shift in the energy. This shows that the subspace of coupling space where the potential exhibits the same transition as (4.1) is two dimensional:

$$(\lambda_6, \lambda_5, \lambda_4, \lambda_3, \lambda_2) = \lambda(1, 6v, 13v^2, 12v^2, 4v^4) \quad (4.4)$$

This special property of the  $\phi^6$  model allows perturbative SSB to be studied from both the unbroken and the explicitly broken phase. The model contains many other semiclassical transitions with higher dimensionalities, which are outlined in Appendix B. In this work, we will focus on the study of the unbroken phase of the model given by (4.1), and will leave the approach from the unbroken phase for future work.

## 4.1 Effective LC description

To apply LCT to this particular field theory, one needs to understand the structure of the effective Hamiltonian first. As usual, the zero modes are explicitly thrown away, despite the fact that they are constrained by the dynamics of the higher momentum states. This leads to the need to change the lightcone Hamiltonian to account for those states. In 1+1 bosonic field theories with a polynomial potential, to all orders in perturbation theory the effect of zero modes is to just renormalize the coupling of the terms that already exist in the Hamiltonian except for the highest order term  $n_{\max}$  by some function of the VEV's  $\langle 0|\phi^n|0\rangle$ , up to some  $N < n_{\max}$ , determined by the equations of motion. This fact is important, because it indicates that we can simulate the field theory in question by diagonalizing a lightcone Hamiltonian of the same exact form as the equal time Hamiltonian:

$$H_{LC} = \int dx_- \left( \frac{m_{LC}^2}{2!} \phi^2 + \frac{\lambda_{4,LC}}{4!} \phi^4 + \frac{\lambda_{6,LC}}{6!} \phi^6 \right) \quad (4.5)$$

In view of this fact, we can think of field theories on the lightcone as effective theory versions of their equal time counterparts: the LC field theory with a trivial vacuum is trying to simulate the ET field theory in spite of the lack of vacuum structure. Because of the lack of vacuum structure, VEV's are not observable in the LC version of the theory, but there exists a mapping between the two theories! One may think that, given our inability to measure VEV's in LCT this would render the scheme useless, but this could not be further from the truth- the vacuum contents of LC are constrained by the non-zero momentum sectors. Due to this, one could argue that all the dynamical information we need about the vacuum is hidden in the spectrum, albeit in a complicated manner. For certain theories, this turns out to be a good approximation. In case this assumption holds, we expect to obtain a qualitatively similar phase diagram as the one of the ET theory, but warped by some functional relation

$$\begin{aligned}
\lambda_{6,LC} &= \lambda_{6,ET} \\
\lambda_{4,LC} &= f(\lambda_{6,ET}, \lambda_{4,ET}, m_{ET}^2) \\
m_{LC}^2 &= g(\lambda_{6,ET}, \lambda_{4,ET}, m_{ET}^2)
\end{aligned}
\tag{4.6}$$

We can quantify this more precisely in perturbation theory using equation (3.6). We can unfold this formula by noting that, it is equivalent to the following substitution

$$\frac{\phi^n}{n!} \rightarrow \sum_{k=0}^n \frac{\phi^{n-k}}{(n-k)!} \frac{\langle 0|\phi^k|0\rangle}{k!}
\tag{4.7}$$

which to be performed by substituting the rule into the LC Hamiltonian expression. With this replacement rule at hand, we can construct the lightcone effective Hamiltonian from it's equal time counterpart to all orders in perturbation theory by substituting the above into the ET interaction potential:

$$\mathcal{H}_{LC} := \sum_{k=0}^N \lambda_{k,LC} \frac{\phi^k}{k!} = \sum_{n=0}^N \lambda_{n,ET} \sum_{k=0}^n \frac{\phi^k}{k!} \frac{\langle 0|\phi^{n-k}|0\rangle}{(n-k)!}
\tag{4.8}$$

Collecting terms in the RHS and equating powers of the field, we obtain the LC-ET correspondence equations

$$\lambda_{k,LC} = \sum_{n=0}^{N-k} \lambda_{k+n,ET} \frac{\langle 0|\phi^n|0\rangle}{n!}
\tag{4.9}$$

We expect this relation to hold reasonably well away from phase transitions, as shown in [40], where the validity of the formula has been benchmarked using perturbative equal time results for the VEV  $\langle 0|\phi^2|0\rangle$  from [81] and LCT results from our group and it was found that LC agrees with ET quantization to within the perturbative expansion's region of validity.

Focusing on a sextic  $\mathbb{Z}_2$  invariant interaction in the unbroken phase, the relationship between LC and ET couplings is given by

$$\begin{aligned}
\lambda_{6,LC} &= \lambda_{6,ET} \\
\frac{\lambda_{4,LC}}{4!} &= \frac{\lambda_{4,ET}}{4!} + \frac{\lambda_{6,ET}}{4!} \frac{\langle 0|\phi^2|0\rangle}{2!} \\
\frac{m_{LC}^2}{2!} &= \frac{m_{ET}^2}{2!} + \frac{\lambda_{4,ET}}{2!} \frac{\langle 0|\phi^2|0\rangle}{2!} + \frac{\lambda_{6,ET}}{2!} \frac{\langle 0|\phi^4|0\rangle}{4!}
\end{aligned} \tag{4.10}$$

It should be noted that this relationship only holds true when the odd VEV's  $\langle 0|\phi^{2k+1}|0\rangle$  vanish identically. This is guaranteed in the unbroken phase, but the moment we allow those VEV's to be non-zero by breaking the above discrete internal symmetry, we open ourselves to the possibility of generating cubic and quintic terms in the effective Lagrangian.

## 4.2 LCT simulations

Using the LC left-handed basis of a free boson field as a starting point, we can compute matrix elements for the LC Hamiltonian (4.5) and diagonalize it for various values of the couplings. The procedure for calculating matrix elements is given in Chapter 2 and is very similar to the  $\phi^4$  model. Normalizing the mass to unity, we are expressing all quantities that we are measuring in units of  $m^2$ .

Firstly, we perform low  $\Delta_{\max}$  simulations to establish the existence of a breakdown curve for the vacuum ansatz and potential bound states. At truncation level  $\Delta_{\max} = 20$  we obtain the lowest lying eigenvalues of the squared-mass matrix, denoted by  $M_n^2$ , as they appear after sorting them in ascending order. The first eigenvalue clearly can be interpreted as the massgap for weak and intermediate coupling, and if it attains negative values this can be considered as a failure of the vacuum ansatz in place, and hence an indicator of a significant rearrangement of the vacuum sector and, therefore, also a phase transition. The ratio of the first two eigenvalues should be equal to 4 whenever there is a single massive bound state in the theory (usually seen after extrapolation to infinite  $\Delta_{\max}$ ). If smaller, it can be considered as a smoking gun for the appearance of one or more bound states under threshold. We plot  $M_1^2$  and  $M_2^2/M_1^2$  against their dependences on the quartic and sextic couplings in Figures 19a,19b.

As we are looking for a proof of principle/sanity check with an cheap computation, we have not included the entire LCT accessible region, but a more in depth analysis will be pursued in later sections. Indeed, as seen in the contour plots with this moderate truncation size, we can easily confirm that much like the  $\phi^4$  model, the  $\phi^6$  LCT model definitely has a phase transition, as there is a curve where the gap is zero. Although it is not visible in Fig. 19a, it turns out that this LCT model's accessible coupling space is also bounded. From Fig. 19b we notice that, additionally, a single near threshold bound state appears at negative values of the coupling,  $\lambda_4 < 0$ . Indeed, as we will explain later, this bound state arises due to the fact that  $-\phi^4$  is an attractive interaction which allows a bound state to form for small and intermediate values of

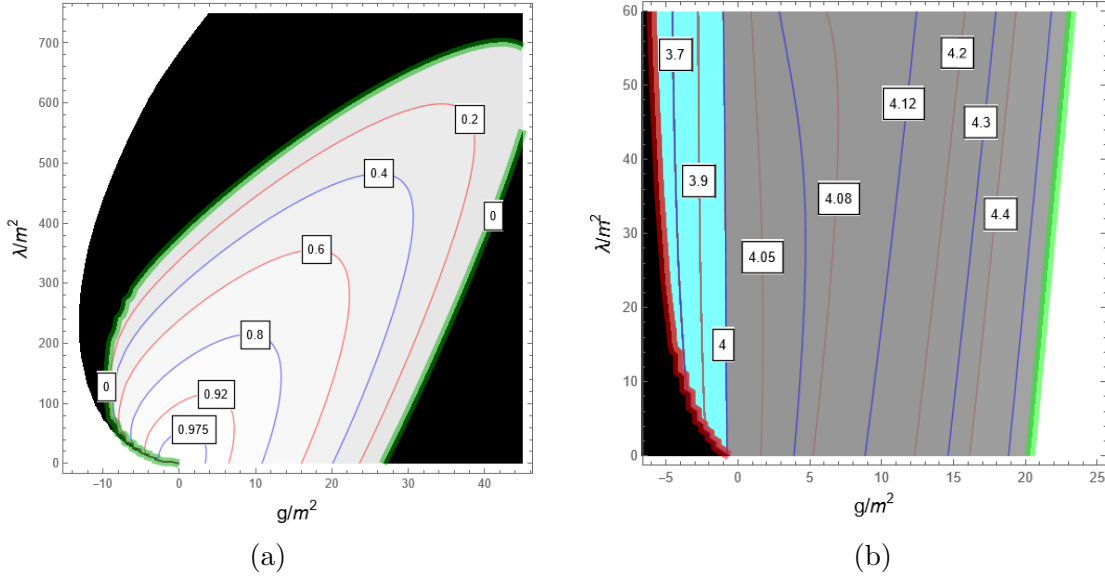


Figure 19: (a) Plot of the massgap  $M_1^2/m^2$ . The curve in green, where the gap is zero, showcases the region where the LCT vacuum ansatz fails. The gap is a smooth function of the couplings in the shown region. (b) Plot of the threshold ratio  $M_2^2/M_1^2$ . The expected value of the ratio  $M_2^2/M_1^2 = 4$  is observed to hold at small and intermediate couplings to within 5% (more accurate threshold estimates require extrapolations). The region where  $M_2^2/M_1^2 < 4$  and the bound state emerges is colored in bright blue. The bound state persists even after extrapolating to infinite matrix size. The thick red and green lines show the position of the (1|2) avoided crossing.

the couplings. The bound state seems to have qualitatively the same behavior as the one in the  $\phi^4$  model; it persists in the SSB theory with 3 minima along the transition curve and it disappears at some, relatively large value of the sextic coupling.

Now that we have established the existence of a breakdown in LCT computationally, we can proceed to study the various regions of the phase diagram separately, at the highest truncation levels possible. We will start with the parts of the phase diagram where analytical results are known, to verify LCT is reproducing the physics correctly. We first look at the weakly coupled SSB phase transition; according to the semiclassical analysis in the beginning of the chapter, we expect the lightcone ansatz breakdown to occur on the curve  $g = -\sqrt{\frac{8\lambda}{5}}$ . We use a simple root finding algorithm to detect the zeroes of the massgap in various directions in the  $(g, \lambda)$  plane, that obey the restrictions  $g < 0$  and  $\frac{|g|}{4!}, \frac{\lambda}{6!} \ll m^2$ , up to truncation level  $\Delta_{\max} = 36$ . The resulting zero gap curves are shown in Fig. 24. The curves at finite truncation

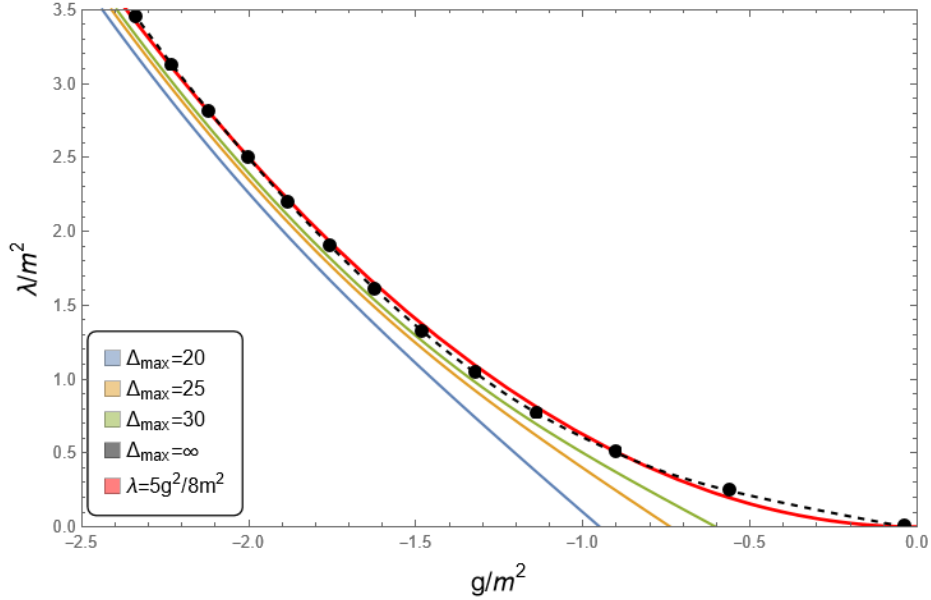


Figure 20: Plot of the curves  $M_1^2(g, \lambda) = 0$  for the region where the continuum theory exhibits a semiclassical first order transition. The transition is expected to happen at  $\frac{\lambda}{m^2} = \frac{5}{8}(\frac{g}{m^2})^2$  (red line). As  $\Delta_{\max}$  increases the curves move closer to the expected transition. An extrapolation to infinite truncation level based on a simple model using data up to  $\Delta_{\max} = 36$  is shown in black, and the comparison with the theoretical prediction shows excellent agreement.

approach, rather slowly, the expected phase transition line. Due to computational limitations, to gauge whether the locations of the zero gap curves actually converge to the expected values, we extrapolate their positions along each direction using a simple power law model. More specifically the data we obtain are given by  $(\Delta_k, s_j(\Delta_k))$ , where  $s$  denotes the roots of the equation

$$s_j(\Delta_k) : M_1^2(s_j(\Delta_k) \cos \theta_j, s_j(\Delta_k) \sin \theta_j; \Delta_k) = 0 \quad (4.11)$$

and  $M_1^2(g/m^2, \lambda/m^2)$  is the gap as a function of the adimensional couplings. Then the dataset is extrapolated according to the simple power law model

$$s_j(\Delta) = s_j(\infty) + \frac{s_j'}{\Delta^{\beta_j}} \quad (4.12)$$

where the exponent  $\beta_j$  is found by performing OLS on the discrete derivative of the data (see Chapter 3). In this range of couplings, the exponents take values in the

range  $2 \lesssim \beta_j \lesssim 3$ , and the extrapolated zero gap points  $(s_j(\infty) \cos \theta_j, s_j(\infty) \sin \theta_j)$  are shown in black. We note that the agreement with the semiclassical predictions for this range of couplings is excellent, to within about 5% accuracy.

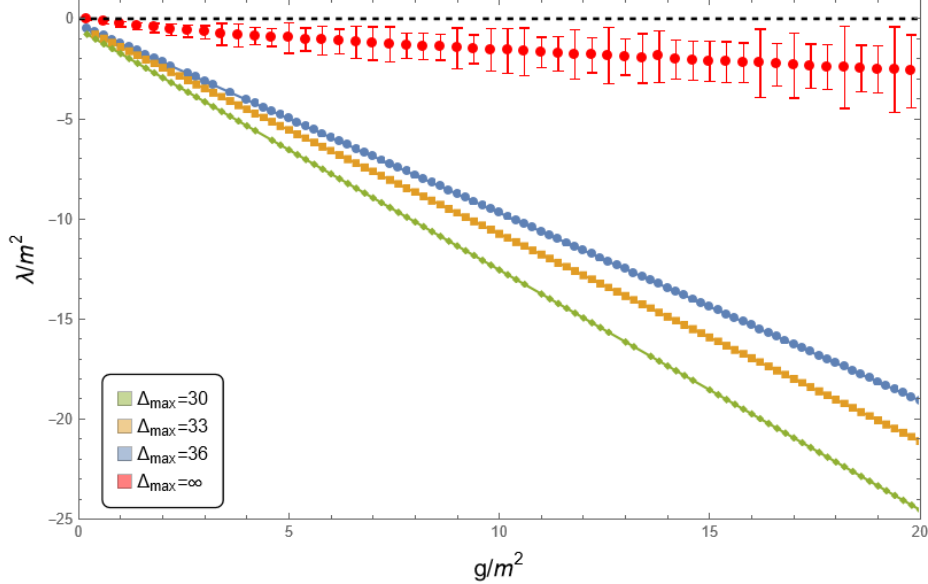


Figure 21: Plot of the curves  $M_1^2(g, \lambda) = 0$  for the region  $\lambda < 0$ . The continuum theory presents with a first order transition at  $\lambda = 0$  (black dashed line). As  $\Delta_{\max}$  increases the curves move rapidly towards the transition line. An extrapolation to infinite truncation level based on a power law iterated once using data up to  $\Delta_{\max} = 36$  is shown in red dots. The extrapolated transition points are to within 1-2 error bars from the predicted continuum transition.

A non-perturbative transition that we can attempt to understand in the context of LCT is the obvious first order transition when  $\lambda = 0$ . As the model passes to negative sextic couplings, the Lagrangian becomes unbounded below, and the VEV will experience a discontinuous transition in the continuum theory. This effect is invisible to perturbation theory and hence represents an important sanity check for a non-perturbative method to reproduce. To achieve this, we find the part of the zero gap curve that lies in the lower half plane  $\lambda < 0$ , at various truncation levels. We see that the curve lies far from the expected continuum transition, and that it requires much higher truncation levels to convincingly reproduce it. Yet again, a reliable extrapolation procedure comes to the rescue; we extrapolate the positions of the gap along lines  $g = \text{const}$ , using a similar power law model as (4.12). The data we obtain are given by  $(\Delta_k, \lambda_j(\Delta_k))$ , where  $s$  denotes the roots of the equation

$$\lambda_j(\Delta_k) : M_1^2(g_j, \lambda_j(\Delta_k); \Delta_k) = 0 \quad (4.13)$$

The data is extrapolated using the power law model

$$\lambda_j(\Delta) = \lambda_j^{(1)}(\infty) + \frac{\kappa_j}{\Delta^{\gamma_j}} \quad (4.14)$$

The exponents  $\gamma_j$  decrease as the quartic coupling gets stronger, indicating weaker convergence; they lie in the range  $1 \lesssim \gamma_j \lesssim 2$ . After extrapolation, the resulting curve is indeed closer to the expected value. Still, it is not clear whether LCT produces a quality result here; we need a way to obtain an reliable estimate on the error of the method to argue that LCT reproduces the phase transition in the continuum limit.

In this particular case, we can improve our estimate. First, we note that the OLS estimates of the exponent  $\gamma_j$  inherently have a bias towards the data they were calculated from; as we vary the maximum achievable truncation of our data  $\bar{\Delta}_{\max} = \max_i \Delta_i$ , we notice that the exponent continually changes, drifting towards its limiting value. This allows us to obtain a sequence of the zero gap position estimators by fitting to smaller data sets  $(\Delta_i, \lambda_j(\Delta_i))$  such that

$$\hat{\lambda}_j^{(p)} : \lambda_j(\Delta) = \hat{\lambda}_j^{(p)} + \frac{\kappa_{jp}}{\Delta^{\gamma_{jp}}} \quad , \quad \Delta_i \leq \bar{\Delta}_p \leq \bar{\Delta}_{\max} \quad (4.15)$$

In this notation, it is easy to see that  $\hat{\lambda}_j^{(\max)} = \lambda_j^{(1)}(\infty)$ : the estimator we obtain from fitting a power law model to the maximum sized dataset is the same as the one obtained in (4.14). If the trend that the exponents follow is monotonic and well-behaved, we can use another quasi-linear model to fit the data points  $(\bar{\Delta}_p, \hat{\lambda}_j^{(p)})$ :

$$\hat{\lambda}_j^{(p)}(\Delta) = \lambda_j^{(2)}(\infty) + \frac{\kappa'_j}{\Delta^{\gamma'_j}} \quad (4.16)$$

This procedure can be repeated as many times as one wishes, but in practice, even

with minimal noise, one cannot perform more than a few iterations of the method before the estimates begin diverging from their limiting value. The main theoretical reason why this iteration does not have a fixed point for real applications is the fact that even very small subleading corrections to the leading power law can lead the iteration process away from the fixed point; in practical applications, the amount of data one can obtain is also finite, and with each iteration, the size of the data set at each iteration strictly decreases, which eventually will lead to inaccuracies in the fitting process. However, we have benchmarked the method in idealized situations, where the noise comes from subleading corrections only, and we noticed that as one takes better data at larger truncations, the iteration output sequence  $\lambda^{(n)}(\infty)$  lingers around the true coupling for an increasing amount of iterations, before it eventually diverges. This process is somewhat analogous to calculating corrections to the limiting power law exponent induced by finite truncation data, which could also have been used to generate an iterative scheme, but we found that, with our datasets, it did not work as well.

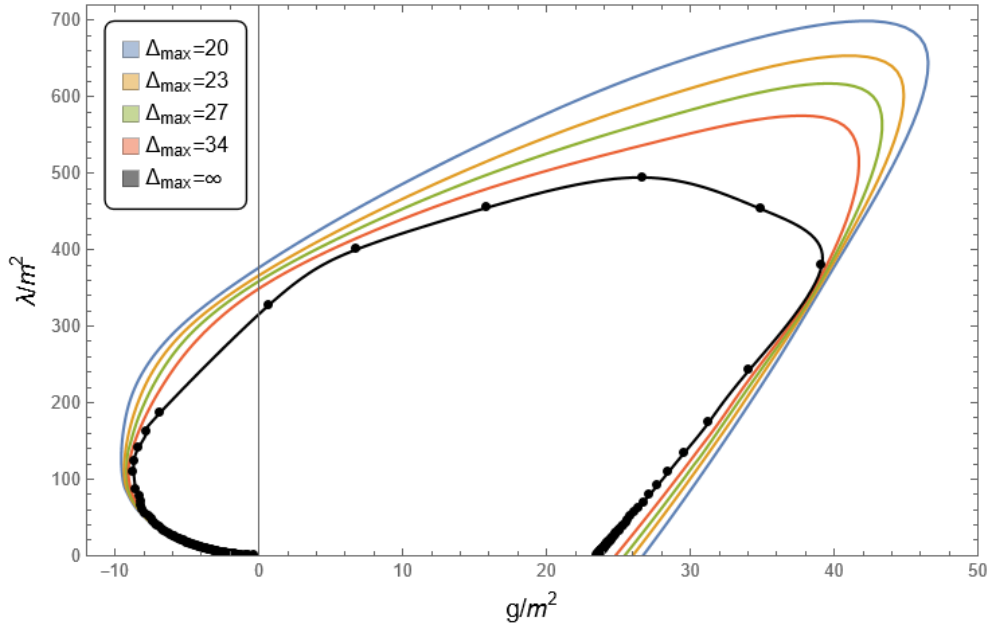


Figure 22: Plot of the zero gap lines for various truncation levels (in color). An extrapolation of said curves to infinite truncation is shown in black, and is the LCT prediction for the position of the phase boundary. The convergence is faster for small sextic coupling and slower for large sextic coupling.

With this technical improvement, the LCT estimate for the first order phase transition line  $\lambda = 0$ , is shown in Fig. 21, along with an associated error bar. Since there is no theoretical guarantee that this procedure will converge, we cannot deem this a rigorous estimate, and therefore we can reason that the difference between estimates  $|\lambda_j^{(2)}(\infty) - \lambda_j^{(1)}(\infty)|$  is a measure of how accurately LCT reproduces the actual phase transition. We report that value as an error bar in our plot, centered around the second order estimates.

Finally, the most computationally expensive task is to map out the entirety of the phase diagram of the theory. This we can do using equations (4.11), (4.12) but this time unrestricting the angles to take values in the interval  $\theta_j \in (0, \pi)$ . The result is shown in Fig. 22. Given the strongly coupled nature of the vast majority of the phase diagram, the convergence of the zero gap curves is relatively slow, and thus we expect a large systematic error to the convergence of strongly coupled directions; in fact we expect that the ansatz failure occurs *closer* to the origin than shown in the plot. Due to the slow convergence, we are also not able to correct for the finite truncation bias. Hence we expect that the accuracy of our data is within 10% in the upper parts of the plot.

### 4.3 Crossings

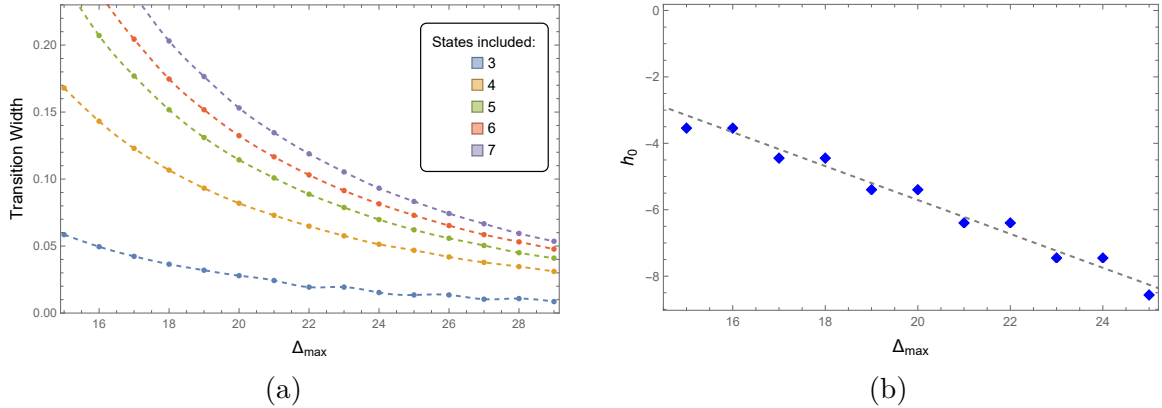


Figure 23: (a) Measurement of the transition width in the  $\phi^6$  model, in the direction  $g = -2.0\lambda$ , for various truncation levels. We see a clear sharpening of the phase transition measurements as the truncation level increases. (b) Plot of the height of the (1|2) crossing for the same direction vs. the truncation level. The height and the width of the crossing decay exponentially with  $\Delta_{\max}$ .

As we mentioned in the case of the  $\phi^4$  model, we need a way to quantify the approach to the phase transition, since just from zero massgap data it is hard to tell whether the LCT scheme has converged sufficiently in any given region of the phase diagram. The associated power law exponent describing the convergence in  $\Delta_{\max}$  may give us hints as to whether the convergence in a certain regime is fast or slow, but as we have seen already in the  $\phi^4$  model and even more prominently in  $\phi^6$ , the exponents are not monotonic with distance from the Gaussian point. In chapter 3, we devised a method to measure an effective width associated with the sharpness of the phase transition as seen by a finite LCT matrix computation, and we showed that this quantity decreases as the truncation level increases. Finally, the transition width measures also approximately decay as a power law in  $\Delta_{\max}$  and the infinite truncation extrapolations indicate that the entire family of transition widths converge to zero at infinite truncation.

In the sextic potential model, we see no deviation from the aforementioned characteristics. As seen in Fig. 23, the transition width based on the lowest neighboring eigenvalue crossings as defined by equations (3.20), (3.24) scales down very nicely in the perturbative regime; the vacuum ansatz breakdown happens over a, quickly

narrowing, region of couplings. Furthermore, we monitor the (1|2) crossing as the truncation increases (it is the one of the few eigenvalue crossings that maintains a robust physical significance as truncation size increases) and we see that its height- and therefore its width- decreases exponentially fast in  $\Delta$ , a hallmark of a well converging phase transition representation.

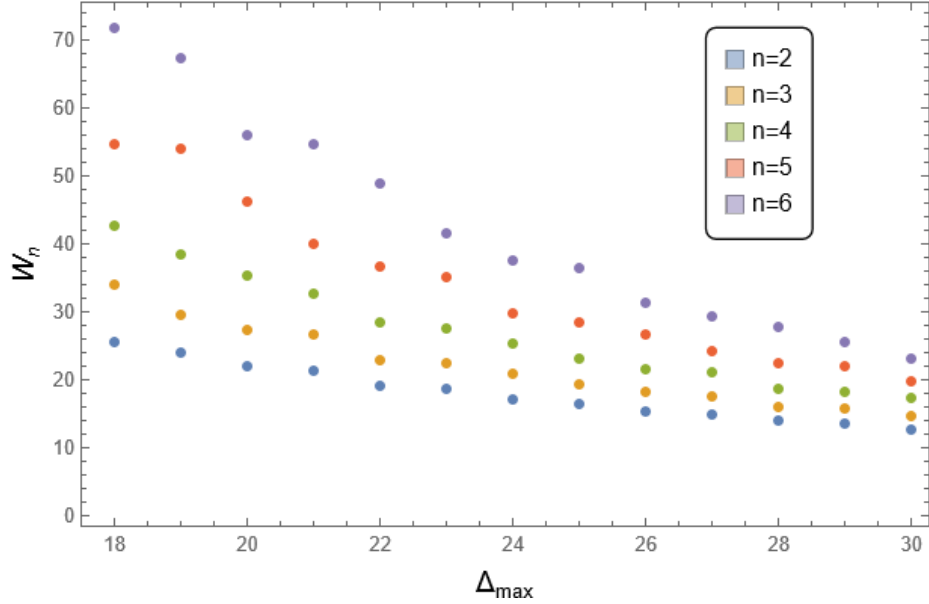


Figure 24: Plot of the width of the phase transition at strong couplings, as defined in (4.18), vs the truncation level. The data has been taken on the direction  $g = 0.1\lambda$ , where the model is strongly coupled ( $\lambda_c \approx 400$ ). There is an overall downward trend for the entire family of measures. We also note a slight instability in the measurements due to the low truncation level.

We also need to understand the size of the phase transition at strong coupling; there the situation is a bit different, in the sense that the vacuum ansatz breaks down due to "pressure" from high particle sectors and not because high particle sectors collapse onto lower ones. We believe that at weak coupling, LCT is trying to reproduce the phenomenology of a first order transition by developing a sharp feature, while at strong positive couplings it is likely that the transition is second order, and LCT is trying to reproduce a massless spectrum with no such sharply discontinuous feature; hence the behavior of eigenvalues near the vacuum ansatz breakdown point is much less steep than at weak coupling. Due to this, we cannot use neighboring eigenvalue crossings to understand the width of the phase transition; the crossings at strong

coupling happen at negative values of the mass, and their behavior is erratic. Instead, we can utilize the distance between the points where eigenvalues hit zero as a measure of the width of the phase transition. We define as usual the position of the unique zero of an eigenvalue in some direction  $s = \frac{g}{\lambda}$

$$\lambda_n : M_n^2 \left( \frac{s\lambda_n}{m^2}, \frac{\lambda_n}{m^2}; \Delta \right) = 0 \quad (4.17)$$

and our definition of the width is the distance between zeroes

$$W_n = |\lambda_n - \lambda_1| \quad (4.18)$$

Indeed, this measure has the correct behavior as  $\Delta_{\max}$  increases; the eigenvalues close to zero have to get closer to each other if they are to reproduce a massless sector. Extracting quantitative statements from it is rather difficult, since much higher truncations are required for this measure to stabilize; strong couplings generally require higher truncation levels to produce more stable results.

## 4.4 Bound states

Another question that arises when examining a particular QFT is how to obtain information on the particle content of the theory. This piece of information is quite important, since it determines the states in the theory that are asymptotically free when separated far from one another, and hence can be used as scattering probes. Knowledge of the particle content can also place very strong constraints on other properties of the theory, like correlation functions and form factors. The spectrum of a generic massive QFT usually contains a low-energy discretum (usually comprised of a few states with masses  $m_1, m_2, \dots$ ) and the multiparticle continua that arise by acting with multiple creation operators for any of the particle types on the vacuum. The discrete states with energy below the lowest multiparticle threshold  $2m_1$  are stable and are the particle content of the theory. Discrete states with higher energy than that are generally metastable, since they can decay into the continuum with an arbitrarily small energy injection, if they have overlap with neighboring states. It should be noted however, that this does not preclude the existence of stable bound states that are well within the multiparticle thresholds, but are protected by symmetry or integrability (as, for example, in the case of the  $\sigma$ -deformation of the Ising CFT, where 5 of the 8 scattering bound states are stable despite being above the lowest two-particle threshold).

Generally, finding bound states in a field theory is a non-perturbative problem. Due to the fact that, more often than not, the theories we consider are perturbations of a free theory. Free theories have simple spectra, that may not be able to analytically deform into the spectra of even weakly coupled deformations thereof. However, in certain spin-0 bosonic field theories with polynomial potentials, there exists a class of bound states for which asymptotic expansions can easily be found: a weakly attractive potential can allow two particles to bind together loosely, which reduces the mass of the resulting state by an amount equal to the negative interaction energy of the pair. To be more specific, work has been done in [43],[44],[82],[83] on theories with  $\mathbb{Z}_2$  invariant potential of the form

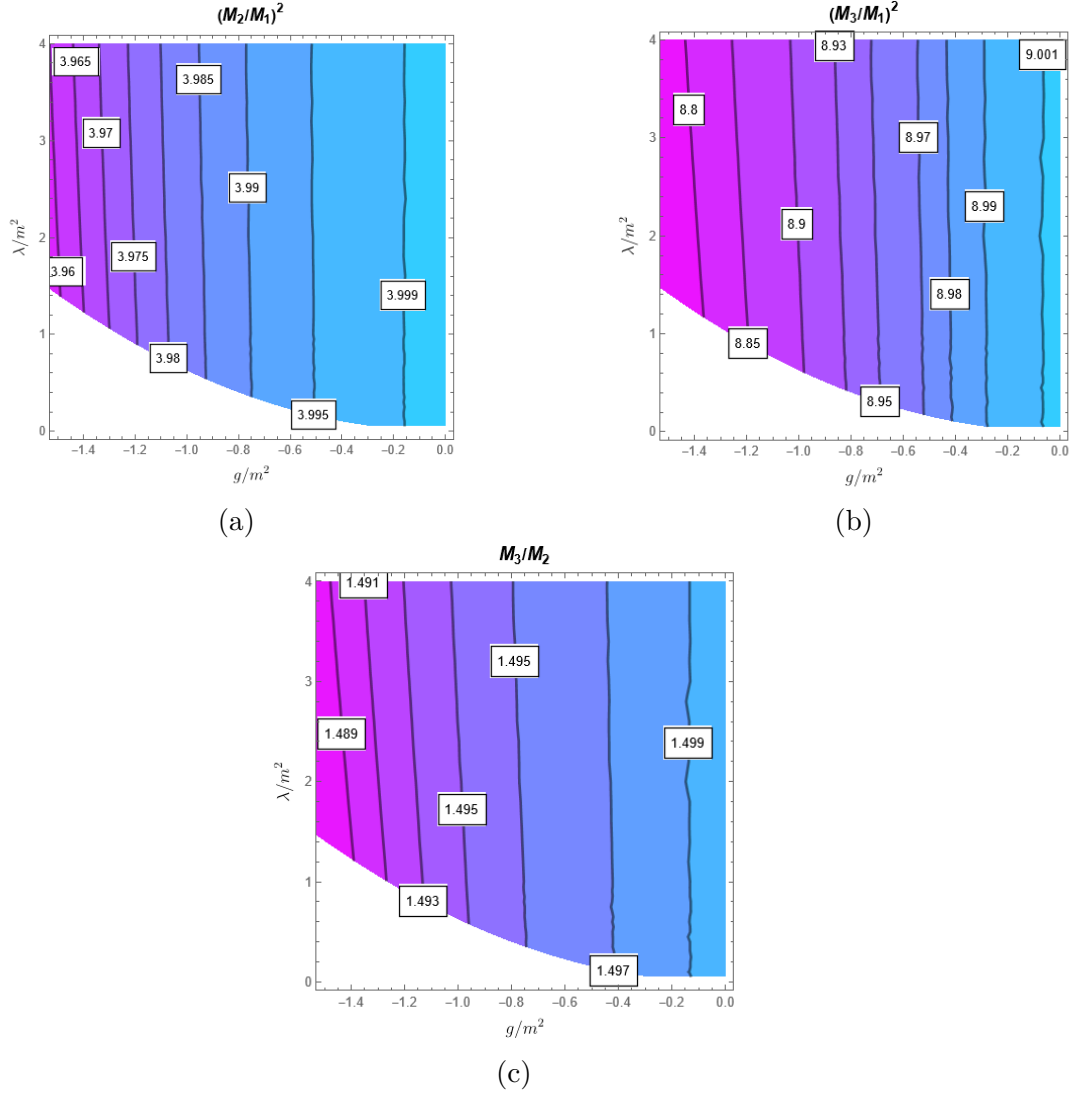


Figure 25: For this diagram we have taken data at even truncation levels in the range  $\Delta_{\max} = 20 - 40$  (a) Contour plot of the mass ratio of 2-particle bound state near threshold, descending in the region  $g < 0$  from the two particle threshold  $M_2^2/M_1^2=4$ . The bound state disappears when  $g \approx 0$  for weak coupling and it is also well defined on the phase transition. (b) The 3-particle bound state mass compared to the massgap. For  $g < 0$  the value is consistently below the 3-particle threshold  $M_3^2/M_1^2 = 9$ . Any values exceeding 9 are due to extrapolation errors. (c) The 3-particle bound state mass compared to the 2-particle bound state mass. The ratio is consistently below  $3/2$ , showing that the 3-particle bound state has higher binding energy, making it energetically preferable to the 2-particle one.

$$\mathcal{V}(\phi) = \lambda \left( \sum_{n=3}^N a_{2n} \phi^{2n} + s \phi^4 \right) + \frac{m^2}{2} \phi^2, \quad a_{2N} > 0, \lambda > 0, s = \pm 1 \quad (4.19)$$

wherein it was found that when the quartic coupling is positive, the theory possesses only one state below the two particle threshold, which is associated with the fundamental particle, while for negative values the theory possesses two such states, the fundamental particle plus a bound state dominantly composed of two-particle states, which appears right below the threshold at weak coupling with eigenvalue

$$m_b = 2m \left( 1 - \frac{9\lambda^2}{8m^4} + \mathcal{O}(\lambda^3 m^{-6}) \right) \quad (4.20)$$

It should be clear that a negative  $\phi^4$  term is required to create a slightly attractive interaction, to guarantee the existence of the bound state. This expansion can be obtained as an approximate solution of the Bethe-Salpeter bound state equation, wherein the Bethe-Salpeter kernel has been approximated to first order by its non-relativistic limit, which strictly involves contact interactions between the bound state constituents. This also explains why the first non-vanishing order estimate (4.20) is universal for such a wide class of polynomial bosonic theories. The bound state result above is not quite as general as the theory we would like to study given in (4.2), and in our notation, it corresponds to the direction  $\frac{g}{\lambda} = -30$ . However, there is nothing that could change the leading order result in the weakly coupled regime; the higher powers of  $\phi^n$ ,  $n > 4$  should contribute to the bound state at next to leading order in the non-relativistic perturbation expansion. The subleading corrections must be positive in sign, since the potentials are repulsive, and eventually the bound state must disappear.

We verify this intuition in Fig. 26a, where we clearly see a bound state emerge from the two particle threshold. It emerges along the line  $g = 0$  for weak coupling and its mass decreases as the negative quartic coupling becomes stronger. This was expected from equation (4.20). We also know that, qualitatively, since the  $\phi^6$  potential is repulsive, increasing its coupling strength should reduce the binding energy of the bound states, although this information is hiding in higher order corrections to (4.20). Indeed, we observe this effect in our simulations, even though for very small couplings,

the effect is negligible.

Additionally, we note that since the model is  $\mathbb{Z}_2$  invariant, the states separate into even and odd sectors, that do not interact with each other. In contrast to the  $\phi^4$  model, the 3-particle threshold now has a well-defined meaning because it is protected by symmetry from mixing with lower energy 2-particle states. This allows the existence of a 3-particle bound state descending from it becomes possible. The reason why we are interested in such bound states is due to the fact that they are generally perturbatively accessible; near-threshold bound states can be effectively treated using the non-relativistic limit of the QFT. Even more importantly, their mass being below the threshold prevents their spontaneous decay and makes them stable; as a result they are robust features of the spectrum. The analytical treatment using the Born approximation becomes increasingly difficult for 3-particle bound states, due to the fact that now one has to solve a three-particle bound state problem, but is nevertheless possible.

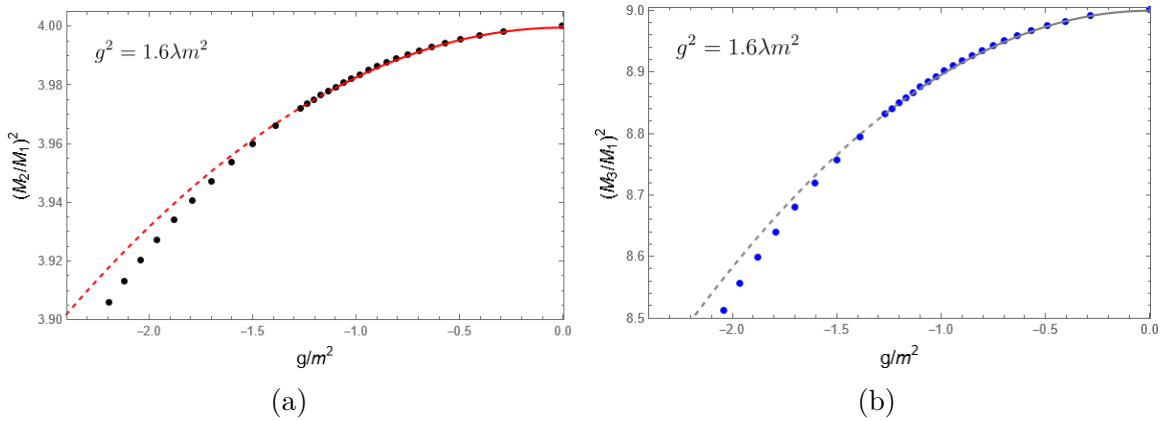


Figure 26: 2-particle and 3-particle bound state values at the SSB triple vacuum critical line  $g^2 = \frac{8\lambda}{5}$ . In this figure we reuse data acquired from the previous figure, in the range  $\Delta_{\max} = 20 - 40$ . The quadratic fit (dashed lines) works well in the region  $|g| < 1$ , if there are no points very close to the origin, where a linear anomaly is observed. Fitting to the form  $r_1 + r_2 g^2$ , we obtain the quadratic coefficient estimate  $r_1 = -0.016 \pm 0.002$  and  $r_2 = -0.036 \pm 0.005$ , and the 3-particle bound state decays faster, as expected.

We would also like to verify equation (4.20) by LCT simulations. This estimate for the bound state energy is robust to lowest order in the quartic coupling, in sharp contrast to (D.9), where the coupling dependence is well motivated, but the specific

coefficients are not necessarily determined by the non-relativistic expansion in powers of the inverse speed of light.<sup>4</sup>

Given this correction, we expect that at weak coupling, the bound state for  $g < 0$ , whether on-or off-critical will be dominated by the second order correction. To this end, we focus on the SSB line  $g^2 = \frac{8}{5}\lambda m^2$ , where we diagonalize the LCT matrix on several points and isolate the masses of the 2- and 3-particle bound states, divided by the 1-particle mass. The results are shown in Fig. 26. We have fit the first few points with the curve  $\frac{M_2^2}{M_1^2} = r_0 + r_2 g^2$ . The result  $r_2 = -0.016 \pm 0.001$  (extracted with a higher order fitting polynomial, including more points in the given range) compares well with the expected value of  $r_2$  from theory

$$r_2 = -\frac{9}{(4!)^2} = -2^{-6} = -0.015625 \quad (4.21)$$

To our knowledge, a theoretical analysis of the 3-particle threshold bound state has not been done before. Here, we measure that the leading correction coefficient is given by

$$r_2 = -0.106 \pm 0.005 \quad (4.22)$$

In the plots we have not included points with  $-0.3 < g/m^2 < 0$ , but simulations with higher resolution seem to indicate that the bound states near the line  $g = 0$  suffer from a small linear anomaly. In fact, if one repeats the procedure outlined in the previous paragraph for more fine grained data points and the fit  $\frac{M_2^2}{M_1^2} = r_0 + r_1 g + r_2 g^2$  one obtains the linear anomaly  $r_1 = 0.0045$ , after extrapolating to infinite truncation. The linear anomaly is most probably a truncation artifact, and it has also been seen in lattice measurements of this bound state. Encouragingly, the value of the anomaly decreases (albeit slowly) with increasing truncation level.

---

<sup>4</sup>This is true in  $\phi^4$  due to the fact that there are contributions with arbitrary powers of  $1/c$  at second order. In other words, one has to compute all non-relativistic corrections to scattering of the same order in the coupling to obtain the exact answer. In  $\phi^6$  the leading correction dominates at weak coupling, and since it is a particle number conserving, tree-level diagram, the contribution is exactly given by its non-relativistic limit.

## A Zero modes in LC

It is well known that in LC quantization the equations of motion are supplemented by extra constraints that bind together spacetime integrals of powers of the fundamental fields. The vacuum sector in LC is dynamically decoupled from the rest of the excitations of the theory, but the vacuum content is in turn determined by those excitations through nonlinear equations that are, generally speaking, extremely difficult to solve. Here we develop some properties of zero modes by looking into simpler systems.

In a canonical quantization setting for a generic QFT (relativistic or not), we are generally faced with the task of quantizing the solutions of a PDE. Of course, in order to define a solution to the PDE, a complete set of boundary conditions have to be imposed and each different complete set of boundary conditions produces distinct sets of solutions. These sets should be in one to one correspondence with each other (each solution in one set only maps to one solution in the other). Since these sets provide equivalent descriptions of the set of solutions to the PDE, quantizing them should produce different descriptions for the quantum system that agree on the values of all potential observables at least in principle (unless the boundary condition is singular, as we will see below).

However, not all boundary conditions are born equal: for example, in order to maintain Hamiltonian-like dynamics in non-relativistic theories with Galilei invariance, one is required to set the boundary condition at a time instant, usually  $t = 0$ , and then evolution is given by the well-known unitary operator  $U(t) = e^{-iHt}$  from quantum mechanics. In this case, it is known that all the interactions have to be included in the Hamiltonian, while all other generators of the Galilei group are non-dynamical.

In relativistic theories on the other hand, the set of boundary conditions one can choose is much less restricted. It is then useful to consider the kinds of hypersurfaces that leave some subgroup of generators of the Poincare group invariant, since in quantization these operators are going to be kinematical and can be then used to classify the states of the system. The most classic example comes from the well-

studied instant form; the boundary condition is taken at  $t = 0$  like in non-relativistic field theories and this results in 6 conserved generators -spatial momenta and rotations. We will refer to this as equal time quantization (ET) from now on. The surfaces that have a non-trivial stability group have been classified in (Pauli, 1949) [70]. The most interesting of them (and second most well studied in the literature) is called the front form, where the boundary conditions are imposed on one of the lightlike surfaces  $x \pm ct = 0$  (in multiple dimensions one can arbitrarily choose one of the spatial coordinates along with the time coordinate to quantize). We will call this boundary condition scheme lightcone quantization (LC). To fix our conventions, from now on we will consider the quantization to be happening in the  $x_+ = x_0 + x_1$  direction, which makes the corresponding momentum component  $P^+$  the "lightcone time" generator, akin to the equal time Hamiltonian, and it will contain information about the interactions of the physical particles.

Lightcone quantization possesses some very intriguing features that are not present in equal quantization, with far reaching consequences:

- For massive physical particles, the lightcone momentum generators along the quantization directions are restricted to have a positive-definite spectrum. In other words, it is required that  $P^+, P^- > 0$ .
- In the process of quantizing along a lightlike direction, the motion is naturally constrained. This means that certain fields are not governed by a field equation that evolves them forward in lightcone time, but instead are constrained in terms of other fields. In order to successfully quantize a lightcone theory, these fields need to be treated separately.

Let us briefly discuss each one of them. The axiom of spectrum positivity for massive particles comes directly from the traditional ET treatment: for physical particles Lorentz invariance requires positivity of masses and energies:  $P^2 > 0, P_0 > 0$ . Given that the Lorentz invariant

$$P^2 = 2P_+P_- - P_\perp^2 \tag{A.1}$$

expressed in terms of lightcone generators, this guarantees that  $P_+, P_-$  need to have eigenvalues of the same sign, and furthermore that sign has to be positive, since  $P_0 \propto P_+ + P_- > 0$  and  $P_+, P_-$  commute. From these considerations, we reason that, interestingly, in lightcone quantization, the  $P^- = 0$  sector is dynamically decoupled from the propagating modes. In ET, this doesn't happen for typical local interactions even in 1+1-d: total momentum ( $P_x$  in this case) is conserved, but the spatial momentum being unbounded from below allows the vacuum to mix with non-empty Fock states. In LC however, it is evident that since there exist no negative  $P^-$  momentum states and this momentum is also conserved, local interactions only have matrix elements between the propagating states and hence the vacuum sector is isolated.

This argument has singlehandedly been the most exciting prospect of LC quantization, since it would imply that if the vacuum is isolated and is the only state in the vacuum sector, then all one has to do is consider the excitations on top of it, and much of the difficulty that comes with numerically/theoretically understanding ET QFT Hamiltonians goes away. This has been coined the name triviality of the vacuum in the literature. In particular, since the vacuum is trivial, it is the same state no matter what the form of the interaction is, so the particle excitations of the field can be always built in a similar way as in a free theory. Specifically, for a bosonic spin 0 field, writing the expansion

$$\phi = \int_{p^- > 0} d\mu(p^-) d^{d-2} p^\perp \left[ a(x_+, p) e^{-i(x-p^- + \mathbf{x}_\perp \cdot \mathbf{p}^\perp)} + a^\dagger(x_+, p) e^{i(x-p^- + \mathbf{x}_\perp \cdot \mathbf{p}^\perp)} \right] \quad (\text{A.2})$$

correctly defines creation and annihilation operators for an interacting particle. The only difference from their non-interacting counterparts is their unresolved lightcone time dependence, which in a free theory is proportional to a factor of  $e^{iE_p x_+}$  with

$$E_p = \frac{m^2 + p_\perp^2}{2p^-} \quad (\text{A.3})$$

With this, a Fock expansion and hence perturbation theory can be developed around a free theory for interacting particles. Spectrum positivity eliminates all Feynman diagrams that contain matrix elements from the vacuum to excited states (tadpoles) and perturbation theory still reproduces ET results for particle scattering, so this was not recognized as a problem in the early literature. However, it is now known that perturbation theory is not the end-all be-all tool to understanding QFT. There are non-perturbative phenomena (for example, phase transitions/spontaneous symmetry breaking), that a few orders of ET perturbation theory alone cannot explain. In LC quantization, the problem is even more severe: the triviality of the vacuum is forcing all vacuum expectation values (VEV's) to vanish. This is in direct violation of the definition of a phase transition which requires an observable quantity (order parameter) to experience a sudden change when the coupling of the interacting theory is increased beyond a threshold value.

As it turns out, the incorrect assumption we have made is, unsurprisingly, the fact that the vacuum sector is trivial and contains only the vacuum state. In fact, there are other states in the  $P^- = 0$  sector, the zero-momentum components of the creation-annihilation operators described above. In fact, the following states are always part of the vacuum sector:

$$a_0^\dagger|0\rangle, (a_0^\dagger)^2|0\rangle, \dots \tag{A.4}$$

where  $a_0^\dagger$  represents the zero mode  $a^\dagger(p_- = 0, p_\perp = 0)$ . How is it, however, that these modes interact with the vacuum to create the non-perturbative complexity in LC quantization? As we will see in the following sections, zero modes in LC don't really have true equations of motion, since their EOM's do not contain any derivatives (the conjugate momentum of the zero mode decouples). The resulting equations are (generally non-linear) constraint equations that determine the zero modes in terms of the evolution of excited modes. Including zero modes in the analysis is a technically difficult task, but in the following we will show some exactly

solvable examples that elucidate further the nature of these modes and how they can contribute in reproducing the ET quantized physics of the theory. <sup>5</sup> gives rise to non-dynamical zero modes, quantities that are determined in terms of other fields instead of having their own evolution equation. The zero mode operators presented above are examples of such quantities in bosonic field theories. The treatment of zero modes is a complex issue in quantum field theories that we are not going to explain in the most thorough detail in this thesis. The interested reader can refer to appendix A for some explicit examples on how zero modes can arise in a discrete classical dynamical system and how one may write appropriate thermodynamic partition functions for those systems.

## A.1 A toy LC quantized field theory

In this subsection we studied the behavior of the zero modes in a discrete setting, and we have shined light on their role as non-dynamical objects that arise from the existing dynamical modes of a system and we have concluded that their presence in a polynomial potential does not pose a threat to the well-definedness of the system, as long as the polynomial potential is bounded from below- which in turn requires the highest degree potential terms to all have a positive sign. This offers evidence in favor of the well-definedness of more complex dynamical systems with a very large number of degrees of freedom, such as a typical lightcone quantized  $\phi^4$  bosonic QFT in 1+1-d flat space with Lagrangian given by

$$\mathcal{L} = \kappa \partial_+ \phi \partial_- \phi - \lambda_2 \phi^2 - \lambda \phi^4$$

---

<sup>5</sup>To explain the meaning of this sentence, consider the 2-d wave equation for a massless particle in lightcone coordinates  $\partial_+ \partial_- \phi = 0$ . The general solution is given by  $\phi(x_+, x_-) = f(x_+) + g(x_-)$  and it is immediately clear that imposing a boundary condition on either of the coordinates is not sufficient to determine a unique solution. Defining a unique solution shouldn't be a problem when a potential term is added, however when adding interactions to a free particle, the degenerate Hamiltonian structure of this problem persists, leading to subtleties in the quantization, like zero modes.

This underlying space of this theory can be discretized into a square lattice with spacing  $a$  and the continuum form above reduces to the following form

$$\mathcal{L} = \frac{\kappa}{a^2} \sum_{i,j=-\infty}^{\infty} \varphi_i \Gamma_{ij} \dot{\varphi}_j - \lambda_2 \sum_{i=-\infty}^{\infty} \varphi_i^2 - \lambda_4 \sum_{i=-\infty}^{\infty} \varphi_i^4$$

where  $\Gamma$  is an antisymmetric tridiagonal matrix. The Lagrangian clearly has the form discussed above and hence is expected to pose a well-defined dynamical system.

Now we present an example of how these zero modes arise by considering the solvable QFT with Lagrangian

$$\mathcal{L} = \frac{1}{2}(\partial\phi)^2 - \frac{m^2}{2}\phi^2 - h\phi \tag{A.5}$$

If we applied naive perturbation theory to this problem we would not recover the correct answer for the VEV's of the field, and here we will show how such quantities can arise as consequences of the existence of zero modes. In ET quantization, this theory can be diagonalized readily by performing a field shift  $\phi \rightarrow \phi + c$ , which leaves the path integral of the theory invariant, and choosing  $c$  appropriately such that the linear term vanishes. The resulting theory is one describing a single massive boson of mass  $m$  with non-zero VEV:

$$\langle 0|\phi(x)|0\rangle = -h/m^2 \tag{A.6}$$

We will proceed by examining briefly the LC Hamiltonian formulation for this theory in 1+1 dimensions, and our goal is to match the results of equal time quantization. We note our conventions

$$x_+ = t + x \quad , \quad x_- = t - x$$

where we treat  $x_+$  as the lightcone time. Then the Lagrangian, the canonical Hamiltonian and the canonical momentum in LC coordinates read

$$\mathcal{L} = 2\partial_+\phi\partial_-\phi - \frac{m^2}{2}\phi^2 - h\phi \quad (\text{A.7})$$

$$H_c = \int dx_- \frac{m^2}{2}\phi^2 + h\phi \quad (\text{A.8})$$

$$\Pi(x_+, x_-) = \frac{\delta\mathcal{L}}{\delta(\partial_+\phi)} = 2\partial_-\phi \quad (\text{A.9})$$

The Lagrangian does not have quadratic terms in either of the  $+$ ,  $-$  coordinates so in the end the Hamiltonian ends up having no kinetic term and the canonical momentum has no lightcone time derivative on it. Hence the equation of the lightcone momentum has the status of a constraint equation. Typically one here goes out to find whether any secondary constraints exist as in section 1.1, but here we will not pursue this avenue, since for this particular system the Dirac-Bergmann algorithm requires special care to be applied. Instead, for clarity we will put the system in a finite volume and impose periodic boundary conditions on the field

$$\phi(x_+, 0) = \phi(x_+, L) \quad (\text{A.10})$$

The periodic BC discretizes the momentum and we now expand the field in creation-annihilation operators in the spirit of A.2:

$$\phi(x_+, x_-) = a_0 + \sum_{n>0} \frac{1}{\sqrt{4\pi n}} (a_n(x_+)e^{-2in\pi x_-/L} + a_n^*(x_+)e^{2in\pi x_-/L}) \quad (\text{A.11})$$

Here  $a_0$  represents a zero mode, which is required to be Hermitian. We insert into the Lagrangian which yields the expression

$$\mathcal{L} = -\frac{m^2L}{2}a_0^2 - hLa_0 + \sum_{n>0} \left[ i(\dot{a}_n a_n^* - \dot{a}_n^* a_n) - \frac{m^2L}{4\pi n} a_n^* a_n \right] \quad (\text{A.12})$$

Before even writing the Euler-Lagrange equations in the new variables, we immediately note that the zero mode has no time derivative, and hence is non-dynamical. The EOMs read

$$\dot{a}_n = -i \frac{m^2 L}{8\pi n} a_n \quad (\text{A.13})$$

$$0 = m^2 a_0 + h \quad (\text{A.14})$$

Here we see the usual set up that lightcone provides for bosonic field theories in 1+1-d. There is always an operator constraint equation that fixes the zero mode of the boson field in terms of non-zero momentum operators and dynamical equations that govern the evolution of the latter. Usually, the operator equations derived in this are intractable, but in this simple problem they can be solved easily for the result derived in (A.6).

## A.2 Zero modes in constrained first order classical systems

We can gain some intuition about how zero mode constraints arise by studying a very simple classical system with finite degrees of freedom, which represents a finite truncation of a LC quantized action with periodic BC's (in fact, corresponding to a discretization of a single interacting boson in 1+1-D). Coincidentally, this system also appears as a classical analogue of light front quantization in [24].

Consider the Lagrangian action

$$S = \int_0^T dt \dot{x}^T A x - \Phi(x), x(0) = x_0 \in \mathbb{R}^{2n} \quad , \quad A^T = -A \in \mathbb{M}_{2n \times 2n} \quad (\text{A.15})$$

Clearly this Lagrangian, being first order in the time derivatives does not lead to a Hamiltonian formulation by naively applying a Legendre transformation, as it turns out that the conjugate momenta and the Hamiltonian are

$$H = \Phi(x) , p_i = (Ax)_i \tag{A.16}$$

One sees that the momenta are not functions of time derivatives like they usually are: they are placing dynamical constraints on the problem. This requires a recipe called the Dirac-Bergmann algorithm in order for one to write a Hamiltonian that reproduces the Lagrangian equations of motion. For now I skip a presentation of this machinery since I found that, interestingly, the system **can** be rewritten as a Hamiltonian system, with  $n$  degrees of freedom identified as positions and the rest identified as momenta. This is not equivalent to applying the DB algorithm, since it requires the matrix to be even dimensional for it to work. We can try to hash out which one is which by looking at the equations of motion:

$$2(Ax)_i = \frac{\partial \Phi}{\partial x_i} \tag{A.17}$$

Now we can diagonalize the matrix  $A$  in the form  $A = S^H \Lambda S$ , if we assume that  $\det A \neq 0$ . Since the matrix is antisymmetric, its eigenvalues are purely imaginary and the eigenvectors that correspond to separate eigenvalues are orthogonal to one another. Also by the fundamental theorem of algebra, the eigenvalues appear in complex conjugate pairs and so do the eigenvectors (since the matrix has real entries only). This means that we can write the  $2n$  equations of motion in the concise form

$$\begin{aligned} 2\lambda_n \dot{e}_n &= -\partial_{e_n} \Phi \\ 2\lambda_n \dot{e}_n &= \partial_{e_n^*} \Phi \end{aligned} \tag{A.18}$$

with  $e_n = \langle v_n, x \rangle$ , and  $v$  represents the eigenvectors of  $A$  satisfying  $Av_n = \lambda_n v_n$ . These equations are in Hamiltonian form if one defines

$$\begin{aligned}\tilde{x}_n &\propto e_n \\ \tilde{p}_n &\propto 2\lambda_n e_n^*\end{aligned}\tag{A.19}$$

These quantities have canonical commutation relations starting from the position variables, if one identifies  $x \rightarrow A^{-1}p$  when calculating the Poisson bracket  $\{\tilde{x}_n, \tilde{p}_n\}$ . This move should be justifiable in the correct setting with the momenta acting as constraints. Let us assume that these quantities have canonical commutation relations anyway, as they are currently written down in equation (1.5). Then the quantities

$$\begin{aligned}Q_n &= \sqrt{\lambda_n}(e_n + ie_n^*) \\ P_n &= \sqrt{\lambda_n^*}(e_n - ie_n^*)\end{aligned}\tag{A.20}$$

also obey canonical commutation relations and are real.

Consider now the case when there are  $(2n + 1)$  dofs and thus  $A \in \mathbb{M}_{(2n+1) \times (2n+1)}$ . In odd dimensions, antisymmetric matrices always have  $\det A = 0$ , and hence a natural zero mode arises. To see this, diagonalize the matrix (assume that there is only a single zero eigenvalue) and the Lagrangian becomes

$$\mathcal{L} = \sum_{k=1}^n \lambda_k (e_k \dot{e}_k^* - e_k^* \dot{e}_k) + \Phi(e_1, e_1^*, \dots, e_n, e_n^*, z)\tag{A.21}$$

which implies the same equations of motion as (1.4) with the addition of

$$\partial_z \Phi(e_1, e_1^*, \dots, e_n, e_n^*, z) = 0\tag{A.22}$$

This in turn shows that the zero mode will be expressed in terms of all the other

dynamical modes upon integration. This creates a lot of trouble for the Lagrangian formalism (which already was in trouble since the resulting equations are not second order in the derivatives, which would imply that the typical formulation of it as a minimization problem is not viable because of the second boundary condition which overconstrains the problem), because the zero mode is completely determined by all the other modes and therefore it's initial value cannot be freely adjusted.

### An explicit example

The simplest nontrivial example one can analyze is the  $3 \times 3$  matrix

$$A = \begin{pmatrix} 0 & a & -b \\ -a & 0 & c \\ b & -c & 0 \end{pmatrix} \quad (\text{A.23})$$

with eigenvalues and eigenvectors given by, (note  $r = \sqrt{a^2 + b^2 + c^2}$ )

$$\lambda_n = \{0, -ir, ir\} \quad , \quad v_n \propto \begin{pmatrix} c \\ b \\ a \end{pmatrix} , \begin{pmatrix} bc - iar \\ -a^2 - c^2 \\ ab + irc \end{pmatrix} , \begin{pmatrix} bc + iar \\ -a^2 - c^2 \\ ab - irc \end{pmatrix} \quad (\text{A.24})$$

Clearly, the first eigenvector generates the requested purely real zero mode (for a single zero mode, the eigenvector must be purely real, or it would have a linearly independent counterpart also assigned to the same eigenvalue- this holds true if there are more zero eigenvalues, since the eigenvectors always have to show up paired up or single but real, and when you have two conjugate eigenvectors  $(u, v)$  then the combinations  $u + v, i(u - v)$  are real). Then, one can write the Lagrangian in the explicit form

$$\mathcal{L} = \lambda_2(\dot{e}_2 e_3 - \dot{e}_3 e_2) + \Phi(x) \quad (\text{A.25})$$

At this point we will analyze a few different potentials to show some different outcomes

of the quantization. According to the analysis preceding this example, given the potentially nonlinear nature of the constraint equation, it is possible that the zero mode is not unique, or doesn't even exist. Non-uniqueness does not necessarily pose a big problem, since every choice of zero mode provides a realization of the dynamical system, and can therefore be quantized into several separate quantum theories by canonical quantization, but there are some cases where the zero mode solutions may be complex, in direct contradiction to the fact that the zero mode can be shown to be real. In those, the real dynamical system posed simply does not exist, and it cannot serve as a basis for a legit quantum theory.

### Constrained harmonic oscillators

Suppose  $\Phi(x) = (x_1^2 + x_2^2 + x_3^2)/2$ . Solving for the coordinates in terms of the eigenmodes yields

$$\begin{aligned} x_1 &= e_1 \frac{ac}{r^2} - K \frac{ac}{r^2} - L \frac{b}{r} \\ x_2 &= e_1 \frac{ab}{r^2} + K \frac{c}{r} - L \frac{ab}{r^2} \\ x_3 &= e_1 \frac{a^2}{r^2} + K \frac{b^2 + c^2}{r^2} \end{aligned} \tag{A.26}$$

$$K := \frac{1}{2}(e_2 + e_3), \quad L := \frac{e_2 - e_3}{2i}$$

Then substituting back into the Lagrangian we finally obtain

$$\mathcal{L} = 2r(\dot{L}K - \dot{K}L) + \frac{a^2}{2r^2}e_1^2 + \frac{b^2 + c^2}{2r^2}(K^2 + L^2) \tag{A.27}$$

The equations of motion set the zero mode to zero. This is a general feature of quadratic potentials: the zero mode can be expressed as a linear combination of other modes, which makes life generally trivial. The equations of motion as shown above decouple to **2=3-1** linear oscillators, and hence the zero mode has been "integrated out" successfully.

This result should also be reflected in the classical thermodynamic partition function of the system. It is known that the partition function at high temperatures is related to the allowed directions that the system can move in, and in particular, the asymptotic behavior should be of order  $\sim T^{D/2}$ , where  $D$  is the number of degrees of freedom of the system. In this model, we need to explicitly implement the dynamical constraint as a Dirac-delta function inside the integral. Since the model is simple enough, we can perform a direct integration, that yields the result:

$$Z = \int \prod_k dx_k dp_k \delta(p_k - (Ax)_k) \delta(cx_1 + bx_2 + ax_3) e^{-\frac{\beta k}{2}(x_1^2 + x_2^2 + x_3^2)} = \frac{1}{r} \left( \sqrt{\frac{2\pi}{\beta k}} \right)^2 \quad (\text{A.28})$$

which agrees with our intuition coming from the equipartition theorem. One can also compute an exact generating function from the usual definition

$$\langle e^{i\frac{\beta}{2k}\lambda \cdot \mathbf{x}} \rangle = \frac{2\pi}{\beta k(a^2 + b^2 + c^2)} e^{-\frac{\beta}{2k}\lambda^T \Sigma \lambda} \quad (\text{A.29})$$

$$\begin{pmatrix} 1 - \frac{c^2}{a^2+b^2+c^2} & -\frac{bc}{a^2+b^2+c^2} & -\frac{ac}{a^2+b^2+c^2} \\ -\frac{bc}{a^2+b^2+c^2} & 1 - \frac{b^2}{a^2+b^2+c^2} & -\frac{ab}{a^2+b^2+c^2} \\ -\frac{ac}{a^2+b^2+c^2} & -\frac{ab}{a^2+b^2+c^2} & 1 - \frac{a^2}{a^2+b^2+c^2} \end{pmatrix} = 1 - \frac{v_1 v_1^T}{r^2}$$

The above decomposition of the covariance matrix allows to express the inner product as a diagonal quadratic form very easily, noticing that it is diagonalizable:

$$\Sigma v_1 = 0, \Sigma v_2 = v_2, \Sigma v_3 = v_3$$

and with  $K, L$  defined as above in terms of the inner products  $e_n$ :

$$\lambda^T \Sigma \lambda = K^2 + L^2 \quad (\text{A.30})$$

$$e_n = \langle v_n / \|v_n\|, \lambda \rangle$$

which clearly shows that since the zero mode dependence has dropped out, the correlation functions of the constraint are zero to all orders, as it should. This discussion indicates that for any odd number of degrees of freedom, the covariance matrix should still be of the form (1.16), albeit the form of the zero mode may be less explicit.

### **Constrained anharmonic motion**

Zero modes can generate complications in the analysis of interacting, non-linear systems. It is clear that zero modes in the class of dynamical systems considered above show up in a form of a non-linear equation that may or may not have solutions. The question that arises then is what kind of interaction potentials define well-posed dynamical systems, with real solutions for the dynamics.

Consider now the potential  $\Phi(x) = x_1^3 + x_2^3$ . This potential is unbounded from below and flat in the  $x_1$  direction so quantizing is maybe not so interesting, but it serves to show that there exist potentials that may not define a good dynamical system for certain values of the kinetic term. It is clear from the form of the potential and a quick calculation that whenever  $bc > 0$ , there is no real solution to the zero mode equation. However, it is easy to see that by the fundamental theorem of algebra, for most potential terms one can write whose highest total power of  $x$  is even, a real solution must always exist. The only way for a real solution to potentially not exist would be to have the highest power in the potential when written in terms of the zero mode to vanish for a certain choice of parameters. However, for even powered potentials that are bounded from below (this implies that all terms  $x_1^{2n}, \dots, x_m^{2n}$  have positive coefficients) this can never happen unless the matrix has a whole row equal to zero, which would imply this matrix has more than one zero eigenvalues.

In all these cases, we have analyzed and found the zero modes of the system without any recourse to a systematic procedure. Such a procedure, however, does exist and is due to Dirac and Bergmann. We showcase the execution of this algorithm below.

### A.3 The Dirac-Bergmann algorithm

It turns out that the procedure proposed in section 1 to write a Hamiltonian system is not entirely unfounded. We will show this by applying the Dirac-Bergmann (DB) formalism to write down a Hamiltonian that one can directly quantize. First of all note that

$$p_i = \frac{\partial \mathcal{L}}{\partial \dot{x}_i} = (Ax)_i \quad (\text{A.31})$$

and therefore one cannot use any of the momenta to determine any velocities in the system<sup>6</sup>. All of the above relations have to be treated as constraints, for the system and must be integrated out. Upon a first look one could think that this system has trivial evolution, but that is simply not true, since there are  $n$  constraints for  $2n$  degrees of freedom of the Hamiltonian system (only the momenta are constrained).

We skip the first step of the DB algorithm, which involves inverting for as many velocities as the rank of the momentum-velocity matrix, and define the constraints

$$\Gamma_i = p_i - (Ax)_i \quad (\text{A.32})$$

The canonical Hamiltonian is clearly  $H_c = \Phi(x)$ , since we inverted for no velocities at all and hence there is no  $p_i \dot{q}_i$  part to the Legendre transformation. The constraints cancel out the kinetic term exactly. With  $R < N$  first order constraints the Hamiltonian that gives the Lagrangian EOM's is:

$$H_{EOM} = H_c + \sum_{i=R+1}^N \dot{q}_i \Gamma_i \quad (\text{A.33})$$

Now we write down the primary Hamiltonian by adding the constraints multiplied

---

<sup>6</sup>This can be concisely written as  $R = \text{rank}(\partial p_i / \partial x_j) = 0$  and hence there are  $N - R$  constraints

by a free parameter:

$$H_p = H_c + \sum_k \lambda_k (p_k - (Ax)_k) \quad (\text{A.34})$$

This Hamiltonian is the one that should reproduce the correct evolution for the constraints (which is no evolution at all!) and should be repeated as many times as needed until one finds all of the secondary constraints. After a bit of algebra we find

$$\dot{\Gamma}_k = \{\Gamma_k, H_c\} = -\frac{\partial \Phi}{\partial x_k} - 2\lambda^\ell A_{\ell k} \quad (\text{A.35})$$

which, when set to zero, determines all of the multipliers when  $\det A = 0$ . For odd  $n$  this implies that there is one (or more but always an odd number) of zero modes that appear as secondary constraints, since the Lagrange multipliers are not determined by this process. For odd dimensions, we need to add the zero mode with another multiplier. Suppose the decomposition of an odd-dimensional matrix  $A = SAS^H$  contains only one zero eigenvalue, which will be arranged to be the first eigenvalue of the matrix. Then the zero mode constraint can be expressed as follows

$$0 = \Lambda_1 S_{1k} \lambda_k = -\frac{1}{2} \left( S \frac{\partial}{\partial x} \right)_1 \Phi \quad (\text{A.36})$$

The new Hamiltonian is ( $z_k = S_{1k}$ )

$$H_p = H_c + \sum_k \lambda_k (p_k - (Ax)_k) + \mu (\mathbf{z} \cdot \nabla_x \Phi) \quad (\text{A.37})$$

To compute the bracket of the zero mode with the Hamiltonian, decompose the matrix  $A$  in eigenvectors and after some algebra<sup>7</sup> arrive at:

$$\{\Gamma_0, H\} \approx \frac{1}{2} \hat{A}_{\ell m}^+ (\partial_\ell \Phi) (\mathbf{z} \cdot \nabla) \partial_m \Phi + (\mathbf{z} \cdot \lambda) (\mathbf{z} \cdot \nabla)^2 \Phi \quad (\text{A.38})$$

---

<sup>7</sup>First, show that all multipliers are determined except one, that lies in the direction of the zero mode, and are given by

$$\lambda = -\frac{1}{2} \sum_{k=2}^N \frac{e_k^H \nabla \Phi}{\Lambda_k} e_k$$

which, unless the potential fulfills very special conditions, determines the zero mode component of the primary constraint. Now in order to check if there are any more constraints, one has to substitute this result back into the Hamiltonian to see if one can determine  $\mu$ . One can readily see that on shell

$$\{\Gamma_k, H_p\} \approx \mu \partial_k (\mathbf{z} \cdot \nabla) \Phi \quad (\text{A.39})$$

which means that the multiplier of the zero mode is determined and equal to zero, unless the potential is linear in the coordinates in the direction of the zero mode, in which case the zero mode has a trivial equation of motion and in a quantum theory, it would be a gauge degree of freedom that needs to be integrated out by imposing a constraint on the path integral.

## B Semiclassical results

### B.1 $\phi^6$ model semiclassics

The kinks of the critical classical theory  $V_c = \lambda\phi^2(\phi^2 - v^2)^2$  play an important role in understanding the structure of the system at small couplings. In fact, instantons control various quantities like for example the behavior of the Borel transform of Green's functions and the semiclassical spectrum of bound states of the theory. It has been shown in [65] that the semiclassical spectrum of the  $\phi^4$  theory in the  $\mathbb{Z}_2$  broken phase is controlled by the kinks of the critical theory, which in general for a bosonic field in 1+1-D, are special, minimum energy, stationary solutions of the equations of motion:

$$\partial_x^2\phi(x) = -\partial_\phi V_c(\phi(x)) \quad (\text{B.1})$$

As a result of the kink analysis, it is argued that for any bosonic system in 1+1-D with a polynomial potential, there can only ever be a maximum of two bound states in the system. In this section, we reproduce the results of [65] for the potential of equation 4.2, which is another bosonic model that undergoes spontaneous  $\mathbb{Z}_2$  breaking.

We can obtain the kinks as solutions of the first integral of equation (B.1) (which can be obtained by multiplying that equation by  $\partial_x\phi$ ):

$$\frac{1}{2}(\partial_x\phi)^2 + V_c(\phi) = E \quad (\text{B.2})$$

which is now separable and can be further reduced to

$$x - x_0 = \int \frac{d\phi}{\sqrt{2(V_c(\phi) - E)}} \quad (\text{B.3})$$

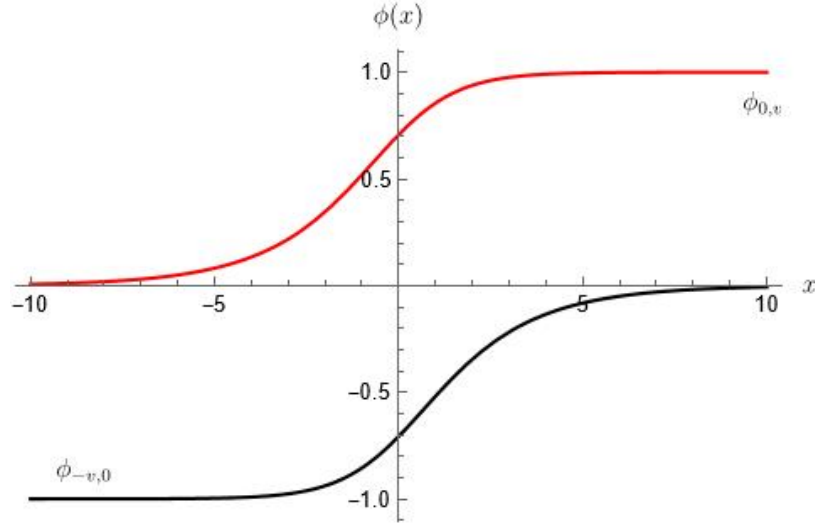


Figure 27: Kinks of the critical classical theory  $V_c = \lambda\phi^2(\phi^2 - v^2)^2$ . The kink that connects the leftmost vacuum to the middle one is shown in black and the one connecting the middle vacuum to the one on the right is shown in red.

In order for this function to have a finite limit at  $x \rightarrow \pm\infty$ , we need to impose the zero energy constraint  $E = 0$ . The field configurations obtained in this manner are called interchangeably instantons/solitons and they connect the zeroes of the equation  $V(\phi) - E$  pairwise. It is obvious that in the critical classical theory the three minima are all solutions of the equation  $V(\phi) = 0$ , so they should be connected by kinks. We denote by  $\phi_{a_1 a_2}$  the soliton that connects vacua at positions  $\phi = a_1$  and  $\phi = a_2$ . The solitons can only connect neighboring vacua in one spatial dimension. Performing the soliton integral is a simple exercise that one can do that results in two different kinds of kinks:

$$\begin{aligned}
 \phi_{-v,0} &= -\frac{v}{\sqrt{1 - e^{2v^2\sqrt{2\lambda}(x-x_0)}}} \\
 \phi_{0,v} &= \frac{v}{\sqrt{1 - e^{-2v^2\sqrt{2\lambda}(x-x_0)}}} \\
 \phi_{v,0} &= -\phi_{-v,0} \quad , \quad \phi_{0,-v} = -\phi_{0,v}
 \end{aligned}
 \tag{B.4}$$

## B.2 Critical surfaces of a general sextic potential

We can begin to understand the structure of the general sextic potential by figuring out what the possibilities are for this potential to induce a transition classically. It turns out that this question is not so simple to answer because of the generality of the potential. A transition in the system is induced every time the VEV, which semiclassically corresponds to the global minimum of the potential, changes, continuously or discontinuously. We can safely assume that every time there is more than one global minimum, a transition has occurred. The idea here lies in obtaining information about the codimension and compactness/shape of the surfaces that these multiple minima coincidences allow.

To illustrate how we can go about this, for the model  $V = \lambda\phi^4 + g\phi^3 + \phi^2$ , we show that the line of first order transitions can be naturally parametrized by the position of the global minima. Note that  $\phi = 0$  is always a minimum of the toy potential, and remains the sole global minimum of the potential in a neighborhood around  $(g, \lambda) = (0, 0)$  the origin of the coupling space. The appearance of another global minimum  $\phi_0$  to induce a transition, we need necessarily  $V(\phi_0) = V'(\phi_0) = V(0) = 0$  and we obtain two equations for the couplings that can be solved to yield a parametric representation of the curve we're looking for:

$$\begin{bmatrix} 1 & 1 \\ 4 & 3 \end{bmatrix} \begin{bmatrix} \lambda\phi_0^2 \\ g\phi_0 \end{bmatrix} = \begin{bmatrix} -1 \\ -2 \end{bmatrix} \Rightarrow (\lambda, g) = (1/\phi_0^2, -2/\phi_0)$$

In other words, the transition will occur on the codimension-1 line  $g^2 = 4\lambda$ , which is what we find from a detailed analysis of the critical points of the potential. We note that a quartic polynomial can have at most 2 minima (if it had three or more distinct ones, all the couplings would have to be zero, however one could have higher order zeroes count as multiple).

We can repeat the analysis for the Hamiltonian (4.3) and we denote  $\mu_k m^2 = \lambda_k/k!$  for

simplicity. This time we want to find the surface on which three global minima appear, since this ansatz includes the critical Hamiltonian found before (note again that we cannot have more than three distinct minima without trivializing the Hamiltonian). We demand that  $V(\phi_1) = V(\phi_2) = V'(\phi_1) = V'(\phi_2) = 0$  which yields the system

$$\begin{bmatrix} \phi_1^4 & \phi_1^3 & \phi_1^2 & \phi_1 \\ \phi_2^4 & \phi_2^3 & \phi_2^2 & \phi_2 \\ 6\phi_1^4 & 5\phi_1^3 & 4\phi_1^2 & 3\phi_1 \\ 6\phi_2^4 & 5\phi_2^3 & 4\phi_2^2 & 3\phi_2 \end{bmatrix} \begin{bmatrix} \mu_6 \\ \mu_5 \\ \mu_4 \\ \mu_3 \end{bmatrix} = \begin{bmatrix} -1 \\ -1 \\ -2 \\ -2 \end{bmatrix}$$

The solution is a parametrized codimension-2 surface ( $X = \phi_1^{-1}, Y = \phi_2^{-1}$ ):

$$(\mu_3, \mu_4, \mu_5, \mu_6) = (-2(X + Y), X^2 + Y^2 + 4XY, -2XY(X + Y), (XY)^2) \quad (\text{B.5})$$

or alternatively in terms of two constraints on the couplings:

$$\mu_6 = \frac{\mu_5^2}{\mu_3^2}, \quad \mu_4 = \frac{\mu_3^2}{4} + 2 \left| \frac{\mu_5}{\mu_3} \right| \quad (\text{B.6})$$

Of course, this is not the only possibility for phase coexistence in this Landau-Ginzburg potential. One could imagine various situations where 2 global minima coincide instead of 3- this is still going to give rise to a first order transition. We would like to find out whether these classical first order transitions can appear in the quantum system- or in other words, find out they contain points arbitrarily close to the origin for small values of the couplings. Given that  $\phi = 0$  is always a minimum there are only two possibilities to consider if the minima present themselves in the positions  $0, \phi_1, \phi_2$ :

1.  $\phi = 0$  is the global minimum in which case for a coincidence we need  $V(\phi_1) = V'(\phi_1) = 0$  and  $V(\phi_2) > 0$
2.  $\phi = 0$  is not the global minimum in which case we demand  $V(\phi_1) = V(\phi_2) =$

$$A < 0, \quad V'(\phi_1) = V'(\phi_2) = 0$$

Both options produce 3-dimensional subspaces of  $\mathbb{R}^4$ , although the first one is somewhat more trivial in the sense that the 2-dimensional cuts of the plane  $\phi_2 = \text{const.}$  always look the same (the 3-dimensional surface is basically a cylinder with cuts given by complicated functions of the VEVs). Option 1 gives only two equations:

$$\begin{bmatrix} \phi_1^4 & \phi_1^3 & \phi_1^2 & \phi_1 \\ 6\phi_1^4 & 5\phi_1^3 & 4\phi_1^2 & 3\phi_1 \end{bmatrix} \begin{bmatrix} \mu_6 \\ \mu_5 \\ \mu_4 \\ \mu_3 \end{bmatrix} = \begin{bmatrix} -1 \\ -2 \end{bmatrix}$$

and a parametrization of the surface is ( $X = \phi^{-1}$ )

$$\begin{aligned} \mu_6 &= X^4 + \frac{\mu_3}{2}X^3 - \frac{\mu_5}{2}X \\ -\mu_4 &= 2X^2 + \frac{3\mu_3}{2}X + \frac{\mu_5}{2X} \end{aligned} \tag{B.7}$$

Option 2 gives us equations that are similar looking to the ones for 3 coinciding phases, but with an extra parameter:

$$\begin{bmatrix} \phi_1^4 & \phi_1^3 & \phi_1^2 & \phi_1 \\ \phi_2^4 & \phi_2^3 & \phi_2^2 & \phi_2 \\ 6\phi_1^4 & 5\phi_1^3 & 4\phi_1^2 & 3\phi_1 \\ 6\phi_2^4 & 5\phi_2^3 & 4\phi_2^2 & 3\phi_2 \end{bmatrix} \begin{bmatrix} \mu_6 \\ \mu_5 \\ \mu_4 \\ \mu_3 \end{bmatrix} = \begin{bmatrix} \frac{A}{\phi_1^2} - 1 \\ \frac{A}{\phi_2^2} - 1 \\ -2 \\ -2 \end{bmatrix}$$

Because the system is linear we get the solution (3.3) plus a term proportional to  $A$  given by

$$\begin{bmatrix} \mu_3 \\ \mu_4 \\ \mu_5 \\ \mu_6 \end{bmatrix} = \begin{bmatrix} -2S \\ S + 2P \\ -2SP \\ P^2 \end{bmatrix} + A \begin{bmatrix} 2S(2S^2 - 3P) \\ -3(S^4 - P^2) \\ 6SP(S^2 - P) \\ -P^2(3S^2 - 2P) \end{bmatrix} \quad (\text{B.8})$$

where  $S := \phi_1^{-1} + \phi_2^{-1}$ ,  $P := (\phi_1\phi_2)^{-1}$ .

## C Avoided Crossings

The presence of eigenvalue crossings is ubiquitous in quantum mechanical problems, and they have been studied as a mathematical and physical peculiarity for the better part of the 20th century. These points are, in a sense that will be defined below, manifestations of a more general class of singularities of matrix spectra under a single deformation parameter, generically called exceptional points. These points generally arise when one perturbs a Hamiltonian in the following manner:

$$H = H_0 + \lambda H_1 \tag{C.1}$$

Suppose that the Hamiltonian is a finite matrix for now. As one varies  $\lambda$  in the complex plane, one can encounter isolated points where neighboring eigenvalues coincide. The existence of these points can be illustrated by considering the  $2 \times 2$  Hamiltonian

$$H = \begin{pmatrix} \epsilon_1 & 0 \\ 0 & \epsilon_2 \end{pmatrix} + \lambda \begin{pmatrix} 0 & \Omega \\ \Omega^* & 0 \end{pmatrix} \tag{C.2}$$

Here  $\epsilon_1, \epsilon_2 \in \mathbb{R}$ . The eigenvalues can be explicitly computed to be

$$E_{\pm} = \frac{\epsilon_1 + \epsilon_2}{2} \pm \sqrt{\frac{(\epsilon_1 - \epsilon_2)^2}{4} + \lambda^2 |\Omega|^2} \tag{C.3}$$

These coincide at two complex values of the interaction coupling  $\lambda_c = \pm i \frac{\epsilon_1 - \epsilon_2}{2|\Omega|}$ . We note however, that for real values of the perturbing field, where the Hamiltonian of interest is also Hermitian, the interaction between the two energy levels only results in an avoided crossing: the two eigenvalues come closer as  $\lambda \rightarrow 0$  and then diverge away from each other again. For a matrix of order 2, the only nontrivial way to induce a true crossing on the real axis is to set  $\epsilon_1 = \epsilon_2$ , in which case the two eigenvalues look like they pass right through each other, giving the appearance of an avoided crossing.

The behavior of the eigenvalues remains regular (there is no singularity). In passing, we also note that, when a two-level crossing is sufficiently isolated, the eigenvectors virtually exchange their identities: before the collision  $\lambda \ll \text{Re}\lambda_c : \{E_1 \rightarrow |1\rangle, E_2 \rightarrow |2\rangle\}$  and after we obtain approximately  $\lambda \gg \text{Re}\lambda_c : \{E_1 \rightarrow |2\rangle, E_2 \rightarrow |1\rangle\}$ , if we maintain that eigenvalues are identified by their ordering:  $E_1 \leq E_2$ ; in other words, the lowest eigenvalue is always identified as  $E_1$  and the highest as  $E_2$ .

It turns out that this feature persists for finite hermitian matrices of arbitrarily high order  $N$ : it is impossible for one to induce a singular crossing of any pair of nearby eigenvalues by simply changing the value of one *real valued* interaction coupling, since the square root branching points of the eigenvalues always appear in complex conjugate pairs, and when they coalesce, the behavior induced is generally regular (it can be seen immediately in the case  $N = 2$ , where imposing  $\text{Im} \lambda_c = 0$  induces linear behavior around the crossing point).

Summarizing, above we discussed avoided crossings in hermitian operator eigenvalue problems, connected their appearance to the existence of exceptional points at complex couplings. This treatment underscores the point that avoided crossings of two eigenvalues are ubiquitous in interacting quantum systems. In the following paragraphs we will discuss why it makes sense to study two level crossings individually for a wide class of problems and we will model them phenomenologically when they present in isolation.

In the discussion above, we limited our inferences to matrices of finite size. However, for studying QFT problems treated with the LCT method, this discussion is general, since the truncated matrices are themselves finite in size. We will discuss avoided crossings in theories of the form C.1 with  $H_0$  being the LCT Hamiltonian for a boson with mass  $m$  and the interaction Hamiltonian given by

$$H_0 = m^2 \int dx_- \frac{\phi^2(x)}{2!} \quad ; \quad H_1(s) = \int dx_- \left( \frac{1}{4!} \phi^4(x) + \frac{s}{3!} \phi^3(x) \right) \quad (\text{C.4})$$

so that for every value of the slope  $s = g/\lambda$  we are studying a one-parameter defor-

mation of the non-interacting Hamiltonian.

Generally, in the full spectra of such LCT Hamiltonians describing scalar bosons with polynomial interactions with no internal symmetries, we notice a proliferation of avoided crossings all throughout the spectrum. As one increases the truncation level, the avoided crossing height generally *decreases*. The lowest lying eigenvalues of LCT Hamiltonians converge to their continuum values the fastest, and avoided crossings between them are especially important to study, while the ones happening at higher eigenvalues bear little physical significance. Experimentally, we notice that avoided crossings in the low energy sector occur within the vicinity of point where the gap vanishes, while as the matrix size increases we note by inspection that the individual crossing length and width, but also their collective width near the phase transition tend to vanish. Therefore, we are justified in viewing these as an indication of a phase transition, and in the following treatment we will provide an effective description for individual two-level crossings, in which we will assign precise meaning to the individual crossing height and width, to aid with our quantitative understanding of avoided crossings.

For the rest of this chapter, we will describe an avoided crossing by the following 5 quantities: the crossing center  $\lambda_c$ , crossing minimum height  $h_0$ , effective width  $w_0$ , incoming eigenvalue slopes  $r_+, r_-$ . Assume that an apparent two-level crossing with center, width, height and energies  $(\lambda_{c1}, w_1, h_1, E_1, E_2)$  is sufficiently isolated- ie the nearest avoided crossing  $(\lambda_{c2}, w_2, h_2, E_3, E_4)$  happens a minimum of a few crossing widths away or a few crossing heights above or below(  $|\lambda_{c1} - \lambda_{c2}| \gg w_1 + w_2$  or  $|\frac{E_1+E_2-E_3-E_4}{2}| \gg h_1 + h_2$  ). If either of these conditions are fulfilled, then we may, in the vicinity of its center, Taylor expand the matrix elements between the two states involved and diagonalize the resulting two level system to study the eigenvalue evolution. This treatment has been hashed out in older literature, but we recast the problem in terms of convenient variables for our numerical treatment. As it turns out, one way of describing the most generic two-level avoided crossing possible is given by analyzing the real, Hermitian Hamiltonian

$$H = \begin{pmatrix} \epsilon_0 & \omega_0 \\ \omega_0 & \epsilon'_0 \end{pmatrix} + (\lambda - \lambda_0) \begin{pmatrix} \omega_1 & \Omega \\ \Omega & \omega_2 \end{pmatrix} \quad (\text{C.5})$$

We can read off upon diagonalizing that

$$\begin{aligned} E_{\pm}(\lambda) &= \frac{1}{2} \left( \epsilon_0 + \epsilon'_0 + (\lambda - \lambda_0)(\omega_1 + \omega_2) \pm \sqrt{D(\lambda)} \right) \\ D(\lambda) &= (\epsilon_0 - \epsilon'_0)^2 + 4\omega_0^2 + 2(\lambda - \lambda_0)(4\omega_0\Omega + (\epsilon_0 - \epsilon'_0)(\omega_1 - \omega_2)) \\ &\quad + (\lambda - \lambda_0)^2(4\Omega^2 + (\omega_1 - \omega_2)^2) \end{aligned} \quad (\text{C.6})$$

We define the crossing height  $h_0$  as the minimum vertical distance between the two eigenvalues, the crossing center  $\lambda_c$  as the point at which the minimum happens and the outward asymptotic slopes of the eigenvalues  $r_{\pm}$  for  $\lambda \gg \lambda_c$  and we calculate them explicitly:

$$\begin{aligned} h_0 &:= \min_{\lambda} |E_+(\lambda) - E_-(\lambda)| = \frac{|\omega_0(\omega_1 - \omega_2) - \Omega(\epsilon_0 - \epsilon'_0)|}{\sqrt{\Omega^2 + \frac{(\omega_1 - \omega_2)^2}{4}}} \\ \lambda_c &:= \operatorname{argmin}_{\lambda} |E_+(\lambda) - E_-(\lambda)| = \lambda_0 - \frac{4\omega_0\Omega + (\epsilon_0 - \epsilon'_0)(\omega_1 - \omega_2)}{4\Omega^2 + (\omega_1 - \omega_2)^2} \\ r_{\pm} &:= \lim_{\lambda \rightarrow \infty} \frac{E_{\pm}(\lambda)}{\lambda} = \frac{\omega_1 + \omega_2}{2} \pm \frac{1}{2} \sqrt{(\omega_2 - \omega_1)^2 + 4\Omega^2} \end{aligned} \quad (\text{C.7})$$

Furthermore, the discriminant  $D(\lambda)$  can be expanded around the critical point and assumes the simple quadratic form

$$D(\lambda) = \alpha^2 + \beta^2(\lambda - \lambda_c)^2 \quad (\text{C.8})$$

$$\alpha^2 = \frac{4(\omega_0(\omega_1 - \omega_2) - \Omega(\epsilon_0 - \epsilon'_0))^2}{4\Omega^2 + (\omega_1 - \omega_2)^2} = h_0^2, \quad \beta^2 = 4\Omega^2 + (\omega_1 - \omega_2)^2 = (r_+ - r_-)^2 \quad (\text{C.9})$$

So far we have defined every quantity mentioned in the previous paragraph, except the width. It's not immediately clear how to construct a width given the shape of the eigenvalue evolution, and the reason why we cannot immediately do this is because

of the non-trivial asymptotes to infinity. However, the derivatives of the difference between the two eigenvalues asymptote to a finite value at infinity and it becomes possible to define a scale. For convenience, we choose the second derivative of the difference, as stated in equation (C.8), whose form we can compute explicitly

$$v(\lambda) = \frac{d^2}{d\lambda^2}(E_+ - E_-) = \frac{(\alpha\beta)^2}{(\alpha^2 + \beta^2(\lambda - \lambda_c)^2)^{3/2}} \quad (\text{C.10})$$

Conveniently, this function has a single maximum at  $\lambda = \lambda_c$  and asymptotes to zero as  $\lambda \rightarrow \pm\infty$ . One can therefore define its full width at half maximum. We use this as our definition of the crossing width

$$w_0 := 2\{\lambda > \lambda_c : v(\lambda) = v(\lambda_c)/2\} = 2\sqrt{2^{2/3} - 1}\frac{\alpha}{\beta} \simeq 1.533\frac{h_0}{r_+ - r_-} \quad (\text{C.11})$$

The width depends directly on the other parameters we defined and is therefore not essential for the complete description of the two-level crossing. Notice how the width is proportional to the height of the crossing, so if one vanishes the other does too. This shows that the shape of the crossing function is somewhat rigid; it cannot be arbitrarily stretched in both directions.

We find that the simplest possible phenomenological description that maintains the independence of these 4 essential parameters is the reduction  $\omega_0 = 0, \omega_1 = \omega_2 = \omega$  which centers the crossing on its center  $\lambda_c$ , while also granting them parallel trajectories when  $\Omega = 0$ . In the light of this we mandatorily impose  $\Omega \neq 0$  which yields

$$\begin{aligned} h_0 &= |\epsilon_0 - \epsilon'_0| \\ \lambda_c &= \lambda_0 \\ r_{\pm} &= \omega \pm \Omega \\ w_0 &= 0.766\frac{|\epsilon_0 - \epsilon'_0|}{\Omega} \end{aligned} \quad (\text{C.12})$$

As far as measuring the crossing parameters is concerned, the simplest way to go

about obtaining them in a quantum system where we can diagonalize the Hamiltonian exactly for values of the coupling with arbitrary precision, is to employ an algorithm to find with good precision the position of the crossing center. Since this is the result of a minimization process, a convergent algorithm for finding the extremum of a function like the golden-section search can be used to obtain it. For our applications, we need to monitor a moderate number,  $\mathcal{O}(10)$  crossings, and obtaining any data point is relatively expensive. We can minimize the number of diagonalizations we have to do by doing a sweep of the transition region containing  $\mathcal{O}(1000)$  points. The detection of a crossing in this setting is almost foolproof for the level of  $\Delta_{\max}$  that we are considering; crossings are usually much further apart than our resolution. Furthermore, the estimation of the crossing parameters is almost perfect, since the crossings are sufficiently well isolated and therefore the functional dependence is robust many crossing widths away from the crossing center, so if one obtains data with enough numerical accuracy there is no possibility of making larger errors. Intuitively, the in and out slope of the crossing can be measured perfectly at long distance. One could be worried that the other crossing parameters are sensitive to near-center crossing data points, but since the functional dependence (C.13) is so robust and noiseless, one can get accurate results by detecting even very small deviations from the straight lines defining the slopes.

Once the crossing center has been found, for any given isolated crossing in our system of interest we may measure the parameters  $\epsilon_0, \epsilon'_0, \omega, \Omega$  very easily by OLS fitting the difference and sum of energies to the functional forms

$$\begin{aligned} E_+ + E_- &= A + B(\lambda - \lambda_c) \\ (E_+ - E_-)^2 &= C + D(\lambda - \lambda_c)^2 \end{aligned} \tag{C.13}$$

Using  $A, C$  one can calculate estimates for  $\epsilon_0, \epsilon'_0$  and from  $B, D$  one gets information for  $\omega, \Omega$ .

## D Non-relativistic bound state in $\phi^4$

It turns out that it is possible to estimate the dependence of the mass of any threshold bound state by appropriately approximating the problem of diagonalizing the QFT Hamiltonian exactly, by a simpler, nonrelativistic version of the problem. To be more precise, it is known that bound states show up as poles to the S-matrix. In particular, for a threshold bound state to form at weak coupling, we expect that it will be composed primarily of a two-particle state, with tiny contributions from higher particle sectors, that dress the free state appropriately to lower its energy. This bound state should show up as an intermediate product in the  $2 \rightarrow 2$  scattering in perturbation theory.

Relativistically, one can compute corrections to this scattering process using diagrammatics and then, by taking the non-relativistic limit, one can reduce the problem the motion of a quantum particle under a Yukawa type potential. The quartic term is the dominant contribution at weak coupling and contributes a quantum mechanical single particle delta-function potential in the non-relativistic limit:

$$\lambda\phi^4 \rightarrow V_1(x) = v_0 \frac{\lambda}{m^2} \delta(x) \quad (\text{D.1})$$

where  $v_0$  is a dimensionless number that fixes the normalization between relativistic and non-relativistic states (see Peskin-Schröder p.121-Yukawa potential for details). The  $\phi^3$  term contributes an *attractive* Yukawa potential of the form

$$V_2(q) = -\frac{g^2}{q^2 + m^2} \quad (\text{D.2})$$

which upon Fourier transforming yields the expression

$$V_2(x) = -v_1 g^2 \frac{e^{-m|x|}}{2m} \quad (\text{D.3})$$

where  $v_1$  is another dimensionless number that can be computed from the match-

ing process. The effective single particle Hamiltonian describing the non-relativistic bound state is given by

$$H = \frac{p^2}{2m} + \lambda_0 \delta(x) - g_0^2 \frac{e^{-m|x|}}{2m} \quad (\text{D.4})$$

which after restoring powers of  $\hbar, c$  we find that, in order to match the units in the quantum theory, must be matched as follows

$$\lambda_0 = v_0 \frac{\hbar^4}{c} \frac{\lambda}{m^2}, \quad g_0 = v_1 \frac{\hbar^{5/2}}{c} \frac{g}{m} \quad (\text{D.5})$$

where  $v_0, v_1$  are the matching dimensionless numbers. The repulsive delta potential does not contain any bound states in its spectrum, so we expect that the bound state will arise at only when  $g$  becomes large enough. Setting  $\hbar = c = 1$  to reduce clutter again, the quantum mechanical potential reads

$$V(x) = v_0 \frac{\lambda}{m^2} \delta(x) - v_1 \frac{g^2}{2m^3} e^{-m|x|} \quad (\text{D.6})$$

The potential is difficult to solve exactly, and perturbation theory around the delta potential will not work, since  $\lambda > 0$  and the delta potential barrier has no bound states in its spectrum to support traditional quantum mechanical perturbation theory. We can make an estimate of the bound state value in the limit  $m \rightarrow \infty$  with  $\lambda/m^2, g/m^2$  constant. Since this limit requires the mass gap to be infinitely large, in the field theory, this is equivalent to weak coupling. In this limit, we first note that the function  $F_m(x) = m e^{-m|x|}$  becomes increasingly sharp as  $m \rightarrow \infty$  and hence

$$\lim_{m \rightarrow \infty} F_m(x) = 2\delta(x) \quad (\text{D.7})$$

The limit of large masses is exactly the limit we want to take, since the region that we are interested in in the continuum theory is  $m^2 \gg g, \lambda$ . We can now approximate

the potential

$$V(x) \stackrel{m \rightarrow \infty}{\sim} \left( v_0 \frac{\lambda}{m^2} - v_1 \frac{g^2}{m^4} \right) \delta(x) \quad (\text{D.8})$$

which shows that to first order in the mass, the expected bound state energy in the non-relativistic approximation is

$$E_b = -\frac{m}{2} \left( v_0 \frac{\lambda}{m^2} - v_1 \frac{g^2}{m^4} \right)^2 \quad (\text{D.9})$$

Returning to the field theory notation, this is the deviation of the bound state mass with respect to the two-particle threshold,  $E_b = M_b - M_{\text{gap}}$ . In (D.9), the mass  $m$  of the quantum particle now corresponds to the mass of the gap  $M_{\text{gap}}$ , which receives corrections with increasing  $\lambda, g$ . However, for a leading order estimate we can ignore these corrections and conclude that, at weak coupling a threshold bound state emerges with mass  $M_b$

$$\frac{M_b}{2M_{\text{gap}}} = 1 - \frac{1}{4} \left( v_0 \frac{\lambda}{m^2} - v_1 \frac{g^2}{m^4} \right)^2 + \dots \quad (\text{D.10})$$

reproducing the equation (3.36) that we were led to conjecture using our intuition gained by LCT numerics.

The nature of the above limit of taking the one particle mass to infinity is somewhat obscure, given that it's taken with the couplings held constant. To obtain a more accurate picture which is also non-perturbative, we use inspiration from the limit above to write an appropriate variational ansatz for the ground state of the quantum mechanical system (D.6). We use the bound state of the delta potential as the variational ansatz centered around the origin, and we use its width as the variational parameter. The normalized trial state can be written as

$$\Psi_q(x) = \langle x|b;q \rangle = \sqrt{q} e^{-q|x|}, \quad q > 0 \quad (\text{D.11})$$

Then, the variational energy can be computed using the formula ( $\hbar = c = 1$ )

$$U(q) = \frac{1}{2m} \int_{-\infty}^{\infty} dx |\Psi'_q(x)|^2 + \int_{-\infty}^{\infty} dx V(x) |\Psi_q(x)|^2 \quad (\text{D.12})$$

The integrals can be easily computed and the explicit formula for the energy estimate is given by

$$U(q) = \frac{q^2}{2m} + v_0 \frac{\lambda}{m^2} q - v_1 \frac{g^2}{m^3} \frac{q}{2m + q} \quad (\text{D.13})$$

We can shed some light into the nature of the perturbative limit that we are taking by employing the following adimensional variables

$$\tilde{U} = m^{-1}U, \quad x = m^{-1}q, \quad \frac{v_1 g^2}{m^4} = a_1 s, \quad \frac{v_0 \lambda}{m^2} = a_0 s \quad (\text{D.14})$$

The variable  $s$  allows us to take the weak coupling limit along lines of constant  $g^2/\lambda$ , which has repeatedly shown up as an important quantifier in our applications. With this rescaling, it becomes apparent that the limit taken in the previous heuristic analysis is, indeed, a weak coupling limit. Finally, we compute the derivative of the variational energy

$$\frac{d\tilde{U}}{dx} = x + s \left( a_0 - a_1 \frac{1}{(2x + 1)^2} \right) \quad (\text{D.15})$$

Computing the roots of this is tantamount to finding the solutions to a cubic equation. This problem is tractable but to obtain enlightening information about the ansatz we will first explore what happens at weak coupling,  $s \ll 1$ . This can be tackled by using a perturbation expansion around the root  $x(s = 0) = 0$ ; we obtain the first few orders to the solution which come in the orderly form

$$x(s) = x_0 + x_1 s + x_2 s^2 + x_3 s^3 + x_4 s^4 + \dots \quad (\text{D.16})$$

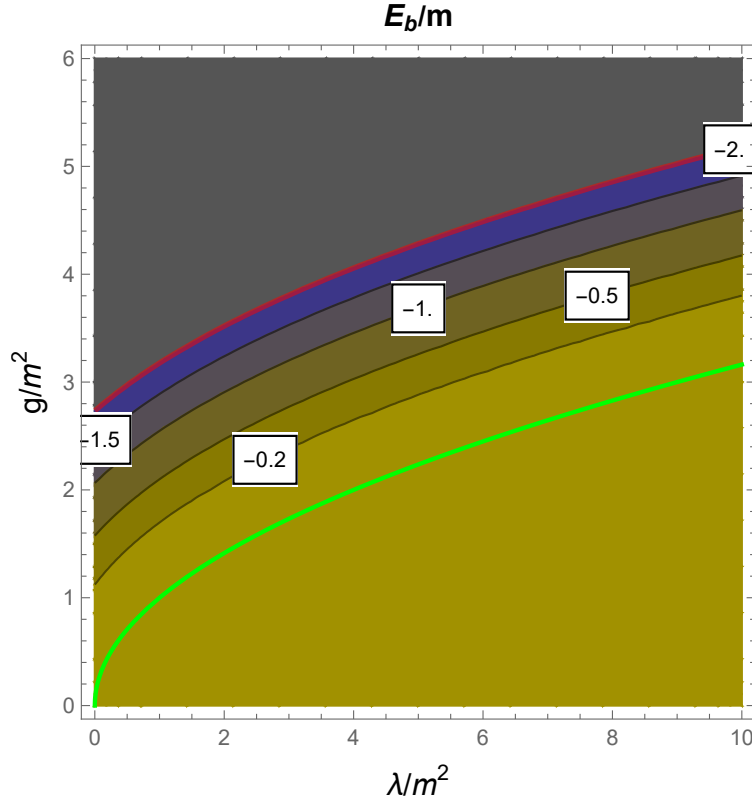


Figure 28: Plot of the binding energy of the threshold bound state in units of the gap  $m$ , with  $v_0 = v_1 = 1$ . The line in green represents the emergence curve  $g^2 = \lambda m^2$ . At the red line  $E_b = -2m$ , and the LCT ansatz breaks down.

Plugging  $x_0 = 0$  in the resulting linear equations yields

$$\begin{aligned} x_1 &= a_1 - a_0, & x_2 &= -4a_1(a_1 - a_0), & x_3 &= 4a_1(a_1 - a_0)(7a_1 - 3a_0), \\ x_4 &= -16a_1(a_1 - a_0)(3a_1 - 2a_0)(5a_1 - a_0) \end{aligned} \quad (\text{D.17})$$

Demanding that  $x > 0$  so that the ansatz makes sense brings out very naturally the tug of war between the attractive cubic and the repulsive quartic interaction: the width of the bound state is proportional to

$$x \propto v_1 \frac{g^2}{m^4} - v_0 \frac{\lambda}{m^2} \quad (\text{D.18})$$

and thus at weak coupling the bound state exists only for values of the couplings that

keep the above quantity positive. This is exactly the result that we wanted to show, now through the lens of a more rigorous tool. Writing out the expansion in terms of couplings

$$x = \left( v_1 \frac{g^2}{m^4} - v_0 \frac{\lambda}{m^2} \right) \left[ 1 - 4v_1 \frac{g^2}{m^4} \left( 1 + 3 \frac{v_0 \lambda}{m^2} - 7 \frac{v_1 g^2}{m^4} + \dots \right) \right] \quad (\text{D.19})$$

reveals that corrections to the expected relationship (D.9) are controlled by the cubic coupling. The bound state energy to the first few orders is given by

$$\frac{E_b}{m \left( \frac{v_0 \lambda}{m^2} - \frac{v_1 g^2}{m^4} \right)^2} = -\frac{1}{2} + 2v_1 \frac{g^2}{m^4} \left( 1 + 2v_0 \frac{\lambda}{m^2} - 6v_1 \frac{g^2}{m^4} + \dots \right) \quad (\text{D.20})$$

and this agrees with our expectations. The strong coupling behavior of this ansatz does not reproduce the results expected from simulations: a bound state appears at  $a_0 = a_1$  and as the couplings increase, it becomes more strongly bound, no matter how large the quartic coupling becomes. This is in contradiction with the fact that the bound state is expected to disappear completely for large enough quartic coupling. However, the non-relativistic calculation fails from the LCT perspective, when  $E_b < -2m$ , since at that point, it has gone below the energy of the vacuum already, agreeing qualitatively with the semiclassical picture. Shown in Fig. 28 is the result of an numerical evaluation of the binding energy as a function of the couplings. The lines where  $E_b = 0$ ,  $E_b = -2m$  are shown for reference.

## LIST OF JOURNAL ABBREVIATIONS

AIP Conf Proc	AIP Conference Proceedings
Ann Math	Annals of Mathematics
Class Quant Grav	Classical and Quantum Gravity
Commun Math Phys	Communications in Mathematical Physics
Int J Mod Phys	International Journal of Modern Physics
J High Energy Phys	Journal of High Energy Physics: JHEP
J Math Phys	Journal of Mathematical Physics
J Stat Mech	Journal of Statistical Mechanics (Online)
JHEP	Journal of High Energy Physics: JHEP
Kong Dan Vid Sel Mat Fys Med	Kongelige Danske Videnskabernes Selskab Matematisk-fysiske Meddelelser
Mod Phys Lett	Modern Physics Letters
Nucl Phys B	Nuclear Physics. B
Nuovo Cim A	Il Nuovo Cimento della Società Italiana di Fisica. A
Phys Lett B	Physics Letters. [Part B]
Phys Rev B	Physical Review. B
Phys Rev D	Physical Review. D
Phys Rev E	Physical Review. E
Phys Rev Lett	Physical Review Letters
Rev Mod Phys	Reviews of Modern Physics

## References

- [1] N. Anand, A. L. Fitzpatrick, E. Katz, Z. U. Khandker, M. T. Walters and Y. Xin, “Introduction to Lightcone Conformal Truncation: QFT Dynamics from CFT Data,” [arXiv:2005.13544 [hep-th]].
- [2] N. Anand, V. X. Genest, E. Katz, Z. U. Khandker and M. T. Walters, JHEP **08**, 056 (2017) doi:10.1007/JHEP08(2017)056 [arXiv:1704.04500 [hep-th]].
- [3] P.W.Anderson, Phys. Rev. Lett. 18,1049(1967)
- [4] M. Asorey, J. G. Esteve, F. Falceto and J. Salas, “Tricritical behavior of two-dimensional scalar field theories,” Phys. Rev. B **52**, 9151 (1995), [arXiv:hep-lat/9410009 [hep-lat]].
- [5] Z. Bajnok and M. Lajer, “Truncated Hilbert space approach to the 2d  $\phi^4$  theory,” JHEP 1610 (2016) 050 doi:10.1007/JHEP10(2016)050 [arXiv:1512.06901 [hep-th]].
- [6] T. Barnes, G.J. Daniell, A numerical study of the bound state spectrum of  $:\gamma(\Phi^6 - \Phi^4)_2:$  In lattice Hamiltonian field theory (1984)
- [7] T. Barnes and G. J. Daniell, Nucl. Phys. B **257**, 173-198 (1985)
- [8] Berger, W.A., Miller, H.G., & Waxman, D. (2007). Threshold bound states. The European Physical Journal A, 37, 357-360.
- [9] B. Borasoy and D. Lee, Nucl. Phys. A **696**, 537-555 (2001) doi:10.1016/S0375-9474(01)01127-7 [arXiv:hep-ph/0101186 [hep-ph]].
- [10] P. Bosetti, B. De Palma and M. Guagnelli, “Monte Carlo determination of the critical coupling in  $\phi_2^4$  theory,” Phys. Rev. D 92 (2015) no.3, 034509[arXiv:1506.08587 [hep-lat]].
- [11] Brooks, E. D., and Frautschi, S. C. (1982). Scalars coupled to fermions in 0+1 dimensions. Zeitschrift Für Physik C Particles and Fields, 14(1), 27–33.

- [12] Brooks, E. D., and Frautschi, S. C. (1984). Scalars coupled to fermions in 1+1 dimensions. *Zeitschrift Für Physik C Particles and Fields*, 23(3), 263–273.
- [13] Bruch, L. W., & Tjon, J. A. (1979). Binding of three identical bosons in two dimensions. *Physical Review A*, 19(2), 425–432.
- [14] M. Burkardt, Light-front quantization of the sine-Gordon model, *Phys. Rev. D* 47, 4628 (1993)
- [15] M. Burkardt, S. S. Chabysheva and J. R. Hiller, Two-dimensional light-front  $\phi^4$  theory in a symmetric polynomial basis, *Phys. Rev. D* **94**, no.6, 065006 (2016) [arXiv:1607.00026 [hep-th]]
- [16] T. Byrnes, P. Sriganesh, R. J. Bursill and C. J. Hamer, *Phys. Rev. D* **66**, 013002 (2002) doi:10.1103/PhysRevD.66.013002 [arXiv:hep-lat/0202014 [hep-lat]].
- [17] M. Caselle, M. Hasenbusch and P. Provero, *Nucl. Phys. B* **556**, 575-600 (1999) [arXiv:hep-lat/9903011 [hep-lat]].
- [18] W. E. Caswell, Accurate energy levels for the anharmonic oscillator and a summable series for the double-well potential in perturbation theory, *Annals of Physics*, Volume 123, Issue 1 (1979)
- [19] Chabysheva, S. S., & Hiller, J. R. (2012). A light-front coupled-cluster method for the nonperturbative solution of quantum field theories. *Physics Letters B*, 711(5), 417–422.
- [20] Sophia S. Chabysheva and John R. Hiller, Basis of symmetric polynomials for many-boson light-front wave functions, *Phys. Rev. E* 90, 063310 (2014)
- [21] S.S. Chabysheva, J.R. Hiller, Light-front  $\phi_2^4$  theory with sector-dependent mass ,[arXiv:1612.09331[hep-th]]
- [22] S. S. Chabysheva and J. R. Hiller, Transitioning from equal-time to light-front quantization in  $\phi_2^4$ , *Phys. Rev. D* **102**, no.11, 116010 (2020) [arXiv:1811.01685 [hep-th]].

- [23] S. S. Chabysheva and J. R. Hiller, Tadpoles and vacuum bubbles in light-front quantization, *Phys. Rev. D* 105, 116006 (2022)
- [24] S. J. Chang, R. G. Root and T. M. Yan, “Quantum field theories in the infinite momentum frame. 1. Quantization of scalar and Dirac fields,” *Phys. Rev. D* **7**, 1133-1148 (1973)
- [25] S.-J. Chang, “The Existence of a Second Order Phase Transition in the Two-Dimensional  $\phi^4$  Field Theory, ” *Phys. Rev. D* 13 (1976) 2778.
- [26] L. Chao, ”Light-cone quantization of scalar field”, *Mod. Phys. Lett. A* 8 (1993) 3165–3172.
- [27] S. Coleman, Quantum sine-Gordon equation as the massive Thirring model, *Phys. Rev. D* 11, 2088 (1975)
- [28] J. Collins, The non-triviality of the vacuum in light-front quantization: An elementary treatment, [arXiv:1801.03960 [hep-ph]]
- [29] Creutz, M., Monte Carlo study of quantized SU(2) gauge theory. *Physical Review D*, 21(8), 2308–2315. (1980)
- [30] Dimock, J., Eckmann, J.P. On the bound state in weakly coupled  $\lambda(\phi^6 - \phi^4)_2$ , *Commun. Math. Phys.* 51, 41–54 (1976).
- [31] Dimock, J. (1977). The non-relativistic limit of  $P(\phi)_2$  quantum field theories: Two-particle phenomena. *Communications In Mathematical Physics*, 57(1), 51–66.
- [32] Dimock, J., and Eckmann, J.-P. (1977). Spectral properties and bound-state scattering for weakly coupled  $\lambda P(\phi)_2$  models. *Annals of Physics*, 103(2), 289–314.
- [33] L. R. Dodd, Exact Solution of the Faddeev Equations for a One-Dimensional System, *J. Math. Phys.* 11, 207–213 (1970)

- [34] P. Dorey, A. Pocklington, R. Tateo, and G. Watts, TBA and TCSA with boundaries and excited states, Nucl. Phys. B525 (1998) 641; arXiv:hep-th/9712197
- [35] G.V. Dunne, M. Unsal, "What is QFT? Resurgent trans-series, Lefschetz thimbles, and new exact saddles", Volume 251 - The 33rd International Symposium on Lattice Field Theory (LATTICE 2015) - Plenary Talks, DOI: <https://doi.org/10.22323/1.251.0010>
- [36] J. Elias-Miro, S. Rychkov and L. G. Vitale, High-Precision Calculations in Strongly Coupled Quantum Field Theory with Next-to-Leading-Order Renormalized Hamiltonian Truncation, JHEP **10**, 213 (2017)
- [37] Joan Elias-Miró and Edward Hardy, Exploring Hamiltonian truncation in  $\mathbf{d} = \mathbf{2} + \mathbf{1}$ , Phys. Rev. D 102, 065001 (2020)
- [38] Discretized light-cone quantization: The massless and the massive Schwinger model Thomas Eller, Hans-Christian Pauli, and Stanley J. Brodsky, Phys. Rev. D 35, 1493 (1987)
- [39] J. Evslin, " $\phi^4$  kink mass at two loops," Phys. Rev. D **104**, no.8, 085013 (2021) doi:10.1103/PhysRevD.104.085013 [arXiv:2104.07991 [hep-th]].
- [40] A. L. Fitzpatrick, J. Kaplan, E. Katz, L. G. Vitale and M. T. Walters, JHEP **08**, 120 (2018) doi:10.1007/JHEP08(2018)120 [arXiv:1803.10793 [hep-th]].
- [41] A. L. Fitzpatrick, E. Katz, M. T. Walters and Y. Xin, JHEP **01**, 182 (2021) [arXiv:1911.10220 [hep-th]].
- [42] A. L. Fitzpatrick and E. Katz, Snowmass White Paper: Hamiltonian Truncation (2022) [arXiv:2201.11696 [hep-th]]
- [43] Glimm, J., Jaffe, A., Spencer, T. : The particle structure of the weakly coupled  $P(\varphi)_2$  model and other applications of high temperature expansions. In: Constructive Quantum Field Theory (ed. G. Velo, A. Wightman), Lecture Notes in Physics, Vol. 25. Berlin-Heidelberg- New York: Springer 1973

- [44] Glimm, J., Jaffe, A., Spencer, T. : The Wightman axioms and particle structure in the  $P(\varphi)_2$  quantum field model: *Ann. Math.* 100, 585–632 (1974)
- [45] Quantization of nonlinear waves J. Goldstone and R. Jackiw *Phys. Rev. D* 11, 1486 (1974)
- [46] R. Haag, *Kong. Dan. Vid. Sel. Mat. Fys. Med.* **29N12**, 1-37 (1955)
- [47] A. Harindranath and J.P. Vary, Solving two-dimensional  $\phi^4$  by discretized light front quantization, *Phys.Rev.D*36, 1141 (1987).
- [48] Heinzl, T., Krusche, S., Simbürger, S., and Werner, E. (1992). Nonperturbative light cone quantum field theory beyond the tree level. *Zeitschrift Für Physik C Particles and Fields*, 56(3), 415–420.
- [49] Hioe, F.T., Macmillen, D., and Montroll, E.W. (1978). Quantum theory of anharmonic oscillators: Energy levels of a single and a pair of coupled oscillators with quartic coupling. *Physics Reports*, 43(7), 305–335.
- [50] V. E. Hubeny, The AdS/CFT Correspondence, *Class. Quant. Grav.* **32**, no.12, 124010 (2015) [arXiv:1501.00007 [gr-qc]].
- [51] Patrick Jentsch, Romain Daviet, Nicolas Dupuis, and Stefan Floerchinger, Physical properties of the massive Schwinger model from the nonperturbative functional renormalization group, *Phys. Rev. D* 105, 016028 (2022)
- [52] E. Katz, G. Marques Tavares and Y. Xu, *JHEP* **05**, 143 (2014) [arXiv:1308.4980 [hep-th]].
- [53] E. Katz, G. Marques Tavares and Y. Xu, [arXiv:1405.6727 [hep-th]].
- [54] E. Katz, Z. U. Khandker and M. T. Walters, *JHEP* **07**, 140 (2016) doi:10.1007/JHEP07(2016)140 [arXiv:1604.01766 [hep-th]].
- [55] Konechny, A., McAteer, D. On asymptotic behaviour in truncated conformal space approach. *J. High Energ. Phys.* 2019, 44 (2019).

- [56] M. Lässig, G. Mussardo, and J.L. Cardy, The scaling region of the tricritical Ising model in two dimensions, Nucl. Phys. B348 (1991) 591.
- [57] H. Leutwyler, J. R. Klauder and L. Streit, Nuovo Cim. A **66**, 536-554 (1970)
- [58] M. A. Lohe, Soliton structures in  $P(\varphi)_2$ , Phys. Rev. D 20, 3120
- [59] Wen-Fa Lu, Guang-Jiong Ni and Zhi-Guo Wang, Symmetry restoration in two  $\phi^6$  models by quantum effects. Journal of Physics G 24, 673 (1998)
- [60] Maclay G.J., History and Some Aspects of the Lamb Shift (2020). Physics. 2020; 2(2):105-149.
- [61] J. M. Maldacena, AIP Conf. Proc. **484**, no.1, 51 (1999)
- [62] Maskawa, T., and Yamawaki, K. (1976). The Problem of  $P_+ = 0$  Mode in the Null-Plane Field Theory and Dirac's Method of Quantization. Progress of Theoretical Physics, 56(1), 270–283.
- [63] A. Milsted, J. Haegeman and T. J. Osborne, “Matrix product states and variational methods applied to critical quantum field theory,” Phys. Rev. D 88 (2013) 085030 doi:10.1103/PhysRevD.88.085030 [arXiv:1302.5582 [hep-lat]].
- [64] G. Mussardo, Neutral bound states in kink-like theories, Nuclear Physics B 779 [FS] (2007) 101–154
- [65] A Coser, M Beria, G. P. Brandino, R. M. Konik and G. Mussardo, Truncated conformal space approach for 2D Landau–Ginzburg theories, J. Stat. Mech. (2014) P12010
- [66] Rajamani Narayanan and Herbert Neuberger, Infinitely many regulator fields for chiral fermions, Physics Letters B, Volume 302, Issue 1 (1993)
- [67] Rajamani Narayanan and Herbert Neuberger, Chiral fermions on the lattice, Phys. Rev. Lett. 71, 3251 (1993)
- [68] Rajamani Narayanan and Herbert Neuberger, Chiral determinant as an overlap of two vacua, Nuclear Physics B, Volume 412, Issue 3 (1994)

- [69] Herbert Neuberger, Exactly massless quarks on the lattice, Physics Letters B, Volume 417, Issues 1–2 (1998)
- [70] P.A.M. Dirac, Forms of relativistic dynamics, Rev. Mod. Phys. 21, 392 (1949)
- [71] Hans-Christian Pauli and Stanley J. Brodsky, Solving field theory in one space and one time dimension, Phys. Rev. D 32, 1993 (1985)
- [72] A. Pelissetto and E. Vicari, “Critical mass renormalization in renormalized  $\phi^4$  theories in two and three dimensions,” Phys. Lett. B 751 (2015) 532 doi:10.1016/j.physletb.2015.11.015 [arXiv:1508.00989 [hep-th]].
- [73] J. Penedones, Writing CFT correlation functions as AdS scattering amplitudes, JHEP 03 (2011) 025, arXiv:1011.1485 [hep-th].
- [74] F. Rose, F. Benitez, F. Léonard, and B. Delamotte: Bound states of the  $\phi^4$  model via the nonperturbative renormalization group Phys. Rev. D **93**, 125018 (2016)
- [75] J. S. Rozowsky and C. B. Thorn, Phys. Rev. Lett. **85**, 1614-1617 (2000) [arXiv:hep-th/0003301 [hep-th]].
- [76] S. Rychkov and L. G. Vitale, Hamiltonian truncation study of the  $\phi^4$  theory in two dimensions, Phys. Rev. D **91**, 085011 (2015)
- [77] S. Rychkov and L. G. Vitale, Hamiltonian truncation study of the  $\phi^4$  theory in two dimensions. II. The  $\mathbb{Z}_2$ -broken phase and the Chang duality, Phys. Rev. D **93**, no.6, 065014 (2016)
- [78] G. Sberveglieri, M. Serone, and G. Spada, Renormalization scheme dependence, RG flow, and Borel summability in  $\phi^4$  theories in  $d < 4$ , (2019) Phys. Rev. D 100, 045008
- [79] M. Serone, G. Spada, G. Villadoro,  $\lambda\phi^4$  theory — Part II. the broken phase beyond NNNN(NNNN)LO, Journal of High Energy Physics volume 2019, Article number: 47

- [80] M. Serone, G. Spada, and G. Villadoro, Instantons from perturbation theory (2017), Phys. Rev. D 96, 021701(R)
- [81] M. Serone, G. Spada, G. Villadoro,  $\lambda\phi^4$  theory — Part I. The symmetric phase beyond NNNNNNNLO, Journal of High Energy Physics volume 2018, Article number: 148
- [82] Spencer, T.: The decay of the Bethe-Salpeter kernel in  $P(\varphi)_2$  quantum field models: Commun. math. Phys. 44, 143–164 (1975)
- [83] 7. Spencer, T., Zirilli, F.: Scattering states and bound states in  $\lambda P(\varphi)_2$ . Commun. math. Phys. 49, 1–16 (1976)
- [84] P. M. Stevenson, Phys. Rev. D **30**, 1712 (1984)
- [85] P. M. Stevenson, Phys. Rev. D **32**, 1389-1408 (1985)
- [86] P. M. Stevenson and I. Roditi, Phys. Rev. D **33**, 2305-2315 (1986)
- [87] E. Tomboulis, Canonical quantization of nonlinear waves, Phys. Rev. D 12, 1678 (1975)
- [88] James P. Vary, Mengyao Huang, Shreeram Jawadekar, Mamoon Sharaf, Avaroth Harindranath, and Dipankar Chakrabarti, Critical coupling for two-dimensional  $\phi^4$  theory in discretized light-cone quantization, Phys. Rev. D 105, 016020 (2022) bibitemweigel2017 Weigel, H. (2017), Emerging Translational Variance: Vacuum Polarization Energy of the  $\phi^6$  Kink, Advances in High Energy Physics, 2017, 1–10.
- [89] K. Yamawaki, Zero-Mode Problem on the Light Front (1998) [arXiv:hep-th/9802037]
- [90] V. Yurov and Al. Zamolodchikov, Truncated Conformal Space Approach To Scaling Lee-yang Model, Int. J. Mod. Phys. **A5** (1990) 3221-3246.

- [91] V. Yurov and Al. Zamolodchikov, Truncated fermionic space approach to the critical 2-D Ising model with magnetic field, *Int. J. Mod. Phys.* **A6** (1991) 4557-4578.
- [92] S. Weinberg (1966). "Dynamics at infinite momentum". *Physical Review*. 150 (4): 1313–1318
- [93] U. J. Wiese, An introduction to lattice field theory (2009). <https://saalburg.aei.mpg.de/wp-content/uploads/sites/25/2017/03/wiese.pdf>
- [94] A. B. Zamolodchikov, A. B. Zamolodchikov and I. M. Khalatnikov, *Physics Reviews. Vol. 10, pt. 4: Conformal Field Theory and Critical Phenomena in two-dimensional systems,*

## Vita

